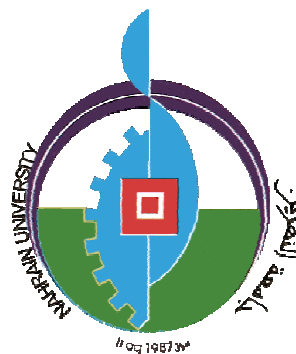


Republic of Iraq
Ministry of Higher Education
and Scientific Research
Al-Nahrain University
College of Science
Department of Physics



Preparation and Characterization of Ferroelectric Compound Like $\text{Ba}_x\text{Sr}_{1-x}\text{TiO}_3$

A Thesis

Submitted to the College of Science / Al-Nahrain University as
a partial fulfillment of the requirements for the degree of
Master of Science in Physics .

By

NATHEER BASHEER MAHMOOD

B.Sc. 2008/ College of Science / Baghdad University

Supervised by

DR.EMAD KHUDAIR AL-SHAKARCHI

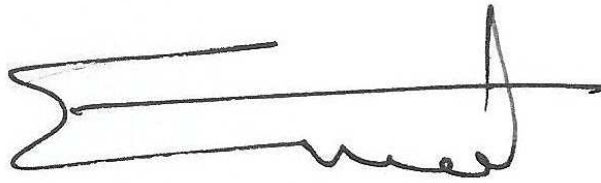
(Prof.)

April,2012

Jamad Al-Awwal,1433

Supervisor(s) certification

We, certify that this thesis entitled "Preparation and characterization of ferroelectric compound like $Ba_xSr_{1-x}TiO_3$ " was prepared by " Natheer Basheer Mahmood " under our supervision at the college of Science / Al-Nahrain university as a partial fulfillment of the requirements for the degree of Master of Science in Physics



Signature:

Name : Emad K. Al-Shakarchi

Scientific Degree : Professor

Date : 9 / 7 / 2012

In view of the available recommendations, I forward this thesis for debate by the examining committee.

Signature:



Name : Dr. Thamir A. Jabbar

Scientific Degree : Assist. Professor

Date : 10 / 7 / 2012

Committee Certification

We, the examining committee certify that we have read the thesis entitled “**Preparation and characterization of ferroelectric compound like $Ba_xSr_{1-x}TiO_3$** ” and examined the student “**Natheer Basheer Mahmood**” in its contents and that in our opinion; it is accepted for the Degree of Master of Science in **Physics**.

Signature:

Name: **Dr. Raad M.S. Al-Haddad**

Scientific Degree: **Professor**

Address: Dept. of Physics, College of Science /
University of Baghdad

Date: 15 / 7 /2012

(Chairman)

Signature:

Name: **Dr. Fadhil A. Rasin**

Scientific Degree: **Assist. Professor**

Address: Dept. of Material Engineering/
Technology University

Date: 11 / 7 /2012

(Member)

Signature:

Name: **Dr. Thamir A. Jabbar**

Scientific Degree: **Assist. Professor**

Address: Dept. Physics, College of
Science/ Al-Nahrain University

Date: 10 / 7 /2012

(Member)

Signature:

Name: **Dr. Emad K. Al-Shakarchi**

Scientific Degree: **Professor**

Address: Dept. of Physics, College of Science/
Al-Nahrain University

Date: 9 / 7 /2012

(Member & Supervisor)

I, hereby certify upon the decision of the examining committee

Signature:

Name: **Dr. Khulood W. Al-Sammarraie**

Scientific Degree: **Professor**

Title: Dean of the College of Science

Date: 19 / 7 /2012



**UNIVERSITE DE LA ROCHELLE
POLE SCIENCES ET TECHNOLOGIES
DEPARTEMENT DE CHIMIE**

Brahim Elouadi, Professeur

La Rochelle, le 20th February 2012

*Professor Dr. Khulood W. Al-Samaraay
Dean
College of Science
Al-Nahrain University
Baghdad, IRAQ*

Object: Sincere & objective evaluation of your Matser Degree Student,
Mr *Natheer Basheer Mahmood Al-Khafaji*

Dear Professor Al-Samaraay,

I would like to confirm you that your Matser Degree Student, Mr *Natheer Basheer Mahmood Al-Khafaji*, has performed a research internship under my direction at La Rochelle University in France, within the period November, 24, 2011 to the 23rd February 2012. In agreement with his Iraqi supervisor, Professor Dr *Emad Khudhair Abbas Al-Shakerji*, the topic of his research work developed with me is entitled: "Preparation and Characterization of Ferroelectric Compound derived from $Ba_xSr_{1-x}TiO_3$ ". Indeed, his research work concerns the correlation between materials composition, structure and dielectric-ferroelectric properties of the systems based on the solid solution $Ba_{1-x}Sr_xTiO_3$.

As he confirmed to me, all his expenses have been covered by the Higher Education Ministry of IRAQ. Indeed, I would like to take this opportunity to thank you and thank warmly the Al Nahrain University and the Higher Education Ministry of IRAQ, for this important support to the young and bright student Natheer Basheer Mahmood Al-Khafaji.

At the end of his internship under my direction, I would like to confirm you and also confirm to the examination Committee of the Master Degree of your College, that the Student Natheer Basheer Mahmood Al-Khafaji, has given very great scientific satisfaction during the whole time he spent in France. Mr AlKhafaji is a very efficient researcher and he has a great insight in the physics and chemistry of materials. He is one of the best students I have had at the level of Master Degree in Materials sciences. He has a sound background in materials investigations. His internship

under my direction has been very useful for him as it allowed him to get another view of materials research.

Mr AlKhafaji has got the capacity to conduct his research work in more autonomous manner! He is also capable to teach various aspects of materials sciences. Therefore, I would like to recommend for an assistantship position if there is any vacancy in your University.

It is also my pleasure to confirm you here my sincerely positive evaluation of Student Natheer AlKhafaji. During his research work under my direction at la Rochelle University, Mr AlKhafaji, has got high expertise in the correlation between the chemical composition, the structure and the ferroelectric properties of materials crystallizing with perovskite structure (ABO_3). Many experiments have been performed on his materials: i) dielectric measurements versus temperature, ii) phase transitions analysis, iii) TEM images and diffractions, iv) EDX analysis, v) etc. Unfortunately the duration of internship was very short. We were not able to investigate deeply all his samples. However, he will leave some samples with me in La Rochelle and I will send him the results of the experiments I will make for the next weeks to come. I will forward him the results and I am confident he will do his best to propose me sound interpretations. He has already started to prepare a draft of a common publication with him and with Dr Emad Al Shakarji, from the Physics Department of your College.

Finally I would like also to recommend him for a PhD scholarship that either your University or the Higher Education Ministry of IRAQ, could provide him. Mr Natheer Basheer Mahmood Al-Khafaji, is certainly one of the best Iraqi students who is worth to encourage for the preparation of PhD Degree either in Iraq or abroad. I am convinced that all investment you can put on him will be, I am sure, very beneficial for Iraq. He is very clever, hard worker, reliable and very serious research student.

With my very best regards

Sincerely yours

Brahim Elouadi,
Professeur des universités

Professeur Brahim ELOUADI
UNIVERSITE DE LA ROCHELLE
Département de Chimie
Av. Michel Crépeau, 17042 La Rochelle cédex 01, FRANCE
Tel: +33-(0)5 46 45 82 95, Fax : +33-(0)5 46 45 82 05
E-MAIL : belouadi-univ-lr.fr

Acknowledgement

Major thanks to my supervisor Prof. Emad K. Al-Shakarchi for his suggestions and checking my thesis thoroughly . It's my pleasure to thank Prof.Brahim Eloudi / La Rochelle University / France, for his acceptance to perform my task and for his important role in this project particularly for his sincere interest, support and numerous technical resources and for his excellent hospitality

Thanks are due to my ant Prof.Zahra M. Al-Khafaji and Prof. Essam A.Al-Jumaily/ Genetic Engineering Institute / Baghdad University / IRAQ for their assistance.

It's my pleasure to thank Mr.Mohammed H.Al-Darub / Ministry of Industry and Minerals / IRAQ for his assistance in XRD; Mr.Mazin Kamil / College of medicine / Al-Nahrain University for his help in TEM; Mr.Ryad S. Majeed Headmaster of Energy Commission / Al-Daura Refinery /IRAQ; Engineer Sami K.Jawad and Miss.Karima F. Salih/Standardization and Quality Control / Al-Daura Refinery /IRAQ for their assistance .

I also wish to thank Mr. Mohammed Tarik and Dr. Thamir Abd Al-Jabar / Solid State Lab./Physics Dept./ Al-Nahrain University for their Lab. assistances to accomplish this task .

I would like to express my gratitude to Dr. Stefano Loreti / ENEA Research Centre/ Italy for providing the requirement for program of XRD Qualitative analysis .

I would like to thank my colleagues who contributed to my work; it is difficult to include all the names, but I would say that God bless all of them.

Finally, I wish to acknowledge the Dept. of Physics / College of Science / Al-Nahrain University and the IRAQI government for the financial assistance for graduate scholarship.

Summary

Summary

Ferroelectric materials possess spontaneous polarization which can be reversed by applying an external electric field over a certain temperature range. Ferroelectric materials belong to special types of crystals (non-centrosymmetric structure). Ferroelectric materials have a lot of industrial applications in medicine, environment and communications, etc. There are many ferroelectric materials such as Barium titanate BaTiO_3 and Strontium titanate SrTiO_3 have perovskite structure. There are different methods for preparing ferroelectrics such as physical and chemical methods which are different in cost and quality.

In this study, $\text{Ba}_x\text{Sr}_{1-x}\text{TiO}_3$ (BST) were prepared with different substitutions (x), where $x = 1, 0.9, 0.8, 0.7, 0.6, 0.5, 0$ by oxalate coprecipitation method, which is an easy method with low cost of power and give good results. Nanopowders with average particle size (50 to 140 nm) were prepared and pressed in a suitable template at pressure = 125 MPa to get disc with diameter = 1 cm, then these discs were sintered under vacuum at temperature of 1200 °C for 8 hr.

The resulted powders have polycrystalline structure. Crystal structure, space group, crystallite size, bond energy and particle size were determined from structural analysis (XRD, FTIR and TEM). Using special software for specifications and estimations such as XRD, FTIR and Microscope software which help in calculations and to make a comparison with some international databases like ICDD PDF2 database, COD database and SDBS database. Some of these results were formatted into CIF files and published into international database (Crystallography open database) from International Union For Crystallography (IUCr).

Physical properties represented by density and dielectric measurements for BST system were studied; density was estimated theoretically, and experimentally and conclude an experimental equation for the ceramic compactness with substitution factor (x)

The dielectric measurements were studied under two conditions, the first was by changing frequency at fix temperature, the second was by changing temperature at fix frequency in role to measure the dielectric constant (ϵ_r) and loss tangent (D) . Curie temperature (T_c) and dielectric constant were determined from dielectric measurements .there are two equations for changing of Curie temperature and dielectric constant versus substitution factor (x) as mentioned in results chapter .

From dielectric measurements, it was clear that the samples BST7, BST6, BST5 had Curie temperature around room temperature, so it might have medical and environmental applications.

The samples BST8 to BST5 had very low values of loss tangent so it might have many applications especially in microwave and communications.

List of Publications

No.	Title	Journal
1	Three Techniques Used to Produce BaTiO ₃ Fine Powder	<i>Journal of Modern Physics, 2011, 2, 1420-1428</i>
2	Crystal Chemistry and Dielectric Properties of Barium Strontium Titanate Fine Powders	<i>Pre-published</i>
3	COD ID : 1507756 (As CIF file)	BaTiO ₃ CIF files were published into international database :
4	COD ID : 1507757 (As CIF file)	<i>Crystallography Open Database (COD)</i> From International Union for Crystallography (IUCr)

List of Tables

Chapter One		
No.	Title	Page
1.1	Types of perovskite structure	6
1.2	Thermodynamic and physical properties of $(\text{Ba}_x\text{Sr}_{1-x}\text{TiO}_3)$	15
Chapter Two		
2.1	Materials , Equipment and software	20
2.2	Conditions and Molarity (M) of starting materials for preparing BST powders	26
Chapter Three		
3.1	Density (g/cm^3) for BST discs after sintering (1200°C / 8hr)	32
3.2	Phases and crystallite sizes of BST samples calcined at(850 °C/5 hr)	38

List of Figures

No.	Title	Page
Chapter One		
1.1	Hysteresis loop	2
1.2	The relation between Ferroelectric , Pyroelectric , Piezoelectric and Dielectric materials	3
1.3	Classification of crystals showing the classes with piezoelectric, pyroelectric, and ferroelectric phenomenon	4
1.4	Perovskite structure	5
1.5	Phase transitions of BaTiO ₃	7
1.6	MFSFET (Metal Ferroelectric Semiconductor Field Effect Transistor)	11
1.7	Variation of capacitance vs electric field for BST	11
1.8	Varactor as tunable LC circuit	11
1.9	Reflectivity (S ₁₁) and Transmittance (S ₂₁) vs frequency of BST	12
1.10	Micro-stripe waveguide	12
1.11	The Phase shifter	12
1.12	Multilayer Ceramic Capacitor (MLCC)	13
1.13	High gain and high directive antenna(4 element BST ceramic array antenna)	13
1.14	(x-T) phase diagram for BST system	18
Chapter Tow		
2.1	Block diagram for Sodium hydroxide-ethanol method	22
2.2	Block Diagram for the Oxalate method	23
2.3	Block Diagram for Sodium hydroxide method	24
2.4	Block Diagram for preparing Barium Strontium titanate (BST)	25
2.5	The template used for pressing the powders	27

2.6	The setup of Dielectric measurement in La Rochelle university France	30
Chapter Three		
3.1	The compactness of the ceramic discs verses Barium concentration (x)	33
3.2	The density of the ceramic discs vs substitution factor(x)	33
3.3	XRD pattern for Sodium hydroxide-ethanol method (a) before calcination (b) after calcination 850 °C / 5hr	35
3.4	XRD pattern for Oxalate method (a) before calcinations, (b) after calcination at 600 °C / 5hr, (c) after calcination at 850 °C / 5hr	36
3.5A	Williamson-Hall plot for Oxalate method (600 °C/5 hr)	36
3.5B	Williamson-Hall plot for Oxalate method (850 °C/5 hr)	
3.6	XRD pattern for Sodium hydroxide method (a) calcination (b) after calcination at 850 °C / 5 hr .	37
3.7A	Williamson-Hall plot for NaOH method before calcinations	38
3.7B	Williamson-Hall plot for NaOH method (850 °C/5 hr).	
3.8	XRD pattern for BT after calcination at 850 °C / 5 hr .	39
3.9	XRD pattern for BST9 after calcination at 850 °C / 5 hr .	39
3.10	XRD pattern for BST8 after calcination at 850 °C / 5	40

	hr	
3.11	XRD pattern for BST7 after calcination at 850 °C / 5 hr .	40
3.12	XRD pattern for BST6 after calcination at 850 °C / 5 hr.	41
3.13	XRD pattern for BST5 after calcination at 850 °C / 5 hr .	41
3.14	XRD pattern for ST after calcination at 850 °C / 5 hr .	42
3.15	XRD pattern for BST after calcination at 850 °C / 5 hr	43
3.16	3D XRD pattern for BST after calcination at 850 °C / 5 hr .	43
3.17	Variation of lattice parameter with substitution factor (x)	44
3.18	Variation of cell volume with substitution factor (x)	44
3.19	Williamson-Hall plot for BT (850 °C/5 hr)	45
3.20	Williamson-Hall plot for BST9 (850 °C/5 hr)	45
3.21	Williamson-Hall plot for BST8 (850 °C/5 hr)	45
3.22	Williamson-Hall plot for BST7 (850 °C/5 hr)	45
3.23	Williamson-Hall plot for BST6 (850 °C/5 hr)	46
3.24	Williamson-Hall plot for BST5 (850 °C/5 hr)	46
3.25	Williamson-Hall plot for ST (850 °C/5 hr)	46
3.26	FTIR spectrum for BT	47
3.27	FTIR spectrum for BST5	48
3.28	FTIR spectrum for ST	48
3.29	FTIR spectrum for BST samples	48
3.30	Variation of absorption in wave number vs substitution factor (x)	48
3.31	Dielectric constant and loss tangent vs frequency for BT	50
3.32	Dielectric constant and loss tangent vs frequency for BST9	50
3.33	Dielectric constant and loss tangent vs frequency for BST8	51

3.34	Dielectric constant and loss tangent vs frequency for BST7	52
3.35	Dielectric constant and Loss tangent vs frequency for BST6	52
3.36	Dielectric constant and Loss tangent vs frequency for BST5	53
3.37	Dielectric constant and Loss tangent vs frequency for ST	53
3.38	The dielectric constant and loss tangent vs temperature for BT at 1KHz	54
3.39	The dielectric constant and loss tangent vs temperature for BT at 10KHz	55
3.40	The dielectric constant and loss tangent vs temperature for BT at 100KHz	55
3.41	The dielectric constant and Loss tangent vs temperature for BT at 1MHz	56
3.42	The current density vs temperature for BT4 at 1MHz	57
3.43	The dielectric constant and loss tangent vs temperature for BST9 at 1 KHz	58
3.44	The dielectric constant and loss tangent vs temperature for BST9 at 10 KHz	58
3.45	The dielectric constant and loss tangent vs temperature for BST9 at 100 KHz	59
3.46	The dielectric constant and loss tangent vs temperature for BST9 at 1 MHz	59
3.47	The current density vs temperature for BST9 at 1 KHz	60
3.48	The dielectric constant and loss tangent vs temperature for BST8 at 1 KHz	61
3.49	The dielectric constant and loss tangent vs temperature for BST8 at 10 KHz.	61
3.50	The dielectric constant and loss tangent vs temperature	62

	for BST8 at 100KHz	
3.51	The dielectric constant and loss tangent vs temperature for BST8 at 1MHz.	62
3.52	The current density vs temperature for BST8 at 1MHz.	63
3.53	The dielectric constant and loss tangent vs temperature for BST7 at 1KHz	64
3.54	The dielectric constant and loss tangent vs temperature for BST7 at 10KHz	64
3.55	The dielectric constant and loss tangent vs temperature for BST7 at 100KHz	65
3.56	The dielectric constant and loss tangent vs temperature for BST7 at 1MHz	65
3.57	The current density vs temperature for BST7 at 1 MHz	66
3.58	The dielectric constant and loss tangent vs temperature for BST6 at 1KHz	67
3.59	The dielectric constant and loss tangent vs temperature for BST6 at 10KHz	67
3.60	The dielectric constant and loss tangent vs temperature for BST6 at 100KHz	68
3.61	The dielectric constant and loss tangent vs temperature for BST6 at 1MHz	68
3.62	The current density vs temperature for BST6 at 1MHz	69
3.63	The dielectric constant and loss tangent vs temperature for BST5 at 1KHz	70
3.64	The dielectric constant and loss tangent vs temperature for BST5 at 10KHz	70
3.65	The dielectric constant and loss tangent vs temperature for BST5 at 100KHz	71
3.66	The dielectric constant and loss tangent vs temperature for BST5 at 1MHz	71

3.67	The current density vs temperature for BST5 at 1MHz	72
3.68	The dielectric constant and loss tangent vs temperature for ST at 1KHz	73
3.69	The dielectric constant and loss tangent vs temperature for ST at 10KHz	73
3.70	The dielectric constant and loss tangent vs temperature for ST at 100KHz	74
3.71	The dielectric constant and loss tangent vs temperature for ST at 1MHz	74
3.72	The current density vs temperature for ST at 1MHz	75
3.73	Curie temperature (K) vs substitution factor for BST samples at different frequencies .	76
3.74	Maximum value of dielectric constant (at T_c) vs substitution factor for BST samples at different frequencies	76
3.75A	TEM image for BST5	78
3.75B	SAED pattern for BST5	78
3.76A	TEM image for BST6	79
3.76B	SAED pattern for BST6	79
3.77A	TEM image for BST6	80
3.77B	SAED pattern for BST6	80
3.78A	TEM image for BST8	81
3.78B	SAED pattern for BST8	81
3.79	Theoretical and experimental Curie temperature vs substitution factor (x) for BST system	82

Contents

Item	Title	Page
Chapter One		
Introduction		
Literature Review		
	Introduction	1
1.1	General aspects	2
1.2	Perovskite structure	4
1.3	Methods for preparation Barium Strontium titanate powder.	7
1.3.1	Solid State Reaction (SSR)	7
1.3.2	Freeze drying method (FDM)	8
1.3.3	Hydrothermal method	8
1.3.4	Sol-Gel method	9
1.3.5	Preparation from complex precursor	9
1.3.6	Citrate process	9
1.4	Properties of BST system	10
1.5	Applications of BST materials	11
1.6	Literature review	13
Chapter Tow		
Materials and Methods		
2.1	Materials and Equipments	20
2.2	Experimental work	21
2.2.1	Preparation of Barium titanate	21

2.2.2	Preparation of Barium Strontium titanate system	25
2.2.3	Pressing process	26
2.2.4	Sintering process	27
2.3	Density estimation	27
2.4	X-ray diffraction (XRD)	28
2.5	Fourier Transform infrared spectroscopy (FTIR)	29
2.6	Dielectric measurements	29
2.6.1	Frequency measurement	29
2.6.2	Temperature measurement	30
2.7	Transmission electron microscope (TEM)	30
Chapter Three		
Results and Discussion		
3.1	The reasons for selecting Oxalate method in preparation	31
3.2	Density estimation	32
3.3	XRD analysis	34
3.3.1	XRD for BT	34
3.3.2	XRD for BST	38
3.4	FTIR spectroscopy	47
3.5	Dielectric measurements	50

3.5.1	Frequency measurements	50
3.5.2	Temperature measurements	54
3.6.	Transmission electron microscope	78
3.7	Conclusions	84
3.8	Recommendations	85

Abbreviations

Abbreviation	Complete version
BST	Barium Strontium titanate
BT	Barium titanate
ST	Strontium titanate
C	Capacitance
D	Loss tangent
ϵ_r	Dielectric constant
ρ	density
XRD	X-ray diffraction
TEM	Transmission Electron Microscope
SAED	Selected Area Electron Diffraction
FTIR	Fourier Transform infrared spectroscopy
θ	diffracted angle
d	interplane distance
λ	Wavelength
β	Full width at the half maximum FWHM
b	crystallite size
ψ	elastic strain
MFSFET	Metal Ferroelectric Semiconductor Field Effect Transistor
MLCCs	Multilayer ceramic capacitors
d₃₃	Piezoelectric coefficient
T_c	Curie temperature
x	substitution factor
κ	Electrochemical coupling
τ	Tolerance factor
ρ_t	Pyroelectric coefficient
K	Wave vector

Chapter One

Introduction

&

Literature Review

Introduction

Ferroelectrics are materials which exhibit spontaneous polarization over certain temperature range. They are special type of pyroelectrics; the later is belonged to piezoelectrics. All these classes belong to dielectric materials. [1]

Ferroelectric materials have special crystal structure; the most important is the perovskite structure. Perovskite structure is a crystal structure which has the formula ABX_3 . Its characters affected by (A, B) which represent cations and (X) the anionic element. Both cationic and anionic elements can be contributed in the characters depending on tolerance factor (x) [1].

There are different methods for preparing ferroelectrics powders. Preparation methods greatly affected the resulted materials. Among these methods are solid state reaction which considered as the conventional method for preparing a wide range of powders .The other is freeze-drying (Lyophilization) which is an expensive one, gives nanopowders. Hydrothermal method is a chemical method carried out in solution media, the main character of this method, its ability to give nanopowders with monosize particles. The other method is sol- gel which characterized by its ability to give more than one form or phase, these can be used for different subsequence preparations. [2, 3] However, the methods could be preformed directly or indirectly .The latter uses different precursors to make the method easier and facilitates getting pure products. [1]

Ferroelectrics have many applications in life. The most important field of application is in construction of electronic devices like capacitors, memory devices, transducers, photonic devices .etc. The other fields get benefits of ferroelectrics are communications, thermal photography (IR photography) . The other uses are of minor importance. [1]

Barium Strontium titanate (BST) is one of the most important ferroelectric materials. It has many different industrial applications. This material is a solid solution between Barium titanate and Strontium titanate, which has perovskite structure that has many phase transitions.

[1]

1.1 General aspects

The term ferroelectrics arose by analogy with ferromagnetics, mainly because they have similar characteristics under electric fields for ferroelectric phenomena and under magnetic fields for ferromagnetic phenomena as shown in Fig.1.1. The prefix ferro- derived from ferum, which means iron in Latin. The term is perfect for ferromagnetic, since all ferromagnetic phenomena are associated with the special type of spin arrangement of the iron atoms. But in ferroelectrics there are no iron atoms, so the prefix does not mean iron, rather, it implies the similarity in characteristics to ferromagnetic. Like ferromagnetic, ferroelectric exhibits a spontaneous electric polarization below the Curie temperature (T_c), a hysteresis loop, and an associated mechanical strain. However, ferroelectrics differ from ferromagnetic in their fundamental mechanisms and also in some of their applications [1].

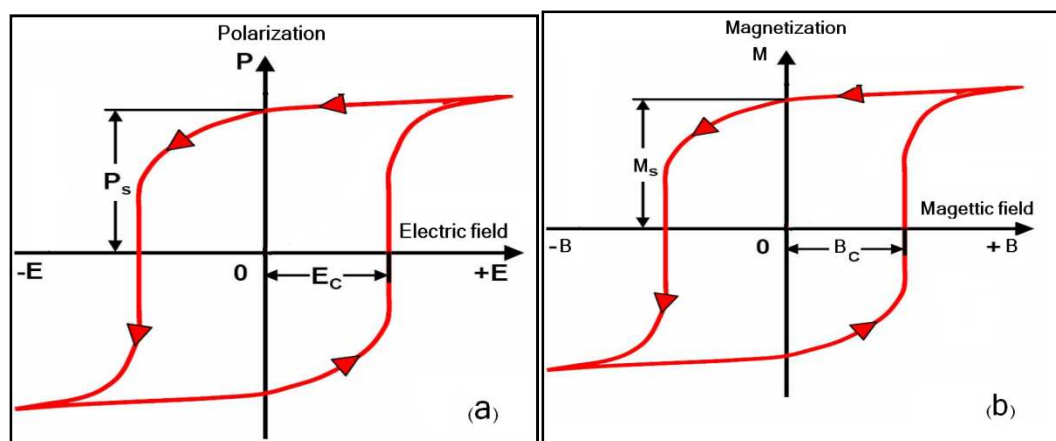


Fig.1.1: Hysteresis loop (a) Ferroelectric hysteresis loop (E-P) (b) Ferromagnetic hysteresis loop (B-M) [1].

Piezoelectrics are materials in which electricity can be generated by applying mechanical stress and vice versa for the mechanical stress can be produced by applying an electric field. This inter-convertible behavior was first discovered by Pierre and Jacques Curie in 1880 in certain crystals, such as quartz [1].

Pyroelectricity means heat-generated electricity. This effect is also convertible, and heat can be generated by electricity resulting from the change of the state of electric polarization. All these types of materials (Piezoelectric, Ferroelectric, and Pyroelectric) are belonged to dielectric materials. Ferroelectric materials are special type of pyroelectric materials, and the pyroelectric materials are special type of piezoelectric materials, all these types are belonged to dielectric materials as shown in Fig.1.2. [4]

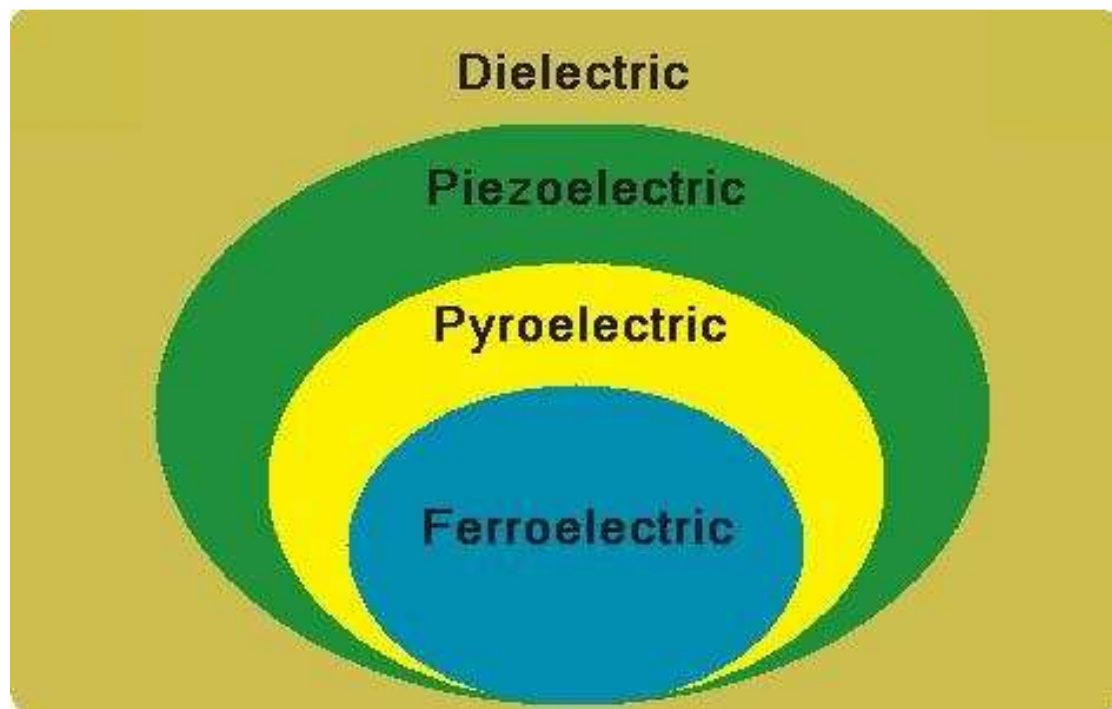


Fig.1.2: The relation between Ferroelectric, Pyroelectric, Piezoelectric and Dielectric materials [4].

Indeed the relation between these types of materials comes from the symmetry of crystal structure. Besides the classification of crystals into seven Bravais systems (14 lattices) according to their geometry, crystals are also classified into 32 point groups according to their symmetry with respect to points. Among the 32 point groups, 11 of them possess a center of symmetry, and the remaining 21 are noncentrosymmetric. Piezoelectric crystals are those without centre of symmetry. These classes of crystals exhibit electric polarity when they are subjected to stress and strain electric field. Among the 21 noncentrosymmetric point groups, 20 are piezoelectric crystal classes. Polarization is a vector quantity, and the existence of spontaneous polarization in a crystal creates a unique

direction or axis whereby the whole crystal is polarized. This polarized axis is not equivalent to any of the symmetric axes of the crystal and it is called the unique polar axis. It has been discovered that only ten out of the 20 piezoelectric crystal classes have unique polar axis and exhibit spontaneous polarization. These 10 polar crystal classes are often called the ferroelectric crystals. So it is obvious that all ferroelectric crystals are piezoelectrics, but the reverse is not true [1, 4]. The block diagram for such classification is shown in Fig 1.3.

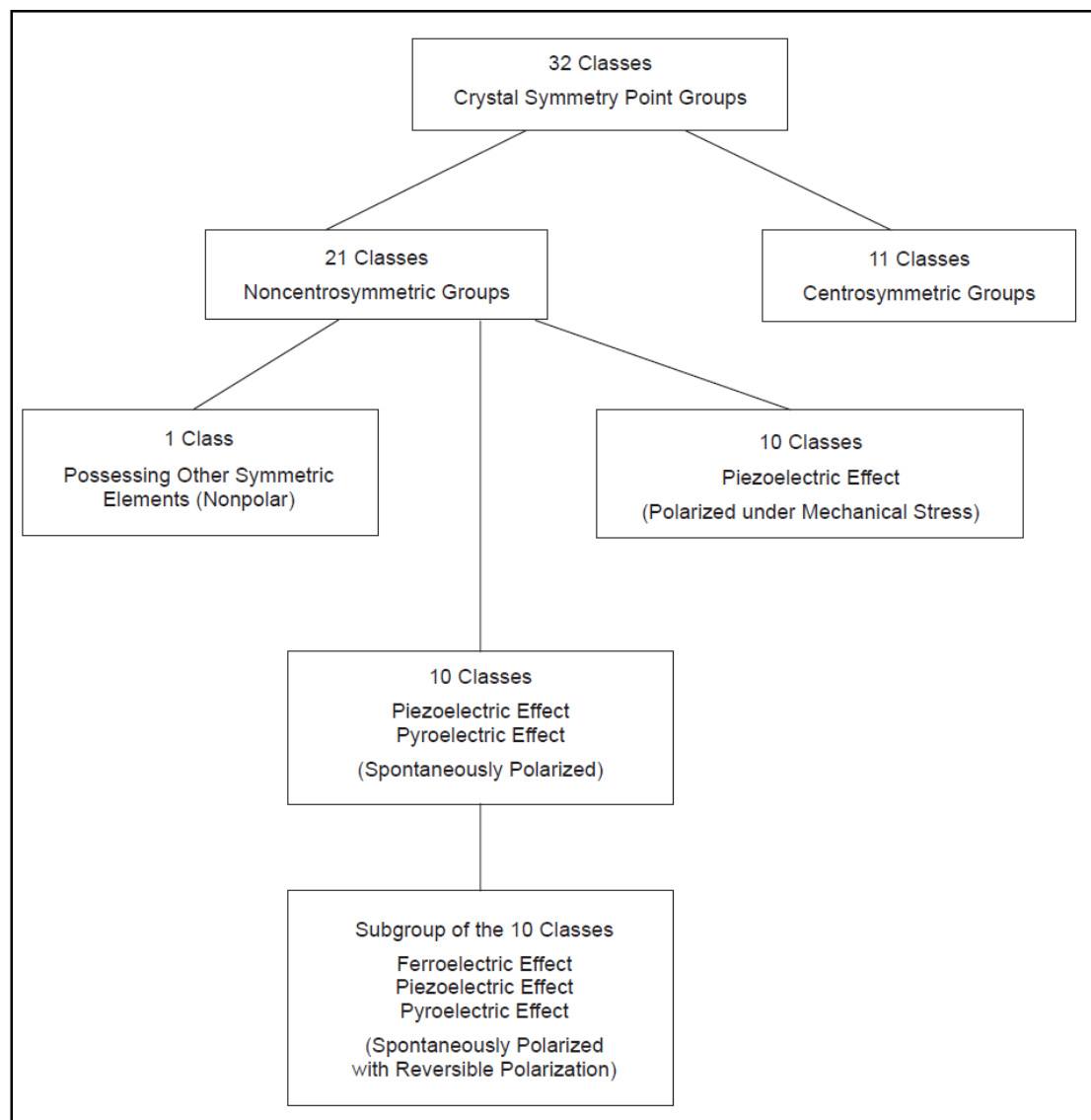


Fig.1.3: Classification of crystals showing the classes with piezoelectric, pyroelectric, and ferroelectric phenomenon [1].

1.2. Perovskite structure

Perovskite structure is one of the most popular structures which founds in ferroelectric materials. The general chemical formula for

perovskite compounds is ABX_3 as shown in Fig.1.4, where A and B are cations with different sizes, and X is an anion that bonds to both.

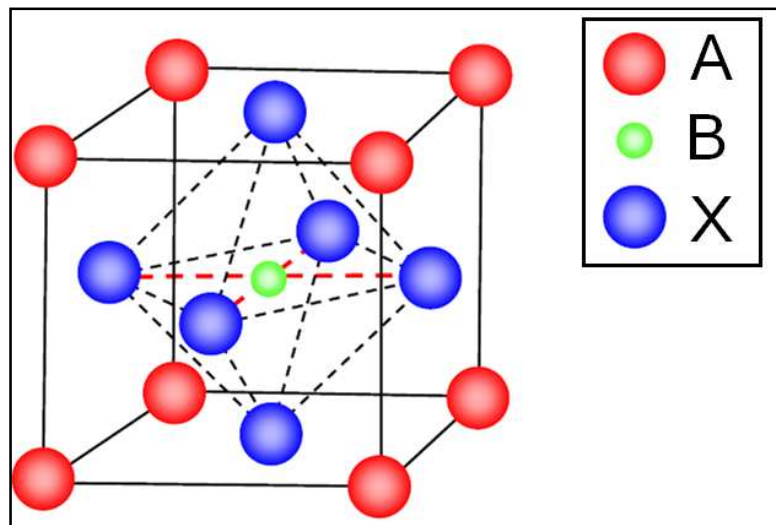


Fig.1.4 : Perovskite structure

The ideal cubic-symmetry structure has the B cation in 6-fold coordination surrounded by an octahedron of anions, and the A cation in 12-fold cuboctahedral coordination [5]. The relative ion size requirements for stability of the cubic structure are quite stringent, so slight distortion can produce several lower-symmetry distorted versions, in which the coordination numbers of A cations, B cations or both are reduced. The tolerance factor (τ) of perovskite can be estimated as in the following equation [1, 4].

$$\tau = \frac{(r_A + r_X)}{\sqrt{2}(r_B + r_X)}$$

Where (r) is the ionic radius.

There are three types of perovskite structure as shown in Table 1.1.

Table 1.1: Types of perovskite structure [1, 6].

Group	Type	Example
I	$A^{+1}B^{+5}(X^{-2})_3$	$\text{NaNbO}_3, \text{KTaO}_3, \text{NaTaO}_3$
II	$A^{+2}B^{+4}(X^{-2})_3$	$\text{BaTiO}_3, \text{PbTiO}_3, \text{SrTiO}_3$ $\text{BaZrO}_3, \text{PbZrO}_3, \text{SrZrO}_3$ $\text{CaTiO}_3,$
III	$A^{+3}B^{+3}(X^{-2})_3$	$\text{YCrO}_3, \text{LaAlO}_3, \text{YAlO}_3$

Perovskite materials exhibit many interesting properties from both the theoretical and the application point of view. Colossal magnetoresistance, ferroelectricity, superconductivity, charge ordering, spin dependent transport, high thermo-power and the interplay of structural, magnetic and transport properties are commonly observed features in this family of compounds. These compounds are used as sensors and catalyst electrodes in certain types of fuel cells and candidates for memory devices and spintronics applications [7].

The most important and popular ferroelectric material is Barium titanate (BaTiO_3), it belongs to perovskite structure. BaTiO_3 has a high dielectric constant, multiple phase transitions and has ferroelectric Curie temperature of (393K) as summarized in Fig.1.5 [1, 4, 6].

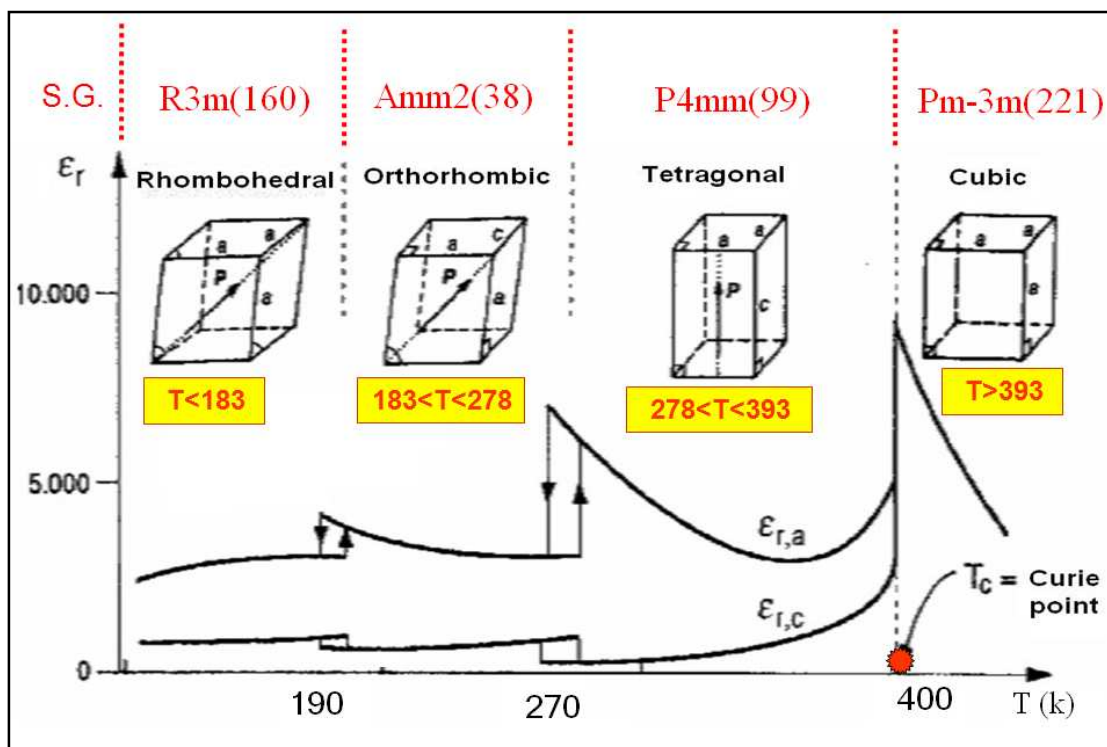


Fig.1.5: Phase transitions of BaTiO₃ (1, 4).

Strontium titanate (SrTiO₃) and Lead titanate (PbTiO₃) are ferroelectric materials with perovskite structure and have ferroelectric Curie temperature (23K) for SrTiO₃ and (763K) for PbTiO₃ [4, 8].

1.3 Methods for preparation Barium Strontium titanate powder.

There are many methods for preparing of Barium Strontium titanate. These methods may be direct or indirect by using some precursors and different catalysts

1.3.1 Solid State Reaction (SSR).

It is a conventional method which means a chemical reaction between solids. The solid-state reaction is the most widely used method for preparation of polycrystalline solids from a mixture of solids starting materials (SrCO₃, BaCO₃, and TiO₂). The mixture was then grounded (or ball milled) with suitable solvent (like ethanol) then calcinations, further grinding and calcinations until get powder [9].

The advantages for this method is cheap and simple. Disadvantages, it produces large particle size, impurity, heterogeneous (multiple phases), so it is difficult to get ultrafine powder [10].

1.3.2 Freeze drying method (FDM)

It is known as Lyophilization or Cryodesiccation , It is a dehydration process freeze-drying works by freezing the material(solution) and then reducing the surrounding pressure to allow the frozen water in the material to sublime directly from the solid phase to the gas phase.

The advantages of this method are formation small particle size (< 20nm). Disadvantages are expensive method, needs long time and power for completely drying. And agglomeration [11].

1.3.3 Hydrothermal method.

Hydrothermal synthesis (sol-precipitation) can be defined as a method for synthesis single crystals or polycrystalline depending on the solubility of minerals in hot water under high pressure. The crystal growth is performed in an apparatus consists of a steel pressure vessel called autoclave. Possible advantages of the hydrothermal method over other types of crystal growth include the ability to create crystalline phases which are unstable at melting point. The materials which have a high vapor pressure near their melting points can be grown by the hydrothermal method [12]. The method is also particularly suitable for the growth of large good-quality crystals when maintaining a good control over their composition and preparation of crystalline powder directly without calcinations, at low temperature .It gives nanopowder particle size <100nm , monosize and mono-dispersion (no agglomeration and no clustering) .

There are some factors these are affected on the resultants when starting with the same materials (BaCl_2 , TiCl_4 , NaOH), these factors include:

- Molarity of NaOH which is inversely proportional to particle size [2, 3].
- Ba/Ti ratio , this considered as another important factor , generally when the ratio < 1 no pure titanate obtained , i.e., there are different impurities ; when the ratio > 1 the product is pure Barium titanate , therefore , the improvement of production is proportional to the ratio .It has been found that the ratio 1.05 is the best [3, 13 - 16] .

- Concentration of Barium and Titanium , increasing the molarity up to 2M of Barium source of starting materials affects the resultant positively , i.e., the high concentrations give ultrafine powder under the condition of balanced ratio mentioned above [2 , 14, 16]

Disadvantages of the method expensive.

1.3.4 Sol-Gel method.

The sol-gel process is a wet-chemical technique widely used in the fields of materials science and ceramic engineering. Such methods are used primarily for fabrication of materials (typically metal oxides) starting from a colloidal solution (sol) that acts as the precursor for integrated network (or gel) of either discrete particles or network polymers. Typical precursors are metal alkoxides and metal salts chlorides, nitrates and acetates, which undergo various forms of hydrolysis and polycondensation reactions. Advantages of this method are cheap, gives nanopowder (particle size <40nm). Allowed to prepare thin film or powder. Disadvantages are production of high agglomeration or clustering which needs to be ground [17].

1.3.5. Preparation from complex precursor

Barium titanate oxalate tetrahydrate preparation leads to production of high-purity barium titanate. To obtain appropriate cation ratios, one must control the precipitation process carefully which indicates that the $Ba^{2+}/Ti^{4+}/C_2O_4^{2-}$ ratio should be 1.05:1:2.2 to obtain a product with Ba/Ti = 1.0. Because $BaCO_3$ is very stable and not easily decomposed, $BaTiO(C_2O_4)_2 \cdot 4H_2O$ is calcined in air [10 , 18] . Advantages seem to be very simple method, need short reaction time, produce fine powder.

1.3.6. Citrate process

In this method, tetrabutyl titanate, citric acid and ethylene glycol are mixed to give a solution and then barium carbonate, dissolved in formic acid and water, is added , then the pH is adjusted (by ammonia) to induce co-precipitation at Ba/Ti = 1:1 of $BaTi(C_6H_6O_7)_3 \cdot 4H_2O$. Under optimum conditions, one should consider the concentrations of citric acid and ethylene glycol, and the mole ratio of (Ba;Ti)/(citric acid , ethylene glycol). The precursor after heat treatment in air produces $BaTiO_3$, obtained via a solid-state reaction between intermediate species. It is noteworthy to notice that the Ba/Ti ratio in solution should be 1:1 at pH <

2.6, and 2:1 at $\text{pH} > 3.2$. This liquid mixing process has been used to synthesize over one hundred different oxides, including titanates, zirconates and niobates. The advantages of this process are: A good control of chemical stoichiometry, low processing temperatures (< 800 °C); and easy dopants addition. The disadvantages are the loss of large mass during calcinations, agglomeration and the method is very expensive [9].

1.4. Properties of Barium Strontium titanate

The main property is Curie temperature which is a parameter can be adjusted by changing the substitution factor (x) between Barium and Strontium [4, 19]. It is usually estimated after sintering process, i.e., at characterization stage.

Sintering process represents the final step in ceramic preparation, this carried out by heating the prepared materials to temperature before their melting points [20]. For example nanocrystalline ($\text{Ba}_{0.7}\text{Sr}_{0.3}\text{TiO}_3$) was prepared by sol-gel process with particle diameter 15 nm [17], so to get pellets with standard characters this should be subjected to sintering process at different temperatures, Somani *et al* [17] used sintering temperature (950, 1000, 1050 and 1100 °C) for 2h, they concluded that 1100 °C was the best. The sintering temperature could be higher as much as 1300-1350 °C as used by many authors [18, 21, 22, 23] when they prepared their pellets by solid-state reactions (SSR), however the sintering time could be varied also, Ioachim and others used sintering temperature 1200-1260 for 2h to for their samples prepared by SSR [24, 25].

Then, after sintering process, the Curie temperature should be estimated as being the most important parameter in ceramic materials. This property has been investigated thoroughly at theoretical and experimental aspects. Theoretical investigations gave rise the equation to calculate the Curie temperature using thermodynamic expectations as follows for the composition $\text{Ba}_x\text{Sr}_{1-x}\text{TiO}_3$:

$$T_c(^{\circ}\text{C}) = 371x - 253$$

Where x = substitution factor [4].

On the other hand, the theoretical aspects were phenomenological and thermodynamic theory [26].

The experimental investigations of Curie temperature are numerous. The temperatures estimated for BST system differ according to substitution factor (x). For $x=0$ (BT), the estimated temperatures were 140 and 132 °C [18, 27]. When $x=0.9$ (BST9) the temperature was 100 °C [21]. When $x=0.8$ (BST8), the temperature was 66 °C [22]. Whereas for $x=0.75$ (BST7.5) the temperature was 79 °C [23]. While for $x=0.65$ (BST6.5) the temperature was 19 °C [24, 25], but when $x=0.6$ (BST6) the temperatures were 1.4, 5 and 7 °C [25, 27, 28]. And when $x=0.5$ (BST5) the temperature was -59 °C [25].

1.5. Applications of BST materials

BST materials have a wide range of applications:

1- BST is used in MFSFET (Metal Ferroelectric Semiconductor Field Effect Transistor) [29], as insulator instead of SiO_2 in MOSFET because BST has a high dielectric constant and very small dielectric loss (loss tangent) which leads to reduce the leakage current (Fig 1.6).

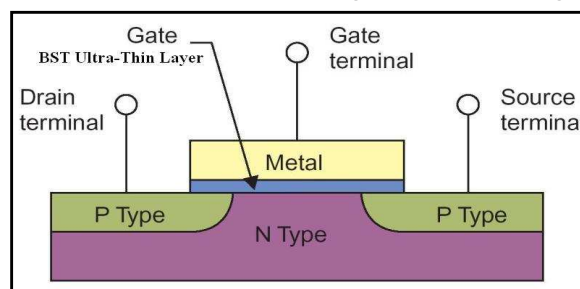


Fig.1.6: MFSFET (Metal Ferroelectric Semiconductor Field Effect Transistor) [29]

2- Tunable circuits

Since the capacitance depends on the voltage $C \propto 1/\sqrt{V}$ [30] as shown in Fig.1.7. So BST system used in varactor (variable-capacitor diode) which is used in tunable circuit as shown in Fig.1.8

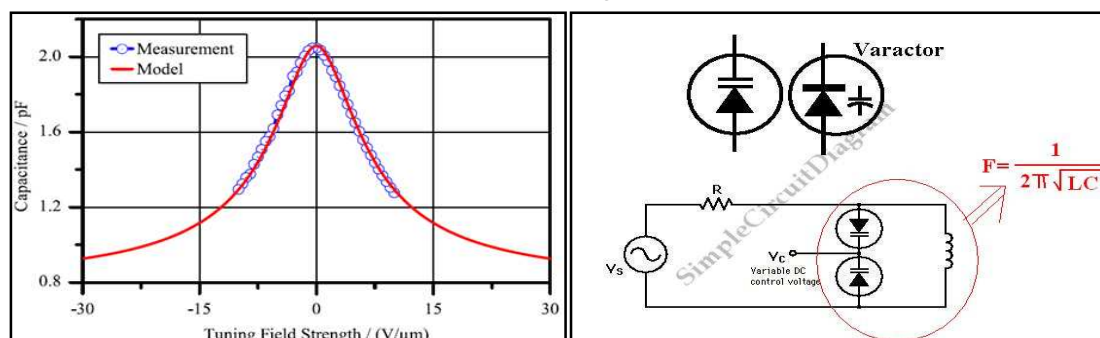


Fig.1.7: Variation of capacitance vs electric field for BST [30].

Fig.1.8: Varactor as tunable LC circuit [31].

3- Microwave BST materials are widely used in microwave applications because BST materials have no reflection at certain frequency as shown in Fig.1.9.

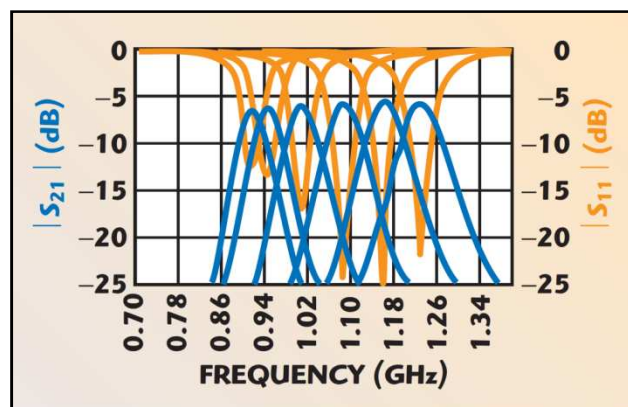


Fig.1.9: Reflectivity (S_{11}) and Transmittance (S_{21}) vs frequency of BST [32].

So that the applications of BST system in microwave can be divided into:

A –Dielectric waveguides (Fig.1.10)

B –Phase shifter (Fig 1 .11) [33].

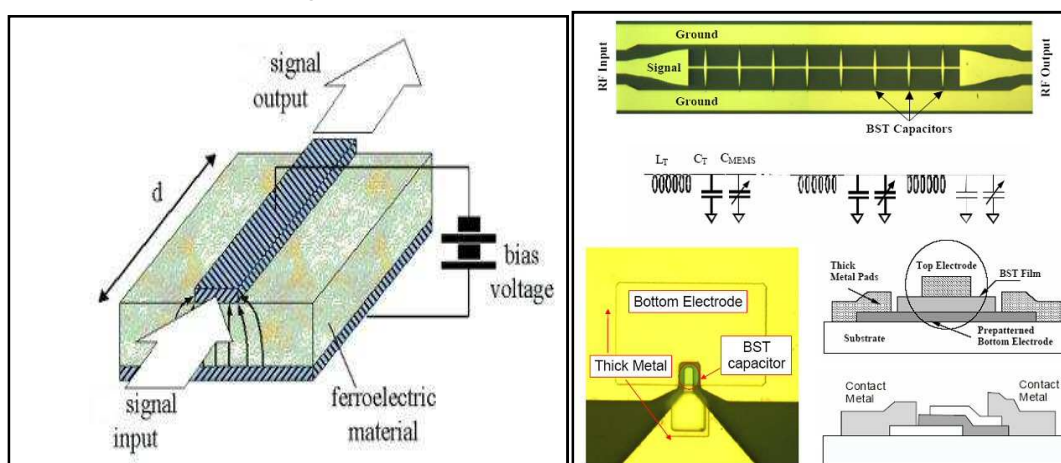


Fig.1.10: Micro-stripe waveguide [32].

Fig.1.11: The Phase shifter [33].

4 –Multilayer ceramic capacitors (MLCCs) , BT is widely used in MLCCs (Fig.1.12) because of its high dielectric constant , while BST has high dielectric constant but lower than the BT , so BST is used in MLCCs but for special applications as in high gain and high directive antenna [34] (Fig.1.13).

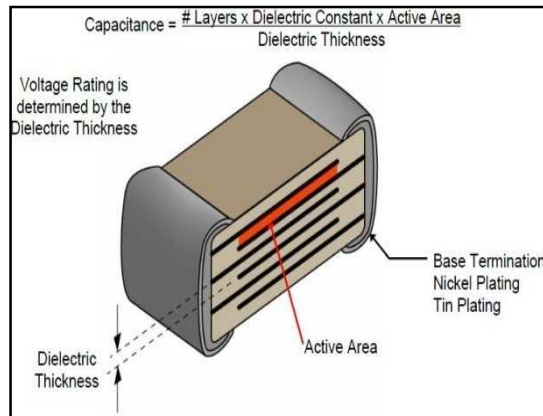


Fig.1.12: Multilayer Ceramic Capacitor (MLCC) [35].

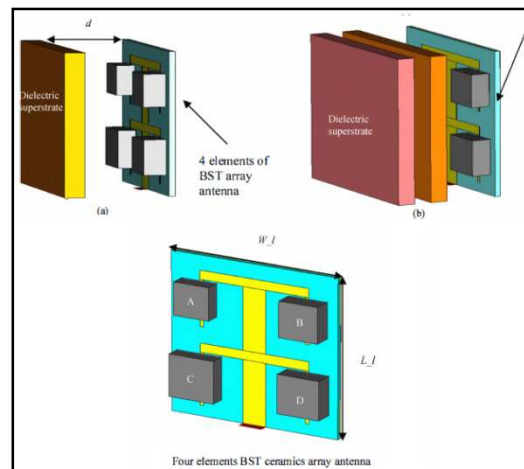


Fig.1.13: High gain and high directive antenna (4 element BST ceramic array antenna)

1.6 Literature Review

Kim *et al.*, (1996) [9] prepared barium tetrahydroxide oxalate tetrahydrate as precursor for BaTiO_3 by using barium chloride, titanium tetrachloride, diethyl oxalate at 80°C and calcined at 850°C . The result is BaTiO_3 with particle size of 200nm.

Kao, *et al.*, (1999). [38] prepared BaTiO_3 , $\text{Ba}_{0.5}\text{Sr}_{0.5}\text{TiO}_3$ and SrTiO_3 by Citrate method (using citric acid as catalyst) using the starting materials $\text{BaCl}_2 \cdot \text{H}_2\text{O}$, $\text{SrCl}_2 \cdot 6\text{H}_2\text{O}$, TiCl_4 and citric acid as starting materials and calcined at 1000°C for 24hr, Then by solid state reaction using BaCO_3 , SrCO_3 and TiO_2 as starting materials and calcined at 1100°C for 24hr. the resulted powders were studied using different techniques FTIR, DSC, TGA and XRD. All the samples pressed at 110MPa and sintered at 1100, 1200, 1300 and 1450°C , for 4 hr in air. The resulted powder from solid state reaction have a particle size of $0.5 - 1 \mu\text{m}$. the resulted precursor from citrate method dried by freeze drying, vacuum

drying air drying and the resulted powder from freeze drying have low agglomeration than the powder from vacuum and air drying . The bulk density is 3.2 g/cm^3 for BaTiO_3 , $\text{Ba}_{0.5}\text{Sr}_{0.5}\text{TiO}_3$ and SrTiO_3 (at 1200°C sintering) and 4g/cm^3 for the same samples (at 1300°C and 1450°C sintering).

Xu, *et al.*, (2002). [2] prepared Tetragonal barium titanate powder with an average particle size of 80 nm by a hydrothermal process at 240°C using TiCl_4 , BaCl_2 and NaOH where the $[\text{Ti}] = 0.15, 0.30, 0.65 \text{ mol/l}$, molar ratio of $[\text{Ba}]/[\text{Ti}] = 1.6$ and $[\text{NaOH}] = 0.25$ to 2.0 mol/l . and the reaction time from 0 to 24 h .They conclude that the tetragonal BaTiO_3 powder with average particle size 80 nm can be synthesized by hydrothermal reaction at 240°C for only 12 h. Increasing the NaOH excess concentration and decreasing the initial titanium tetrachloride concentration are benefit for preparation of tetragonal BaTiO_3 powder; and increasing the reaction temperature and time also obtain same result . And there may be a relationship between BaTiO_3 phase and particle size, and the particle size of the cubic BaTiO_3 powder is finer than the tetragonal BaTiO_3 powder.

Khollam *et al.*, (2003) [37] have prepared $[\text{Ba}_{0.65}\text{Sr}_{0.25}\text{TiO}(\text{C}_2\text{O}_4)_2 \cdot 4\text{H}_2\text{O}]$ powder by using barium hydroxide, strontium nitrate, Oxalic acid and isopropanol and obtain $\text{Ba}_{0.65}\text{Sr}_{0.25}\text{TiO}_3$ at $750^\circ\text{C} / 2 \text{ hr}$. They study the synthesis conditions for producing BST using DTA/TGA, XRD, IR,

Jhung *et al.*, (2004). [13] study Effects of reaction conditions in microwave synthesis of nanocrystalline barium titanate . They study the effect of synthesis parameters such as $\text{H}_2\text{O}/\text{Ti}$, Ba/Ti and OH/Ti ratios and heating methods (microwave irradiation and hydrothermal heating). They synthesized nano-crystalline BaTiO_3 (less than 30 nm) with microwave irradiation of reaction mixture prepared from chloride precursors. They conclude that the crystal size decreases with the increase of hydroxide and barium concentration, whereas the size decreases with the decrease of the water concentration. Synthesis of BaTiO_3 with microwave irradiation has the advantages of fast crystallization and decreased crystal size

Hwu, *et al.*, (2005). [10] prepared BaTiO_3 from TiCl_4 , BaCl_2 and $\text{H}_2\text{C}_2\text{O}_4$ with mole ratio of $\text{Ba/Ti/C}_2\text{O}_4 = 1.05/1/2.2$ with different reaction temperature ($5^\circ\text{C} - 70^\circ\text{C}$) and studying the effect of the reaction temperature on the morphology and particle size of $\text{BaTiO}(\text{C}_2\text{O}_4)_2 \cdot 4\text{H}_2\text{O}$ TGA. And studying the effect of calcination temperature on $\text{BaTiO}(\text{C}_2\text{O}_4)_2 \cdot 4\text{H}_2\text{O}$. They obtain BaTiO_3 at the calcination temperature $> 600^\circ\text{C}$. The sizes of the particles of BaTiO_3 increased with the increasing of calcination temperature

Guangneng *et al.*, (2005). [36] synthesized cubic phase ($a = 4.035 \text{ \AA}$) barium titanate nanoparticles with an average diameter of about 20nm via a one-step sol-precipitation route in water bath (about 80°C) for 5 hr without surfactant and any post-treatment. The as-synthesized BaTiO_3 nanoparticles exhibit the nature of single-crystal and non-agglomerate.

Mantese *et al.*, (2005). [4] discuss the effect of (x) in $\text{Ba}_x\text{Sr}_{1-x}\text{TiO}_3$ by thermodynamics and summarized the thermodynamic and physical properties of BaTiO_3 , SrTiO_3 and $\text{Ba}_x\text{Sr}_{1-x}\text{TiO}_3$ in a table

Table 1.2: Thermodynamic and physical properties of $\text{Ba}_x\text{Sr}_{1-x}\text{TiO}_3$ [4].

	BaTiO_3	SrTiO_3	$\text{Ba}_x\text{Sr}_{1-x}\text{TiO}_3$
T_0 ($^\circ\text{C}$)	118	-253	$371x-253$
C ($^\circ\text{C}$)	1.7×10^5	0.8×10^5	$(9x+8) \times 10^4$
α (m/F)	$6.65 \times 10^5(T-118)$	$1.41 \times 10^6(T+253)$	$1.12 \times 10^7(T-71x+253)/(9x+8)$
β ($\text{m}^5/\text{C}^2\text{F}$)	3.56×10^9	8.4×10^9	$(-11.96x+8.4) \times 10^9$
γ ($\text{m}^9/\text{C}^4\text{F}$)	2.7×10^{11}	-	2.7×10^{11}
C_{11} (N/m^2)	1.76×10^{11}	3.48×10^{11}	$(3.48-1.72x) \times 10^{11}$
C_{12} (N/m^2)	8.46×10^{10}	1.00×10^{11}	$(1-0.154x) \times 10^{11}$
Q_{12} (m^4/C^2)	-0.043	-	-0.034

So they expect that the Curie temperature for BST is x dependant ($T_c(^\circ\text{C}) = 371x-253$) by thermodynamic

Yan *et al.*, (2005). [15] prepared BaTiO_3 by hydrothermal method using the starting materials BaCl_2 , TiCl_4 , NaOH , thus by different Ba/Ti ratio (1.07 – 1.4) the best result for preparing BaTiO_3 was mono-

dispersive and spherical particle of size 70–90 nm under the conditions (Ba/Ti = 1.05 , at 100 °C) by re-crystallization

Guo *et al.*, (2006). [3] obtained BaTiO₃ powder is monosized distribution equi-axed particles of size 150 nm can be obtained at ratio 1.6 of [Ba] / [Ti] in precursor in 2.0 M [NaOH] solution at 80 °C in microwave oven for 30 min. The results showed that with the increase of the reaction time, the grain size of BaTiO₃ powder increases

Xu *et al.*, (2006). [14] obtained Monosized spherical particles of BaTiO₃ by a sonochemical method in a strong alkaline environment using BaCl₂ , TiCl₄ and NaOH . They briefly investigated that the effects of reactant concentrations and molar ratio R=[Ba]/[Ti] (0.9 to 1.5) on the precipitation of BaTiO₃ particles. The particles have a monosized spherical morphology and the particle size ranges from submicron (600–800 nm) to nanometer (60–70 nm) by increasing the reactant concentration (from 0.072 mol/l to 0.72 mol/l). The molar ratio R must be ≥ 1 because (Ba/Ti<1) would cause a contamination of BaTiO₃ and the increasing of R lead to decreases the particle size .

Zhigang *et al.*, (2006). [16] prepared BaTiO₃ nanoparticles via the reaction of BaCl₂, TiCl₄ and NaOH in aqueous solution , and they study the effect of the reaction temperature , [Ba /Ti] ratio (R) and BaCl₂ concentration on the preparation of BaTiO₃ and the particle size . They conclude that the increasing of the reaction temperature lead to decrease the particle size , the [Ba/Ti] ratio (R) must be ≥ 1 , the BaCl₂ concentration must be (0.1 – 2) M and the higher concentration is perfect because lead to higher nucleation rate , nucleation a larger number of smaller nucleus which is better for precipitation of particle with much smaller size and uniform size distribution .

Simon-Seveyrat, *et al.*, (2007). [18] studied the formation of barium titanate powder by solid-state reaction and oxalate co-precipitation route with different calcination temperature (25 °C to 1100 °C) and sintering temperature 1350 °C , studying dielectric and piezoelectric properties of the ceramics prepared via the two processes and concludes that BaTiO₃ perovskite phase obtained by the oxalate co-precipitation chemical way is formed at approximately 700 °C instead of 900 °C for the solid-state reaction and the room temperature dielectric

constant is 2050 for solid state reaction route and 2200 for oxalate route and $\tan\delta$ is 1.8 for solid state reaction route and 1.4 for oxalate route. Curie point ($^{\circ}\text{C}$) is 140°C for the solid state reaction and 139°C for Oxalate route

Ioachim *et al.*, (2007). [24] prepared BST ceramic ($\text{Ba}_{1-x}\text{Sr}_x\text{TiO}_3$) with $x=0.35$ and 0.60 by conventional solid state reaction, then doped the BST samples with (Mn, Mg) and sintering at ($1200^{\circ}\text{C} - 1260^{\circ}\text{C}$ for 2h). They study the dielectric measurement at 1 kHz for the doped and pure samples. They obtain the Curie temperature (for pure BST sintering at $1260^{\circ}\text{C} / 2\text{h}$) is 19°C for $x=0.35$ and -93°C for $x=0.6$. While doped with 1.0 wt% MgO and 1 wt% MnO_2 , the BST samples exhibit a more diffuse ferroelectric transition than the undoped samples. Moreover, the doped samples present a smaller Curie temperature than that for the undoped samples

Somani *et al.*, (2007). [17] synthesized nanocrystalline BST ($\text{Ba}_{0.7}\text{Sr}_{0.3}\text{TiO}_3$) powder with average particle-diameter of 15 nm through sol-gel process using barium acetate, strontium acetate and titanium isopropoxide as the precursors, acetic acid as a solvent and 2-methoxy ethanol as stabilizer, calcination of gel at ($400^{\circ}\text{C} - 700^{\circ}\text{C}$ for 2h) and sintering ($950, 1000, 1050, 1100^{\circ}\text{C}$) for 2 h.

Berbecaru *et al.*, (2008). [25] Prepared ceramics ($\text{Ba}_{1-x}\text{Sr}_x$) TiO_3 , (BST) with $x=0.25, 0.35, 0.40, 0.50, 0.60, 0.75$ and 0.90 by conventional solid state reaction calcined at $1150^{\circ}\text{C}/2$ hr. and mixed with MgO and MnO_2 and sintered at 1200 to 1260°C . / 2hr and the obtained Curie temperature is -59°C for $x=0.5$, 1.4°C for $x=0.4$ and 19°C for $x=0.35$

Kajtoch *et al.*, (2007). [21] Prepared $\text{Ba}_{0.9}\text{Sr}_{0.1}\text{TiO}_3$ by conventional solid state reaction at 1330°C and obtained the Curie temperature 100°C for $\text{Ba}_{0.9}\text{Sr}_{0.1}\text{TiO}_3$

Gabryoe. (2008). [27] prepared ($\text{Ba}_{0.6}\text{Sr}_{0.4}$) TiO_3 and ($\text{Ba}_{0.6}\text{Sr}_{0.4}$) $\text{Ti}_{0.8}\text{O}_3$ samples by solid state reaction at 1340°C . and studying the dielectric measurement at different frequencies ($20\text{ Hz} - 5\text{MHz}$) and obtained Curie temperature 7°C for ($\text{Ba}_{0.6}\text{Sr}_{0.4}$) TiO_3 and 132°C for BaTiO_3 (cooling cycle).

Shirokov *et al.*, (2008). [26] developed thermodynamic method of construction of the potential in the framework of the phenomenological and thermodynamic theory for description of the concentration phase diagram of non-ordering solid solutions. They developed concentration ($x - T$) phase diagram of $Ba_xSr_{1-x}TiO_3$ solid solution as shown in the following figure.

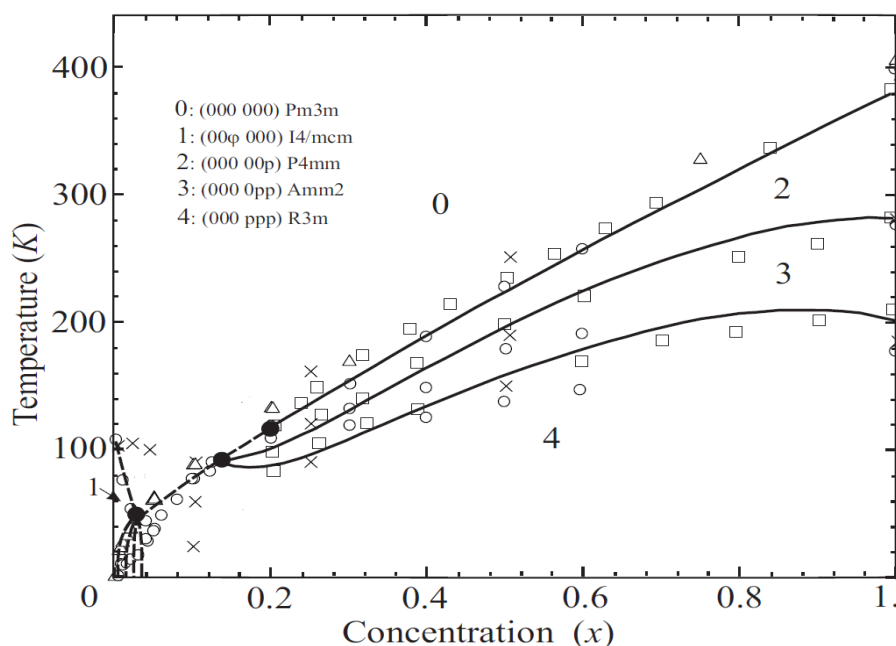


Fig.1.14: ($x - T$) phase diagram of $Ba_xSr_{1-x}TiO_3$ solid solution [26]

Kajtoch *et al.*, (2009). [22] Prepared $Ba_{0.8}Sr_{0.2}TiO_3$ by conventional solid state reaction at $1350\text{ }^\circ\text{C}$ and study the dielectric measurement, they obtained the curie temperature $66\text{ }^\circ\text{C}$ for $Ba_{0.8}Sr_{0.2}TiO_3$

Wang *et al.*, (2010). [23]. prepared BST ($Ba_{0.75}Sr_{0.25}TiO_3$) by conventional solid-state reaction and sintering by sol-assistant sintering at ($1300\text{ }^\circ\text{C}$ to $1320\text{ }^\circ\text{C}$ / 2h). The obtained Curie temperature is $79\text{ }^\circ\text{C}$ for different sintering temperature and time.

Wee *et al.*, (2010). [34] have Designed for elements BST ceramic array antenna and they study the Gain and directivity for this antenna, they obtain high gain of over 6.94 dBi and directivity of 7.53 dBi for the case of double layer.

Nedelcu *et al.*, (2011). [28] synthesized $Ba_{0.6}Sr_{0.4}TiO_3$ by solid state reaction (calcination at $1150\text{ }^\circ\text{C}$ for 2 h) then sintered at $1210\text{--}1450\text{ }^\circ\text{C}$ range and the Curie temperature is $5\text{ }^\circ\text{C}$ for different frequency ($120\text{ Hz} - 5\text{ MHz}$)

The aims of this work are:

1. Preparation of Barium titanate (BaTiO_3) using different methods. And specified the most applicable method through its parameter of preparation.
2. Choosing the best method produces an ultra fine powder to be used in preparation of Barium Strontium Titanate ($\text{Ba}_x\text{Sr}_{1-x}\text{TiO}_3$) with different substitutions , where x is the substitutions factor ($x= 1.0, 0.9 \dots\dots 0.5$)
3. Studying the structural properties (crystal structure, space groups lattice, bond energy and particle size) of the resultant Barium strontium titanate using special software and databases.
4. Studying the effect of substitutions factor (x) on some physical properties of BST system such as Curie temperature, dielectric constant, density, crystal structure, lattice parameters, space group, particle size, bond energy

Chapter Two
Materials & Methods

Materials and Methods

2.1 Materials and Equipments

The following items were used in this study

Table 2.1: Materials, Equipment and software

Materials			
Item	Formula	Source , Origin	Description
Titanium tetrachloride	TiCl ₄	BDH ,UK	Density =1.726 (g/cm ³)
Barium chloride	BaCl ₂ .2H ₂ O	Thomas Baker, India	
Strontium chloride	SrCl ₂ .6H ₂ O	Merck ,USA	
Oxalic acid	(COOH) ₂ .2H ₂ O	Merck , USA	
Sodium hydroxide	NaOH	Fluka , USA	
Absolute ethanol	CH ₃ CH ₂ OH	BDH , UK	99%
Filter papers		Whatman , UK	#42
Equipments			
Item	Source , Origin	Description	
Sensitive balance	STATON 462AL	4-digits	
Water bath	DT Hetotherm , Germany	Heating and cooling	
XRD diffractometer	XRD7000 , SHEMADZU , Japan	$\lambda = 1.5406 \text{ \AA}$, Ni filter Voltage = 40 KV Current = 100 mA	
Transmission Electron Microscope		JOEL	
FTIR	FTIR 8000 Series SHEMADZU , Japan	400 cm ⁻¹ – 4000 cm ⁻¹	
Programmable LCR meter	TEGAM 3550 , USA	42 Hz - 5 MHz 0.01 V - 5 V 0.1 mA - 100 mA	
Programmable LCR meter	HIOKI 3532-50 , Japan	42 Hz - 5 MHz 0.01 V - 5 V 0.1 mA - 100 mA	
Electrical press	Carver auto series , USA	15 ton	
Tube furnace	Carbolite Shevold , UK	1000 °C	
Vacuum tube furnace	SGL-1600 , China	1600 °C	
Oven	Hearus , German	250 °C	
Software			
Xpowder	v.2004 with ICDD PDF2 database	For phase identification , Lattice parameter refinement and crystallite size calculations	
Full prof suit package	V.2011	For Lattice parameter refinement	
Crystal impact package	Crystal impact match v1.11 And crystal impact diamond v.3.2g	Lattice parameter refinement and space group estimation	
Refine95		Unit cell refinement	
Labview	LabView8.5	For programming the LCR meter	

2.2 Experimental work

Different chemical techniques have been used to prepare the $\text{Ba}_x\text{Sr}_{1-x}\text{TiO}_3$ starting from $x=1$ (BaTiO_3) and ending with $x=0$ (SrTiO_3). Titanium tetrachloride (TiCl_4) was used as a source material for Titanium. Barium chloride ($\text{BaCl}_2 \cdot 2\text{H}_2\text{O}$) was the source material for Barium whereas Strontium chloride ($\text{SrCl}_2 \cdot 6\text{H}_2\text{O}$) was Strontium source. Sodium hydroxide (NaOH) and Oxalic acid ($(\text{COOH})_2 \cdot 2\text{H}_2\text{O}$) were used as catalysts. The purpose of using different chemical process rather than freeze drying method (FDM) is the efficient but it is not compatible with our situation in the laboratory related to discontinuity in electric power in the college and this method need a continuous electric power at least (48hr) for operating freeze drying apparatus. This was the reason for looking for a simple chemical process producing a fine powder of BaTiO_3

2.2.1 Preparation of Barium titanate

A. Sodium hydroxide–ethanol method [36]: This method was started by adding 10 ml of TiCl_4 to 20 ml of absolute ethanol to get yellow gummy solution. Then 10 ml of distilled water was added to the gummy solution gradually to get transparent solution. The resultant transparent solution was mixed with 70 ml of 0.385 M solution of BaCl_2 . Later 220ml of 12 M NaOH was added to the mixture as shown in block diagram in Fig.2.1. The reaction was carried out in water bath at 80°C for 5hr. The resultant precipitate was washed and filtered (5 times), dried at 90°C for 12 hr. These periods are short enough to done in the laboratory without any failure in the preparation of the composition. Finally, calcination process was carried out using carbolite furnace at 850°C for 5 hr to get BaTiO_3 ultra fine powder.

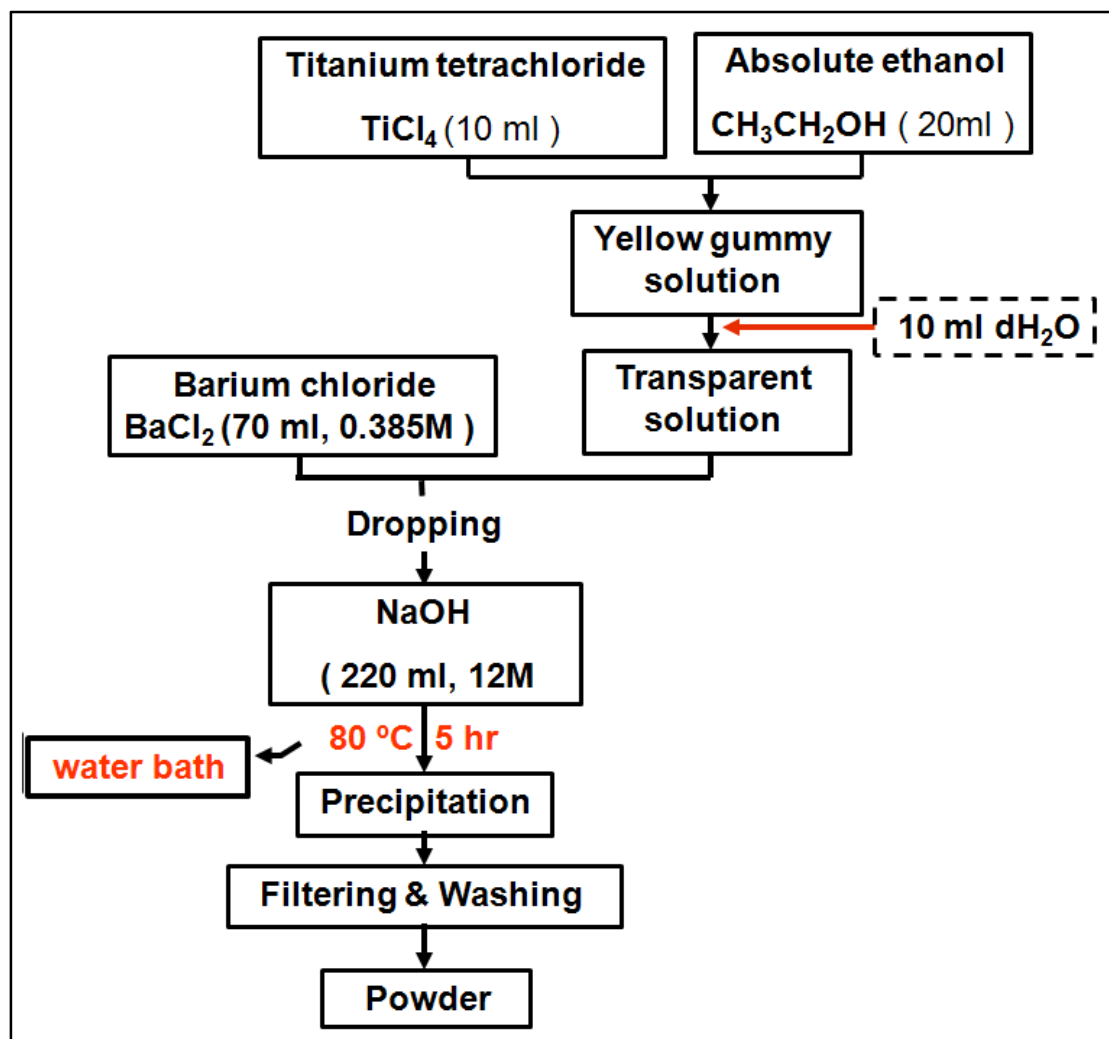


Fig. 2.1: Block diagram for Sodium hydroxide-ethanol method.

B. Oxalate method [10, 18, 37] : This method was carried out by mixing 50 ml of 1M solution of TiCl_4 with 50 ml of 1.05 M solution of Barium chloride. The mixture was added gradually to 50 ml of 2.2 M solution of Oxalic acid. The reaction was carried out in water bath at 80°C for 15min. The resultant powder " Barium titanyl oxalate tetrahydrate [$\text{BaTiO}(\text{COO})_2 \cdot 4\text{H}_2\text{O}$]" separated by filtration, washed and dried at 90°C for 12hr. These periods are suitable to done in our laboratory. Calcination process was performed on two different stages, the first one by using carbolite furnace at $T=600^\circ\text{C}$ for 5hr, the second stage was at $T=850^\circ\text{C}$ for 5 hr to get BaTiO_3 powder. The block diagram for this method is shown in Fig. 2.2.

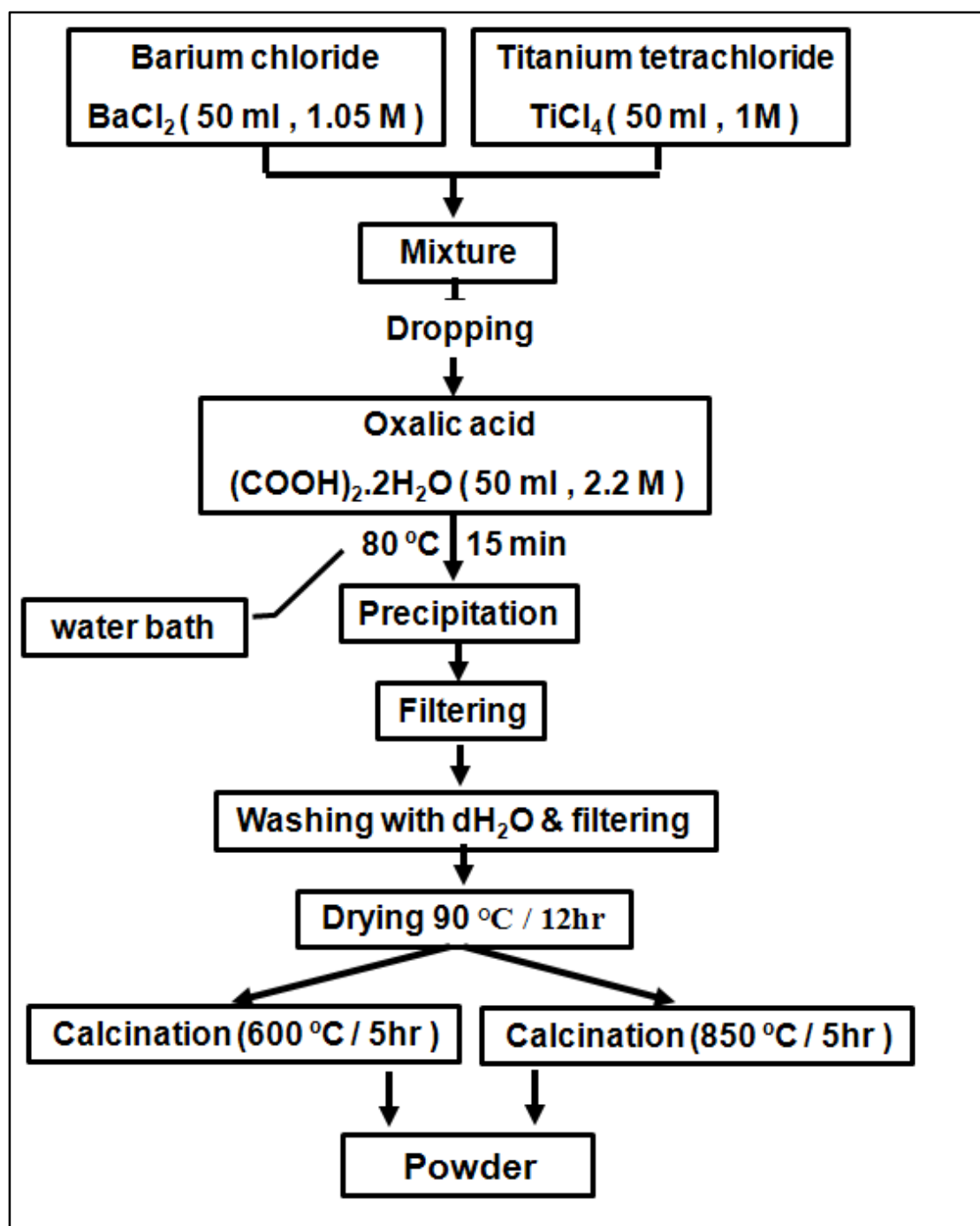


Fig. 2.2: Block Diagram for the Oxalate method .

C. Sodium hydroxide method [2, 14, 16]: This method was done by mixing 50 ml of 1 M solution TiCl_4 with 50 ml of 1.05 M Barium chloride. The mixture was added to 50 ml of 7 M NaOH gradually. The reaction was carried out in water bath at 80 °C for 5hr, the resultant precipitate was washed five times and dried at 90°C for 12 hr. Calcination process was done in carbolite furnace at $T=850^\circ\text{C}$ for 5hr.

Producing the fine powder of BaTiO_3 . The block diagram for this method is shown in Fig.2.3.

Regarding to these three simple chemical methods and depends on XRD analysis for the resulted powders. The results showed that the Oxalate method is the best one according to the power management, the output data of the crystallite size and phase of the produced BaTiO_3 .

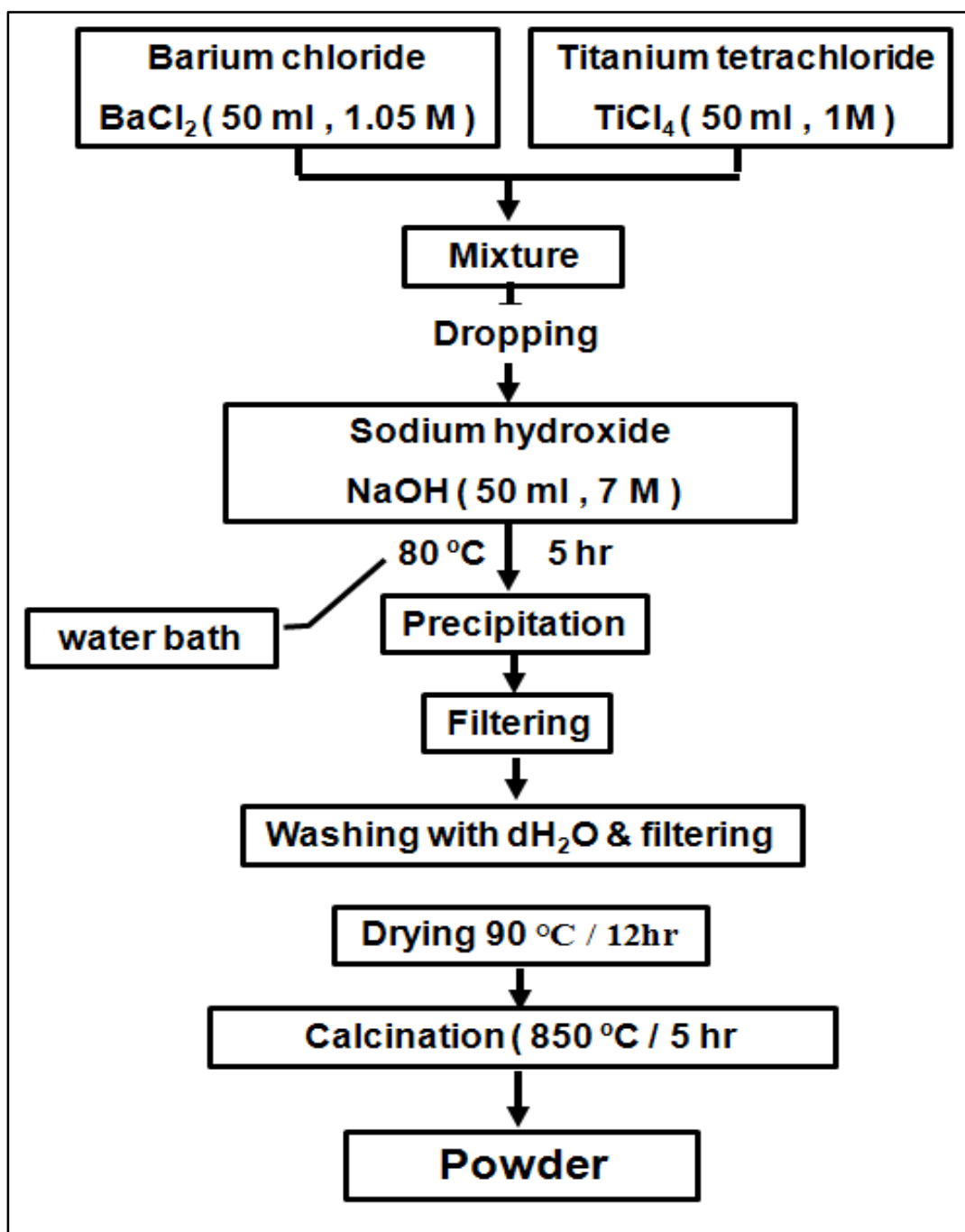
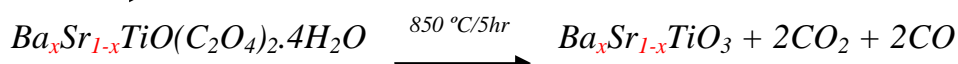
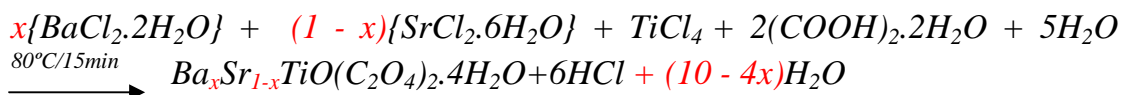


Fig. 2.3: Block Diagram for Sodium hydroxide method.

2.2.2 Preparation of Barium Strontium titanate system.

After the comparable between the three methods for preparation and select the best one to complete the requirement for this project .This has been done by using the Oxalate method to prepare $Ba_xSr_{1-x}TiO_3$ powders with $x= 1 , 0.9 , 0.8 , 0.7 , 0.6 , 0.5 , 0$. It was prepared by using the following chemical equations. Table 2.2 shows the conditions for prepare BST



The steps are shown in block diagram in Fig.2.4

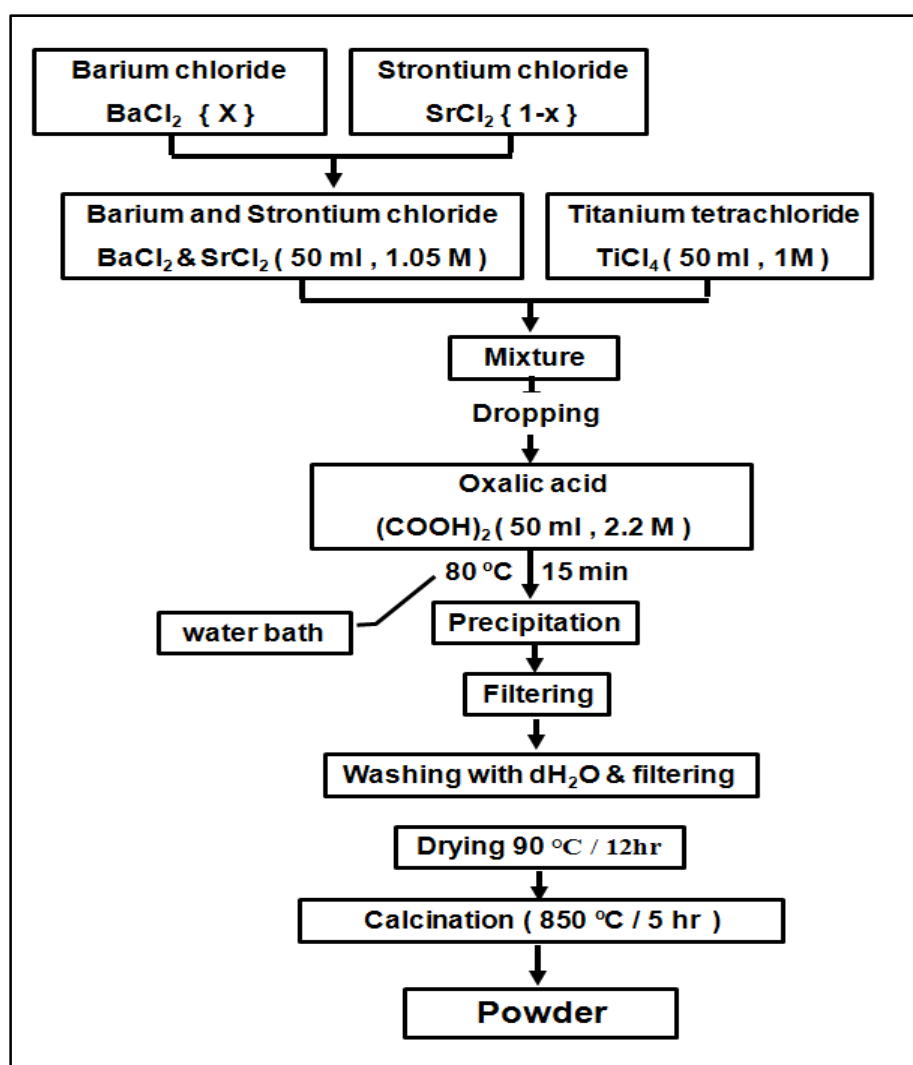


Fig. 2.4: Block diagram for preparing Barium Strontium titanate (BST)

Table 2.2 : Conditions and Molarity (M) of starting materials for preparing BST powders

Sample	Formula	BaCl ₂ (M)	SrCl ₂ (M)	BaCl ₂ & SrCl ₂ (M)	TiCl ₄ (M)	Oxalic acid (M)	Precursor
BT	BaTiO ₃	1.05	0	1.05	1	2.2	BaTiO(COO) ₂ .4H ₂ O
BST9	Ba _{0.9} Sr _{0.1} TiO ₃	0.945	0.105	1.05	1	2.2	Ba _{0.9} Sr _{0.1} TiO(COO) ₂ .4H ₂ O
BST8	Ba _{0.8} Sr _{0.2} TiO ₃	0.84	0.21	1.05	1	2.2	Ba _{0.8} Sr _{0.2} TiO(COO) ₂ .4H ₂ O
BST7	Ba _{0.7} Sr _{0.3} TiO ₃	0.735	0.315	1.05	1	2.2	Ba _{0.7} Sr _{0.3} TiO(COO) ₂ .4H ₂ O
BST6	Ba _{0.6} Sr _{0.4} TiO ₃	0.63	0.42	1.05	1	2.2	Ba _{0.6} Sr _{0.4} TiO(COO) ₂ .4H ₂ O
BST5	Ba _{0.5} Sr _{0.5} TiO ₃	0.525	0.525	1.05	1	2.2	Ba _{0.5} Sr _{0.5} TiO(COO) ₂ .4H ₂ O
ST	SrTiO ₃	0	1.05	1.05	1	2.2	SrTiO(COO) ₂ .4H ₂ O

2.2.3 Pressing process [20]

The pressing is a mechanical process used to press the powder into a pellet shape to reduce the vacancies and porosity between the particles and shrinkage the size by packing the particles to each other. Pressing is very important stage to complete the sample preparation and produce discs for LCR measurements. The calcined powders were put in cylindrical templates with diameter of 1cm that was designed in solid state laboratory; the template is shown in Fig. 2.5 .The powders were pressed using CARVAR electrical press at pressures, 124 MPa, 300 MPa and 500 MPa. The resulted discs were subjected to sintering .



Fig. 2.5: The template used for pressing the powders.

2.2.4 Sintering process [20]

The sintering process is heating the discs to a temperature that in the range of 0.5–0.75 of the melting temperature of the material [20, 48]. The powder did not melt, instead, the particles joined together and reduce the porosity (i.e., densification) of the body. The obtained samples from 300 MPa and 500 MPa pressing were very brittle, while the samples pressed at 124 MPa were strong enough to fired. Therefore only the samples pressed at 124 MPa were sintered at 1200 °C for 8 hr to obtain BST discs (using vacuum tube furnace SGL-1600 with heating and cooling rate 5 °C / min).

2.3 Density estimation [20]

The density for all sintered samples was estimated according to geometrical density , and calculated according to the following equation.

$$\rho = \frac{W}{\text{thickness} \times \text{area}} = \frac{W}{V}$$

Where ρ = density (g/cm^3), W = mass of the sample (g), V = volume of the sample (cm^3). Where $\{V = \text{thickness} \times \text{area}\}$ for the ceramic discs. Theoretical density measurements were calculated by using the following equation.

$$\rho = \frac{\text{molar mass}}{\text{cell volume} \times N_a}$$

Where N_a is Avogadro number in mol^{-1}

There is another parameter represented by compactness. The last one is a function of the successful of pressing and sintering mechanism. The compactness was calculated by the following equation.

$$\text{Compactness} = \frac{\rho (\text{geometrical})}{\rho (\text{theoretical})}$$

2.4 X-ray diffraction (XRD)

The prepared samples by the chemical methods were subjected to the X-ray diffraction analysis that was carried out at room temperature, lattice parameters estimated according to Bragg law as in the following equation [39].

$$n\lambda = 2d\sin\theta$$

Where n = diffraction order, λ = wavelength of the XRD diffractometer, d = interplane distance and θ = diffracted angle. While crystallite sizes estimated from Williamson-Hall equation as follow [39].

$$\frac{\beta \cos\theta}{\lambda} = \frac{0.89}{b} + 4\psi \frac{\sin\theta}{\lambda}$$

Where β = full width at the half maximum (FWHM), b = crystallite size, ψ = elastic strain and θ = diffracted angle.

The analysis was performed using X Powder v. 2004 software [40] for determination the lattice parameters and crystallite sizes. The second software was crystal impact Match v1.11 and crystal impact Diamond v3.2e [41] software used for phase identification (lattice determination and space group determination) the third one was Refine95 for cell refinement [42] with XRD database (PDF2# 81-2205 for BT, PDF2# 44-

0093 for BST77, PDF2# 89-0274 for BST67, PDF2# 34-0411 for BST6, PDF2# 39-1395 for BST5 and PDF2# 86-0179 for ST) from International Center for Diffraction Data (ICDD) [43] and (COD# 210_0858 for BT and COD# 900-6864 for ST) crystallography open database from International Union for Crystallography (IUCr) [44] were used for specifications of the produced powder.

2.5 Fourier Transform infrared spectroscopy (FTIR)

The aim of this analysis is to give more details on the production of the powders and the phase identifications. A small quantity of powder were mixed with KBr to get transparent disc. This disc was sandwiched in FTIR cell (NaCl cell), and the FTIR spectrum was estimated with FTIR spectrometer.

The analysis was performed using Essential FTIR software [45] with FDM library database (Fiveash Data Management # 00334 for ST) [46] and SDBS# 40058 for BT (Japanese structure organic database) [47] were used for specifications of powders.

2.6 Dielectric measurements

These studies were performed in different sites; the first was solid state laboratory at Al-Nahrain University by using TEGAM-3550 LCR meter at 5 volt. The second was at La Rochelle university in France using HIOKI 3532-50 LCR meter at 3 volt .The discs were placed in a suitable testing cell for dielectric discs as shown in Fig.2.6 under vacuum, Argon pressure, Nitrogen pressure and Helium pressure, the following measurements were performed :

2.6.1 Frequency measurement

This study has been done by changing the applied frequency from 42 Hz to 5 MHz with irregular steps at constant temperature (room temperature, high temperature, low temperature) and recording the capacitance(C) with loss tangent (D).

2.6.2 Temperature measurement

This study has been performed by changing the applied temperature from 100 K to 500 K at constant frequencies (1 kHz, 10 kHz, 100 kHz, 1 MHz) and recording the capacitance (C) with loss tangent (D).

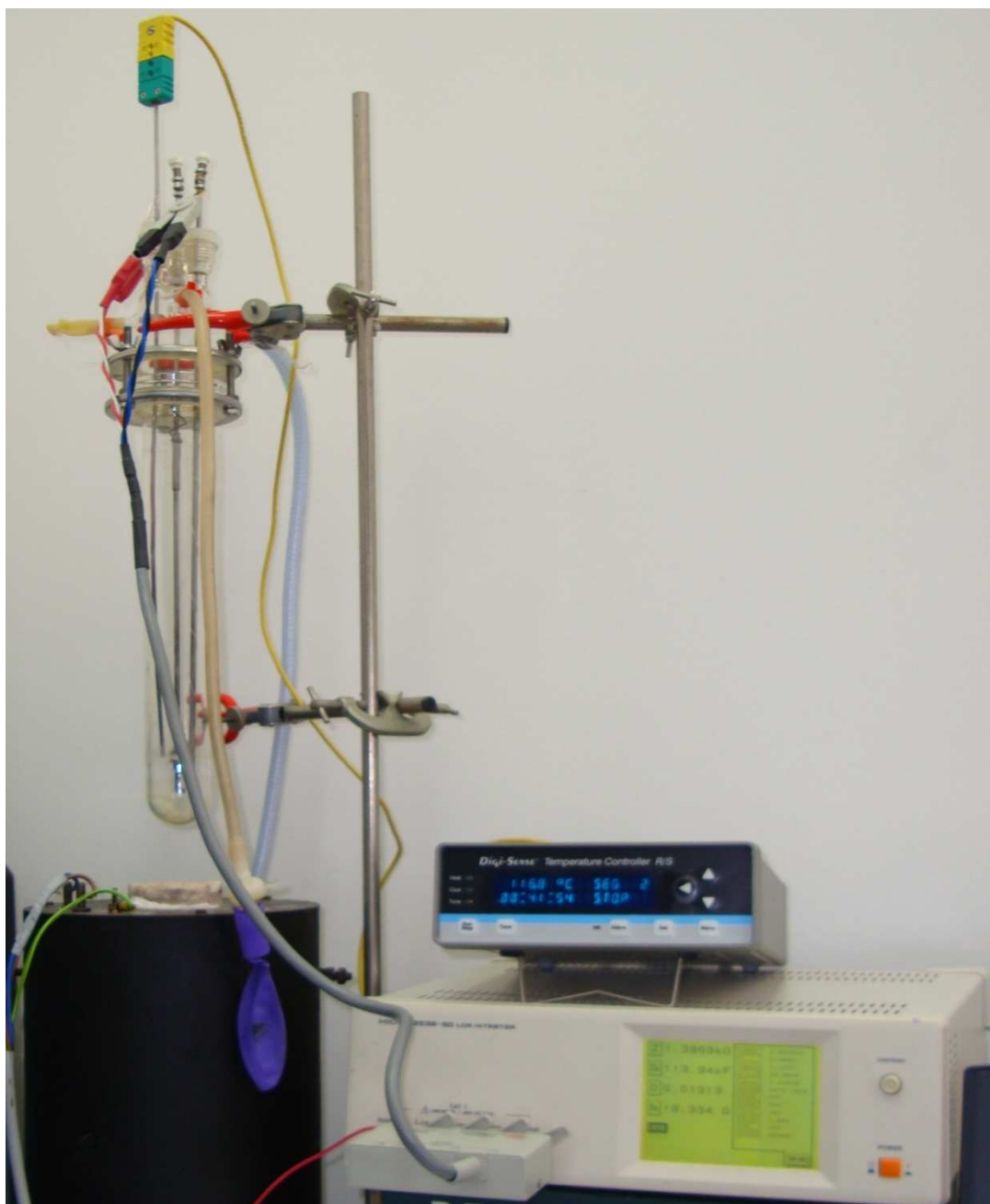


Fig. 2.6: The setup of dielectric measurement in La Rochelle University / France.

2.7 Transmission electron microscope (TEM).

The samples were prepared by mixing the powder with ethanol and mixing in Ultrasonic bath for 1 hr., then dropping on copper grid. The samples were put into to TEM chamber. Particle size and electron diffraction were calculated from TEM.

Chapter Three
Results and Discussion

Result and Discussion

Barium titanate was prepared using three chemical methods as mentioned in previous chapter. The best method for preparation (Oxalate method) was used to prepare Barium Strontium titanate ($\text{Ba}_x\text{Sr}_{1-x}\text{TiO}_3$) with $x = 1, 0.9, 0.8, 0.7, 0.6, 0.5$. XRD was used for determination of crystal structure (lattice parameters, crystallite size and space group) by using different software. FTIR spectroscopy was used for diagnosis of the obtained samples. Dielectric measurements were used for determination of Curie temperature. TEM analyses were used to estimate the particle size, particle shape and electron diffraction.

3.1 The reasons for selecting Oxalate method in preparation

During preparation of ceramic powders, it was obvious that the chemical methods (sol-precipitation) gave homogeneous and ultrafine powders. Whereas the conventional one (solid state reaction) needed high temperature of approximately 1000 °C to 1400 °C followed by grinding and further calcination. The resultant structure has a large grain size and multiple phases (heterogeneous) and high porous and needed high sintering temperature of about 1350 °C to 1450 °C. While the chemical method that produced ultrafine powder, homogeneous with high purity and low grain size which led to reduce calcination temperature (600 °C to 900 °C) with low porosity and low sintering temperature (1000 °C to 1300 °C). Solid state reaction might be considered as indirect method while chemical method (solution method) is direct method because that the reaction was done in the solution directly between Ba^{+2} , Ti^{+4} and O^{-2} to get BaTiO_3 precursor.

The criteria for choosing the best method to produce BT (NaOH-ethanol, Oxalate method and NaOH method) were cost effective, time management, crystallite size and the relative presences of impurities by XRD pattern.

It has been found that the best method for producing BT was the Oxalate method because:

- 1- Reaction time was 15 min while for the other methods was 5 hr which led to reduction of the cost

- 2- The Oxalate method has the smallest crystallite size while the other methods had a larger crystallite size.
- 3- The XRD pattern for the Oxalate method showed all the peaks of BT , while the first and the third methods had unknown peaks in XRD pattern

For these reasons the Oxalate method were used in this study to prepare BST system ($Ba_xSr_{1-x}TiO_3$) where $x = 1, 0.9, 0.8, 0.7, 0.6, 0.5$.

3.2 Density estimation

The parameters of density for sintered samples play an important role in Ceramic. There is a theoretical value of density for the prepared samples as in appendix 1. The simple method for measuring density is by using a principle concept in physics represented by Archimedes experiment. The second method for measuring density is by using geometrical method. It is clear that there is a variation in densities of the samples between theoretical and experimental values as in Table 3.1 and Fig.3.2. These differences might be return to the compactness, the last one increased as (x) increase as in the following equation and Fig.3.1. The estimated densities are shown in Table 3.1

Table 3.1: Density (g/cm^3) for BST discs after sintering ($1200^\circ C / 8hr$) (appendix 1)

Sample	Substitution factor (x)	Geometrical Density (g/cm^3)	Theoretical Density (g/cm^3)	Compactness (%)
ST	0	1.57	5.14	30.58
BST5	0.5	1.99	5.59	35.69
BST6	0.6	2.13	5.66	37.62
BST7	0.7	2.25	5.74	39.14
BST8	0.8	2.29	5.83	39.20
BST9	0.9	2.23	5.93	37.58
BT	1	3.02	6.03	50.06

The compactness is changing with the substitution factor (x) as in Fig.3.1, the estimated equations for the ceramic compactness, theoretical density and experimental densities are:

$$\text{Compactness (\%)} = 14.56x + 29.19$$

$$\text{Theoretical density (g/cm}^3\text{)} = 0.878x + 5.138$$

$$\text{Geometrical density (g/cm}^3\text{)} = 0.987x + 1.6$$

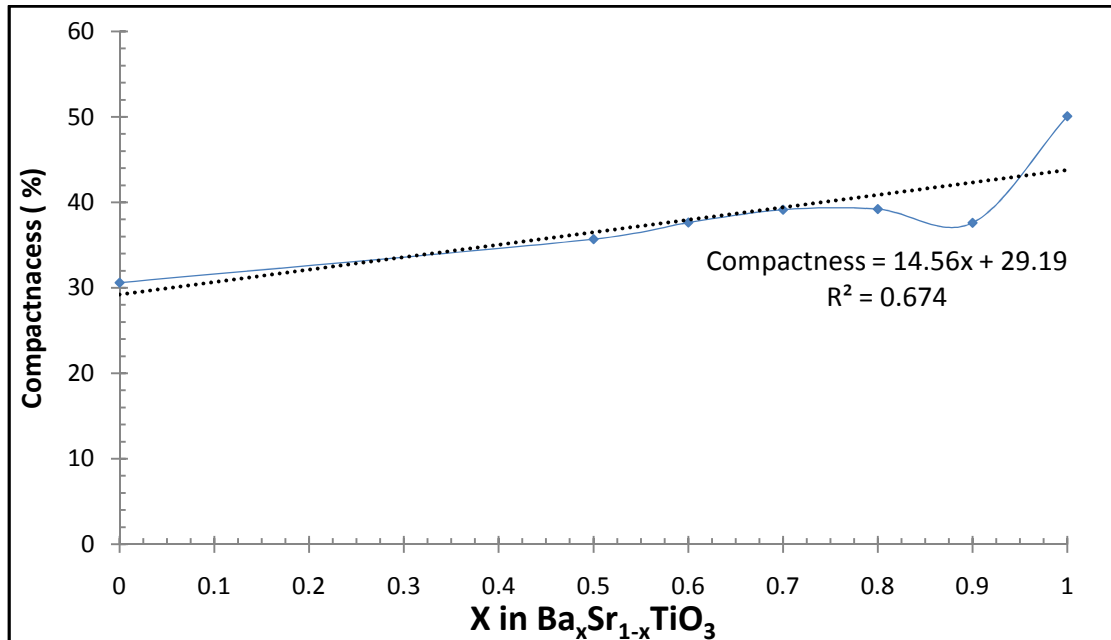


Fig. 3.1: The Compactness of the ceramic discs vs substitution factor (x)

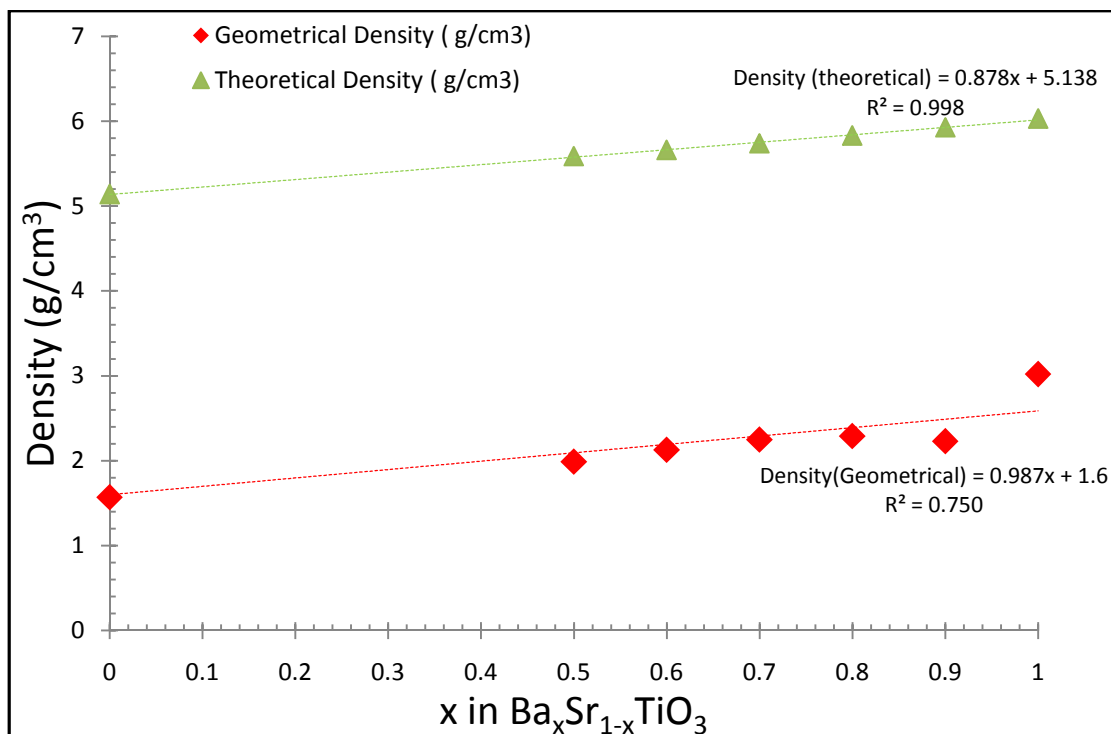


Fig.3.2: The density of the ceramic discs vs substitution factor(x)

This changing in density is due to the substitution of Sr ions, where (Ba⁺²) radius = 1.35 Å and molar mass = 137.33 g/mol while (Sr⁺²) radius = 1.13 Å and molar mass = 87.62 g/mol (Appendix 2) [49], so the

substitution of Sr ions leads to shrinkage in lattice volume and decreasing in molar mass of BST. All these reasons lead to decreasing in density. Theoretically increasing of Ba ions(or increasing x) lead to increase the density , experimentally for the geometrical density the increasing of (x) leads to increase the density while for Archimedes density the increasing of (x) leads to decreasing of density which means that when (x) increase the porosity decrease (i.e. inversely proportion)

3.3 XRD analysis

The XRD is an important technique to determine the structural properties (crystal structure, lattice parameter, crystallite size and space group) of materials. The prepared samples were subjected to XRD diffractometer as mentioned in chapter two. XRD software were used to determine the structural properties of the prepared samples. XRD patterns are shown in the following:

3.3.1 XRD for BT

A. XRD for Sodium hydroxide-ethanol method:

The XRD pattern had amorphous phase for BT before calcination, and crystalline phase (tetragonal lattice $a=b=3.9841\text{\AA}$, $c=4.0162\text{\AA}$, with space group {P4mm}), after calcination at $850\text{ }^{\circ}\text{C}$ / 5hr as shown in Fig 3.3. The crystallite size was in the range (26-42 nm) and the non-uniform strain is about 0.180 .

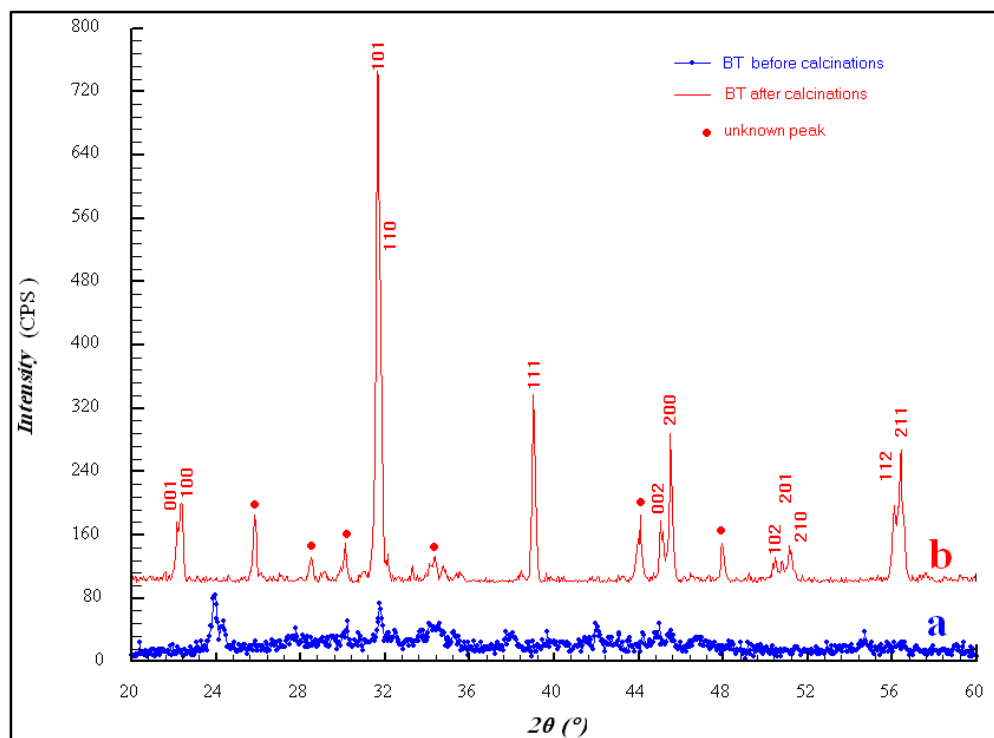


Fig 3.3: XRD pattern for Sodium hydroxide-ethanol method (a) before calcination (b) after calcination 850 °C / 5hr.

B. XRD for Oxalate method:

The XRD pattern showed amorphous phase for Barium titanate Oxalate tetrahydrate before calcination, and crystalline phase (cubic lattice $a=b=c=4.0073 \text{ \AA}$, with space group {Pm-3m}) after calcination at 600 °C / 5 hr, and crystalline phase (tetragonal lattice $a=b=3.9999 \text{ \AA}$, $c=4.017 \text{ \AA}$, with space group {P4mm}) after calcination at 850 °C / 5 hr as shown in Fig 3.4.

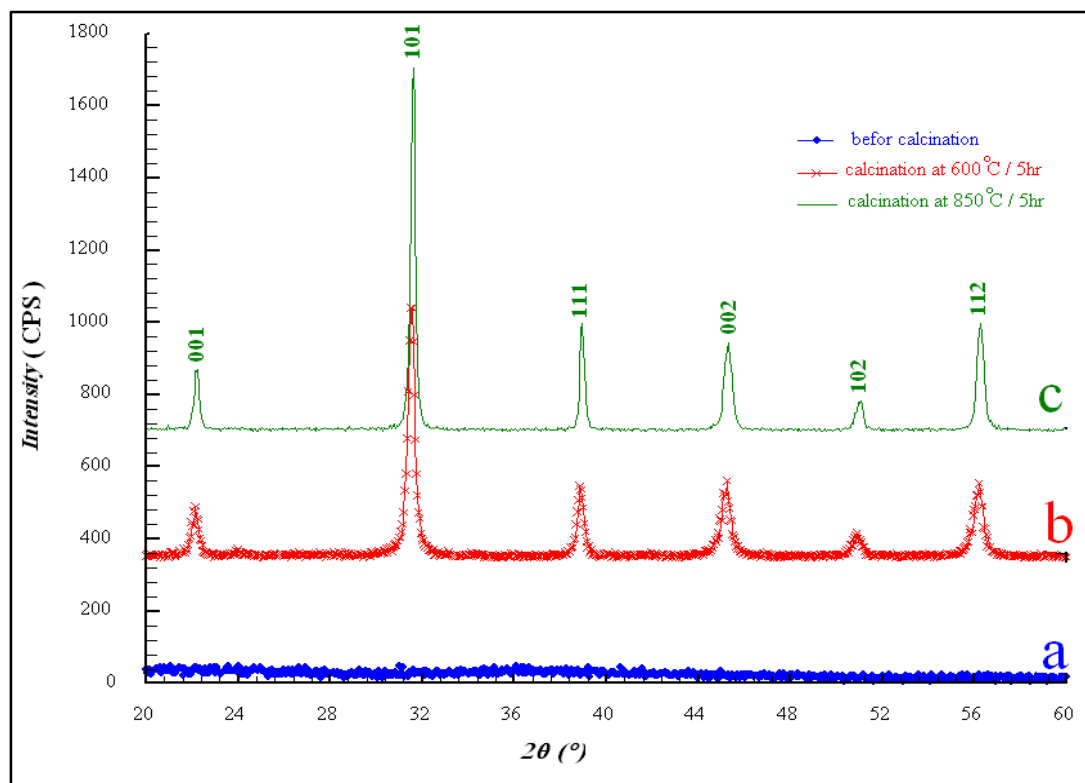


Fig 3.4: XRD pattern for Oxalate method (a) before calcinations, (b) after calcination at 600 °C / 5hr, (c) after calcination at 850 °C / 5hr.

On the other hand, the crystallite size was in the range (21-25 nm) and the non-uniform strain was 0.246 for the sample calcined at (600 °C/5 hr) as shown in Fig.3.5.a. Whereas the crystallite size was in the range (25-37 nm) and the non-uniform strain was 0.253 for the sample calcined at (850 °C/5 hr) as shown in Fig.3.5.b.

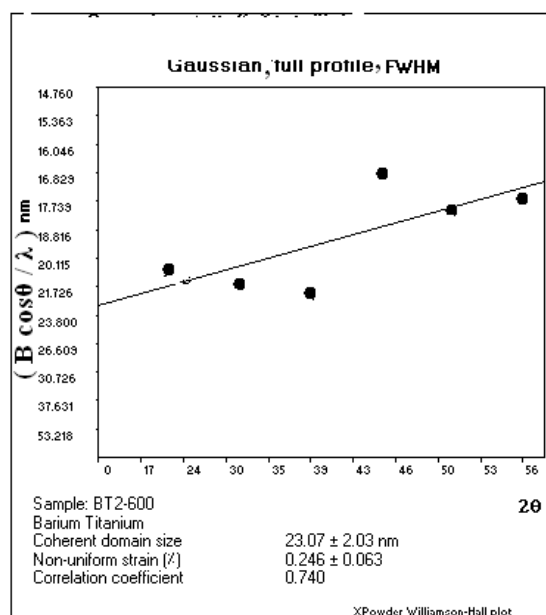


Fig.3.5.a: Williamson-Hall plot for Oxalate method (600 °C/5 hr)

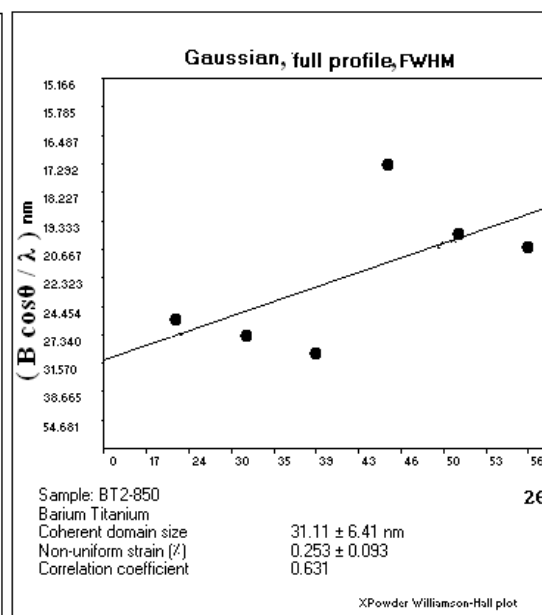


Fig.3.5.b: Williamson-Hall plot for Oxalate method (850 °C/5 hr)

C. XRD for Sodium hydroxide method.

The XRD pattern showed crystalline phase for BT before calcination (cubic lattice $a=b=c= 4.0247 \text{ \AA}$, with space group $\{Pm-3m\}$), and crystalline phase (cubic lattice $a=b=c=4.0025 \text{ \AA}$, with space group $\{Pm-3m\}$) after calcination at $850 \text{ }^\circ\text{C} / 5\text{ hr}$ as shown in Fig 3.6.

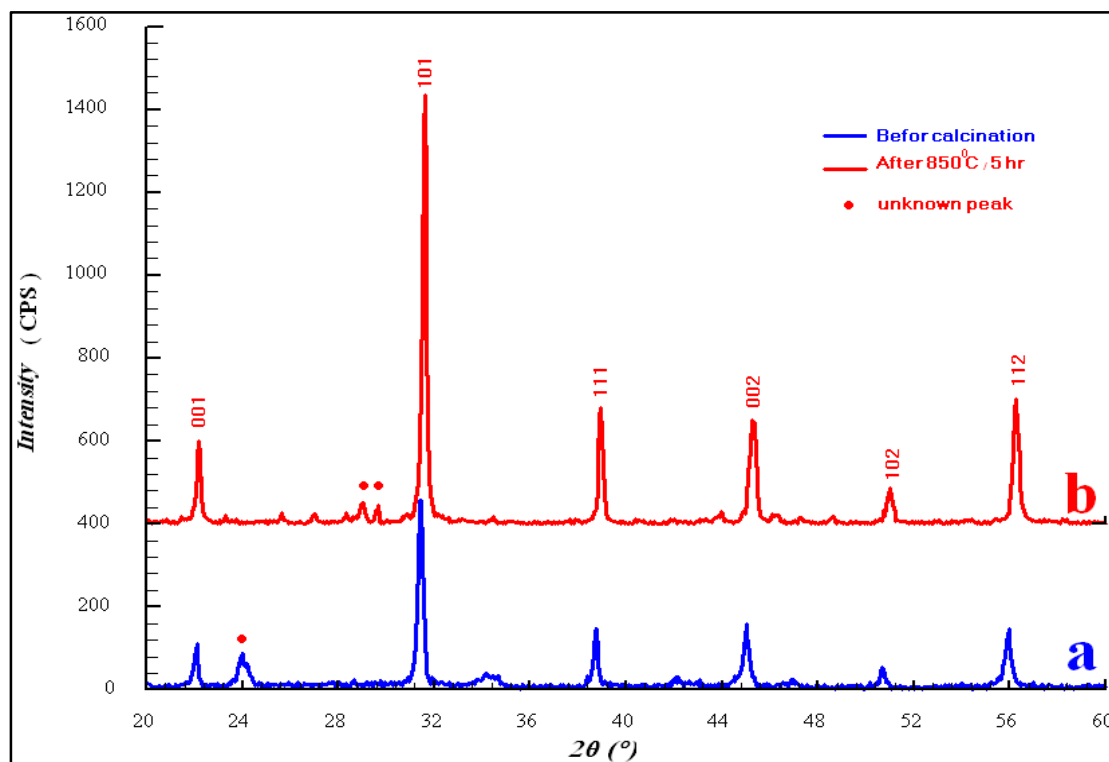


Fig.3.6: XRD pattern for Sodium hydroxide method (a) calcination (b) after calcination at $850 \text{ }^\circ\text{C} / 5 \text{ hr}$.

The crystallite size was in the range (26-36 nm) and the non-uniform strain was 0.152 for the sample before calcinations as shown in Fig.3.7.a. The crystallite size was in the range (27-35 nm) and the non-uniform strain was 0.184 while for the sample calcined at $850 \text{ }^\circ\text{C} / 5 \text{ hr}$ as shown in Fig.3.7.b.

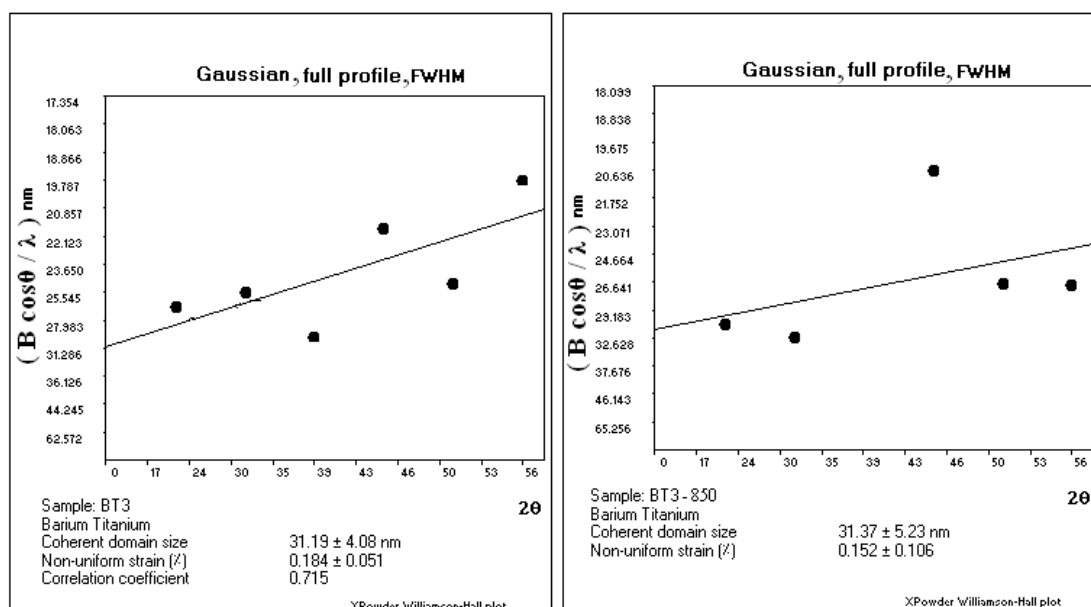


Fig.3.7.a: Williamson-Hall plot for NaOH method before calcinations.

Fig.3.7.b: Williamson-Hall plot for NaOH method (850 °C/5 hr).

3.3.2 XRD for BST

The XRD patterns had amorphous phase of Barium Strontium titanyl Oxalate tetrahydrate before calcination (for all BST samples) and crystalline phases after calcination at 850 °C / 5hr as shown in table 3.2.

Table 3.2: Phases and crystallite sizes of BST samples calcined at (850 °C/5 hr)

Sample	a (Å)	c (Å)	Lattice	Space group	Crystallite size (nm) from XRD	Particle size (nm) from TEM
ST	3.899	3.899	Cubic	Pm-3m	24 - 29	
BST5	3.956	3.956	Cubic	Pm-3m	23 - 28	70
BST6	3.969	3.969	Cubic	Pm-3m	24 - 90	95
BST7	3.982	3.983	Tetragonal	P4mm	25 - 38	
BST8	3.989	3.995	Tetragonal	P4mm	21 - 26	40
BST9	3.994	4.008	Tetragonal	P4mm	21 - 45	
BT	3.9999	4.017	Tetragonal	P4mm	29 - 89	

The following figures (Fig.3.8 – Fig.3.16) show the XRD patterns for BST samples.

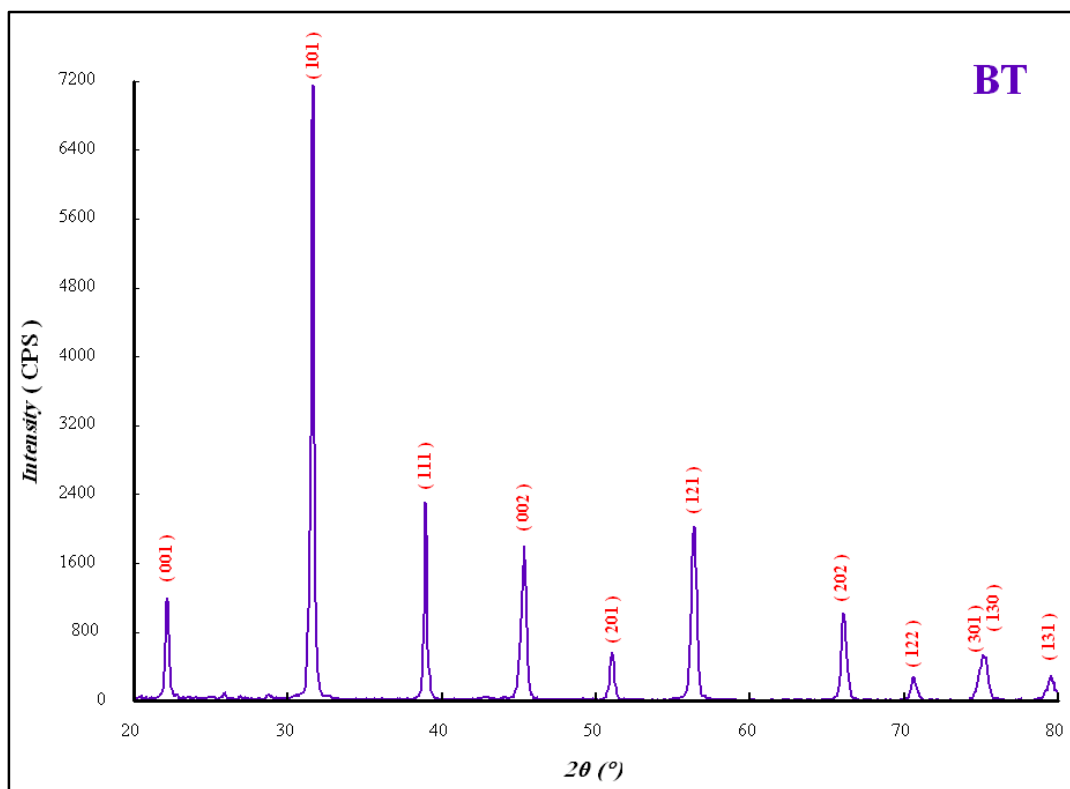


Fig.3.8: XRD pattern for BT after calcination at 850 °C / 5 hr.

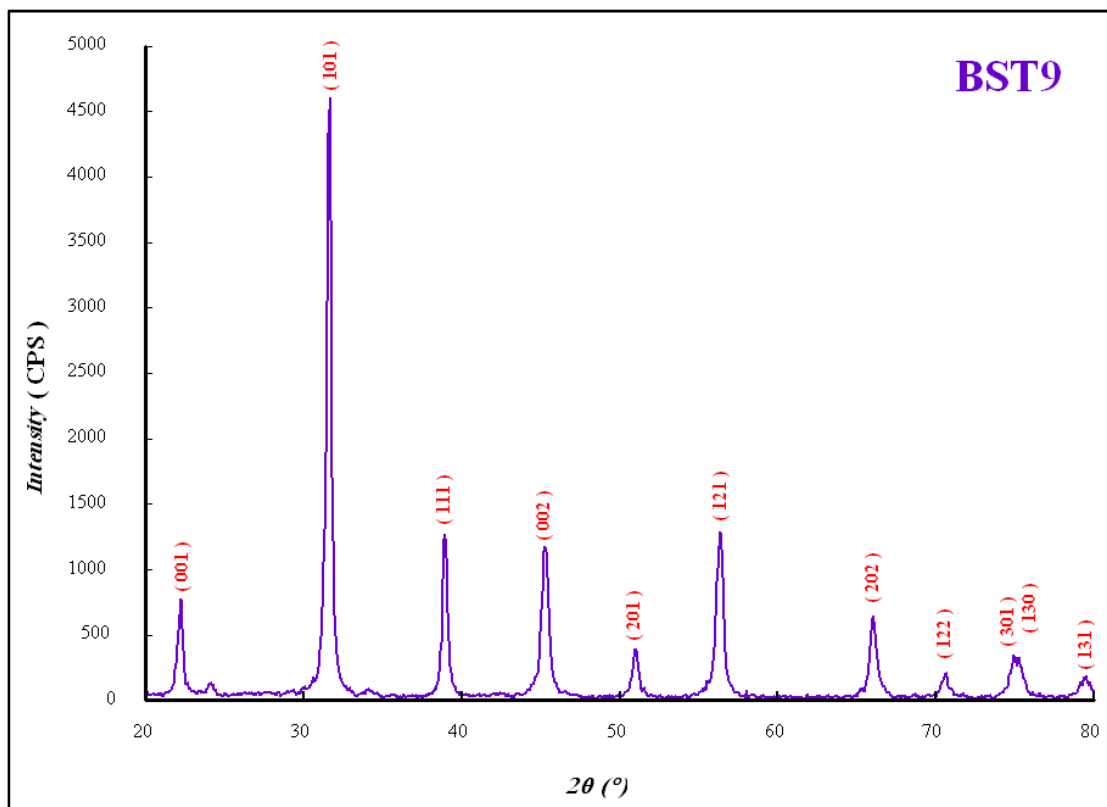


Fig.3.9: XRD pattern for BST9 after calcination at 850 °C / 5 hr.

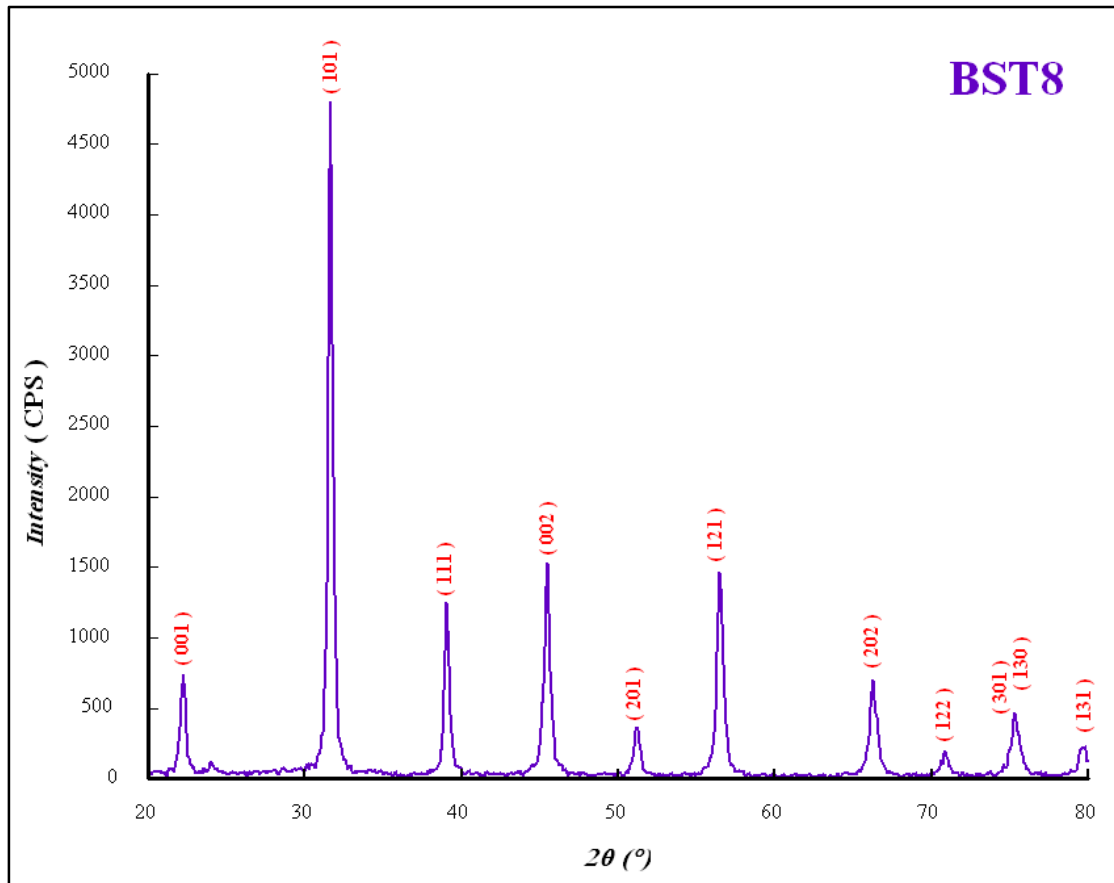


Fig.3.10: XRD pattern for BST8 after calcination at 850 °C / 5 hr.

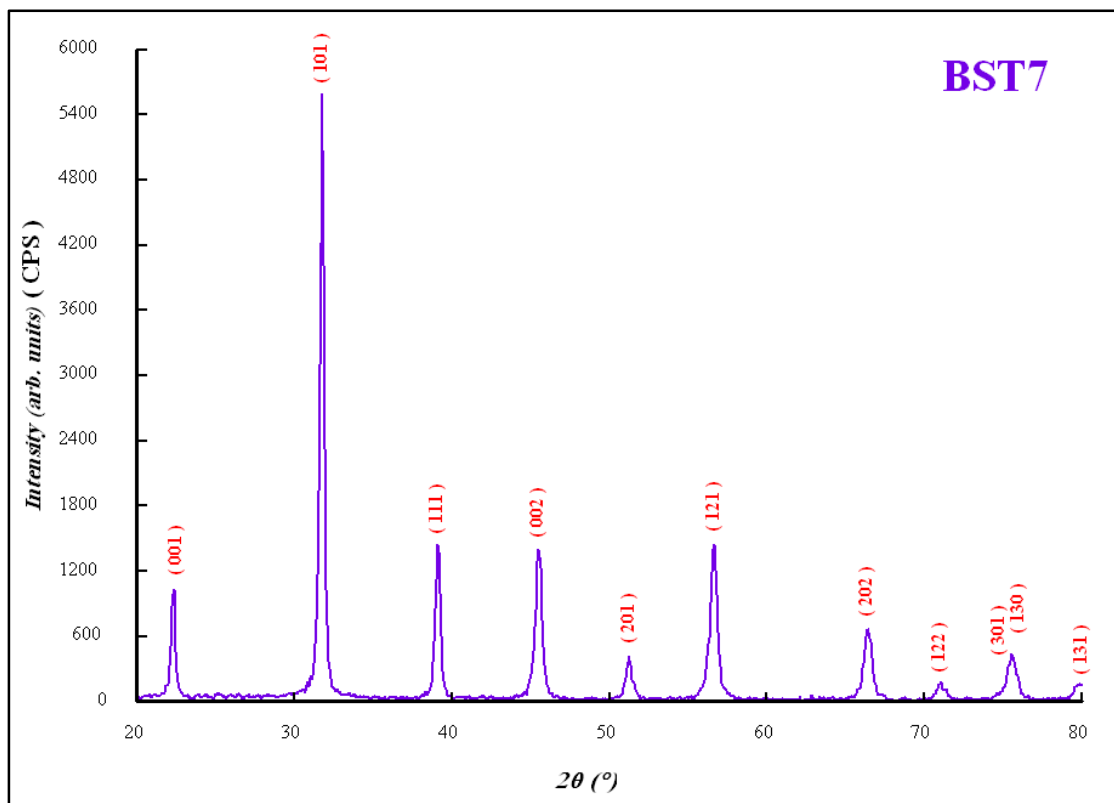


Fig.3.11: XRD pattern for BST7 after calcination at 850 °C / 5 hr.

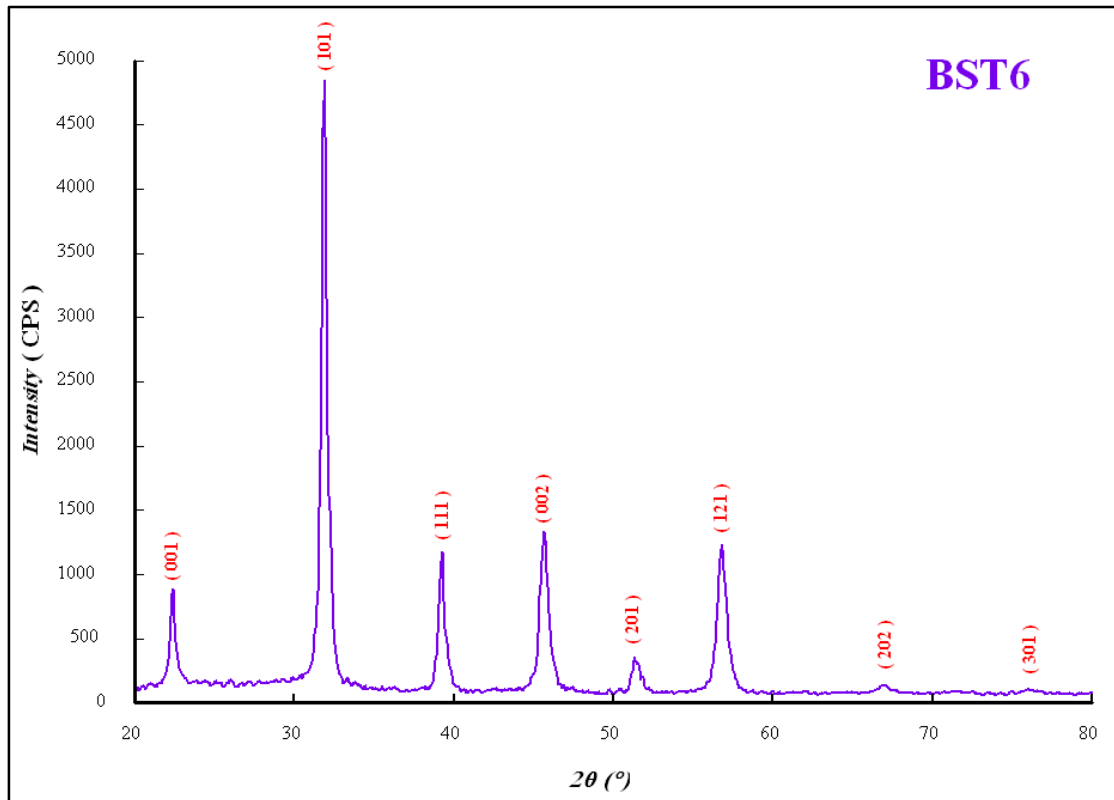


Fig.3.12: XRD pattern for BST6 after calcination at 850 °C / 5 hr.

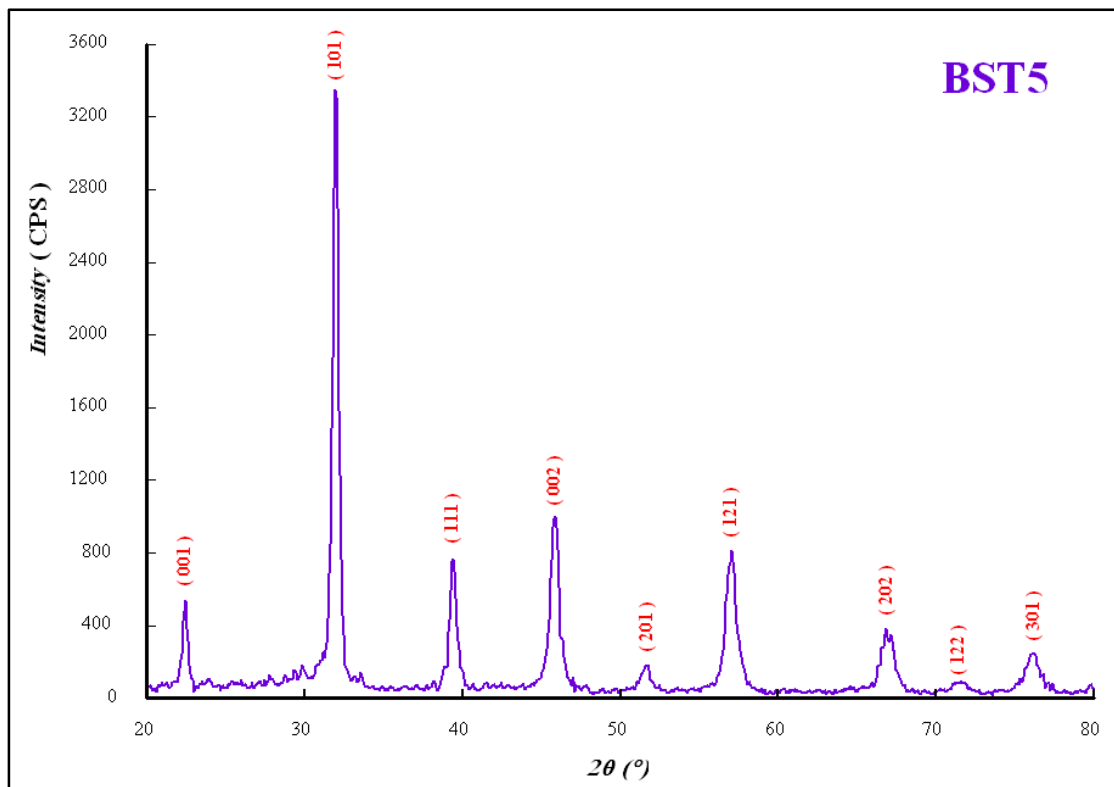


Fig.3.13: XRD pattern for BST5 after calcination at 850 °C / 5 hr.

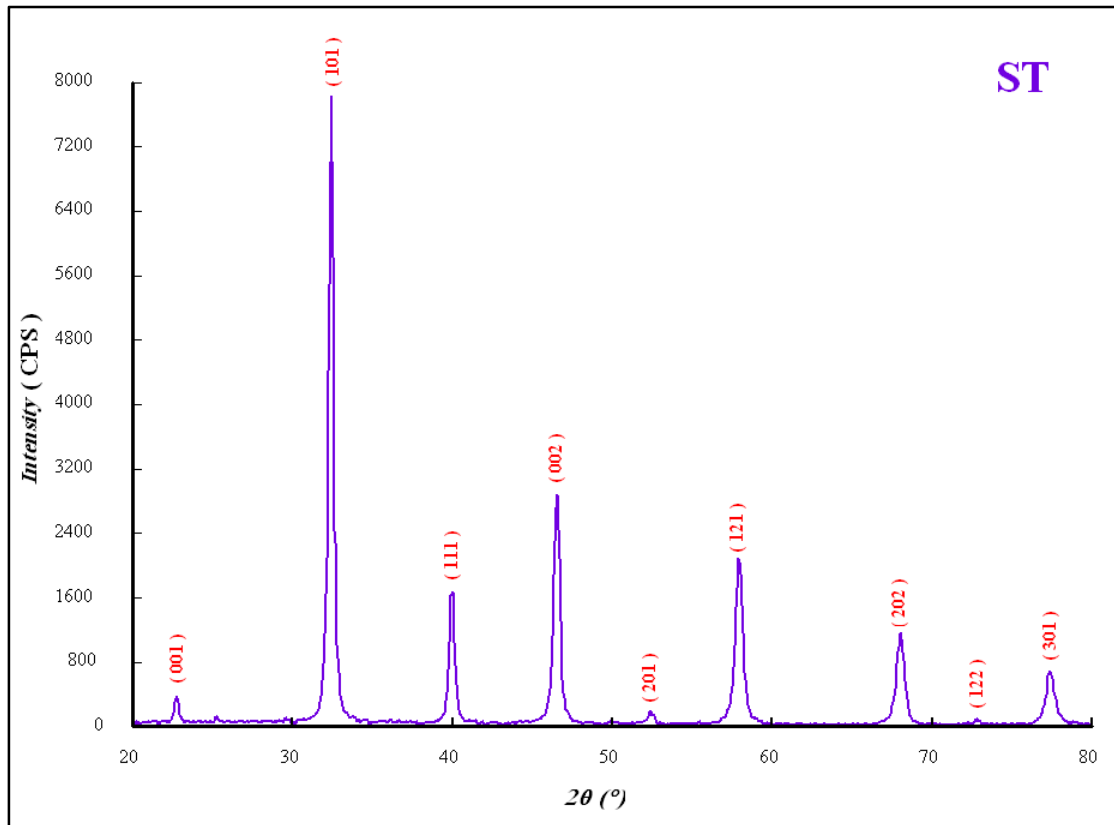


Fig.3.14: XRD pattern for ST after calcination at 850 °C / 5 hr.

For all BST patterns there is a slightly shifting in 2θ as shown in Fig.3.15 and Fig.3.16 that means there is a limited variation in lattice parameter as a function of (x) as shown in Fig.3.17 and Fig.3.18.

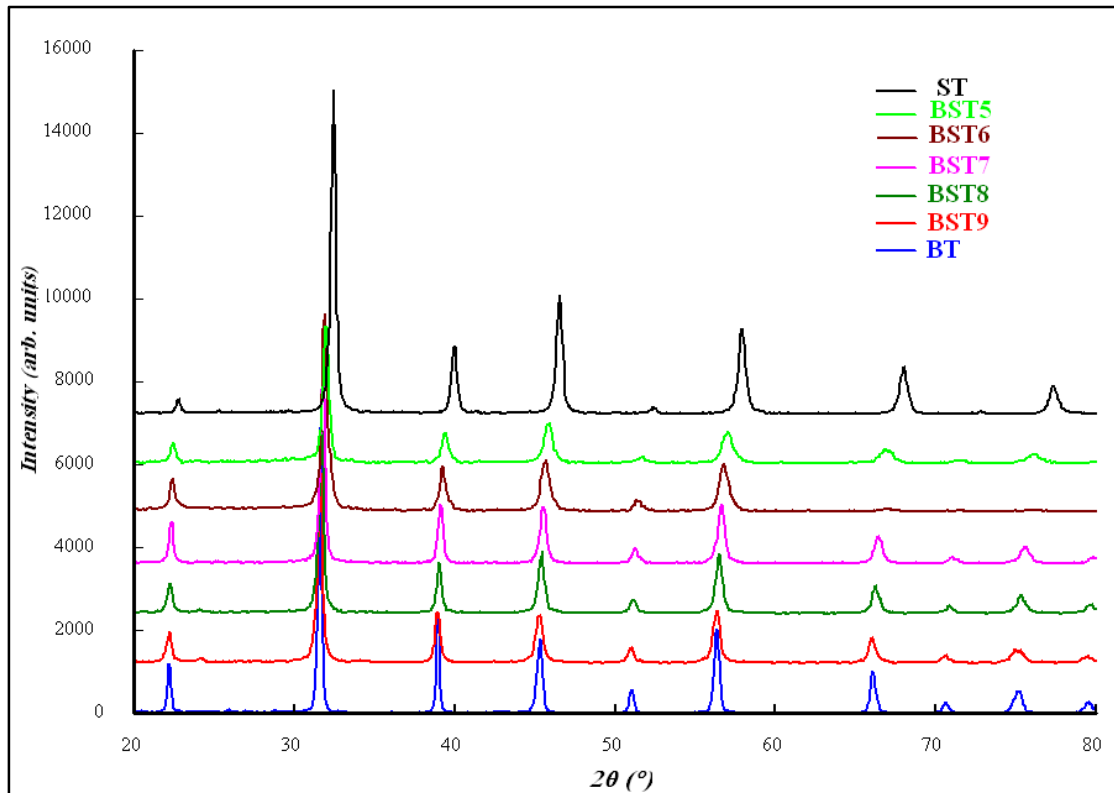


Fig.3.15: XRD pattern for BST after calcination at 850°C / 5 hr.

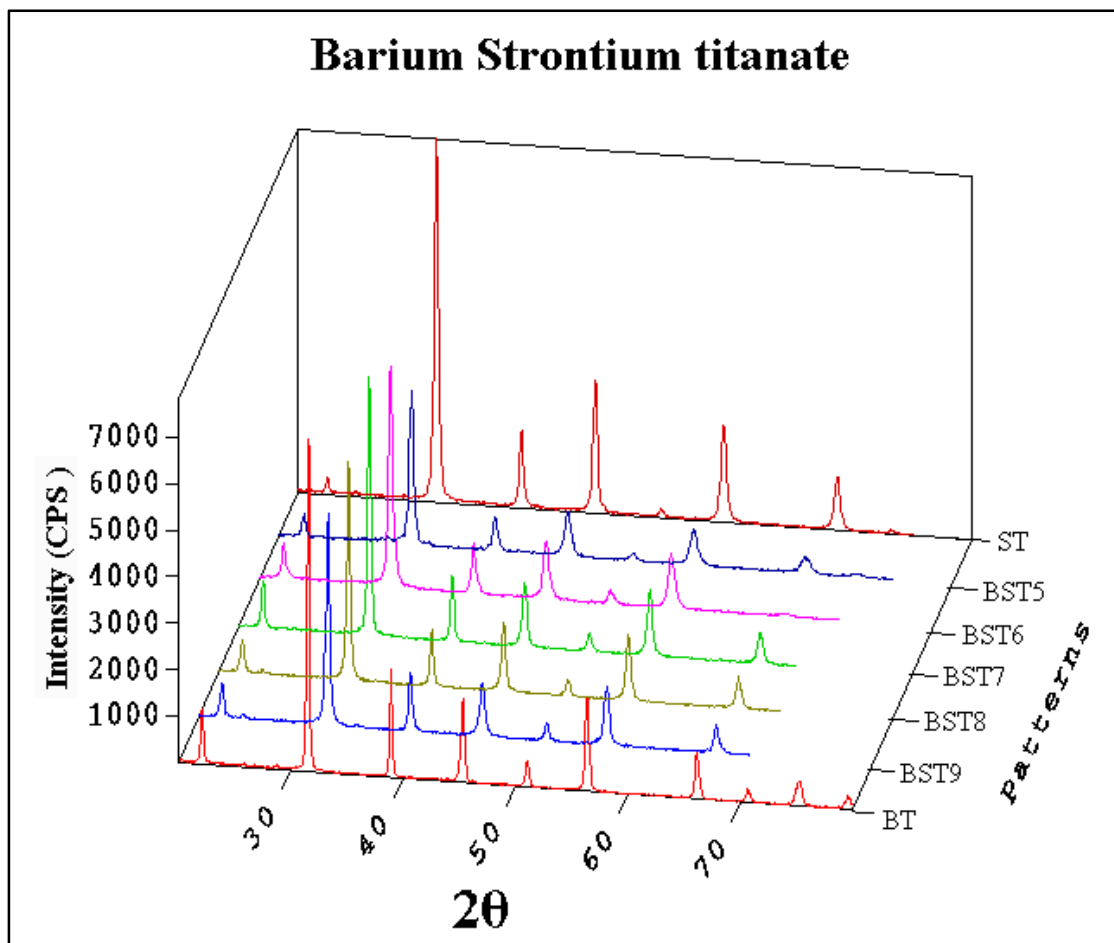


Fig.3.16: 3D XRD pattern for BST after calcination at 850°C / 5 hr.

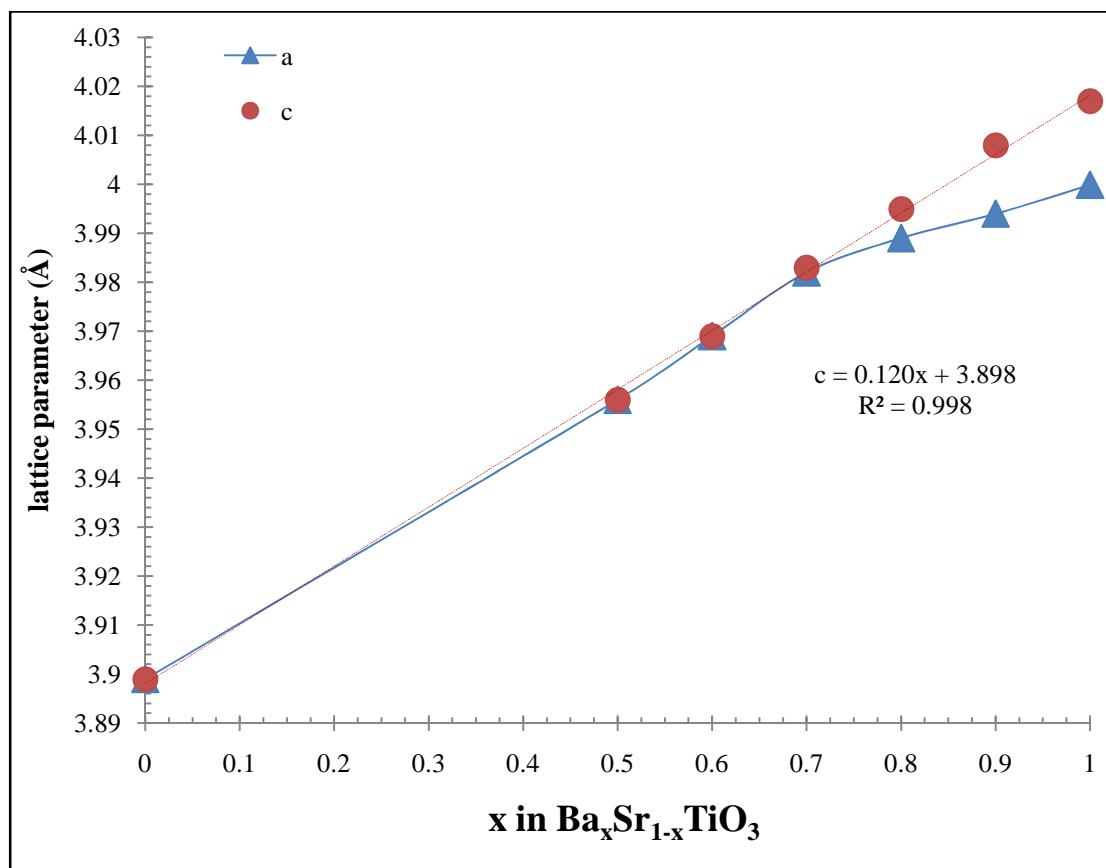


Fig. 3.17: Variation of lattice parameter vs substitution factor (x)

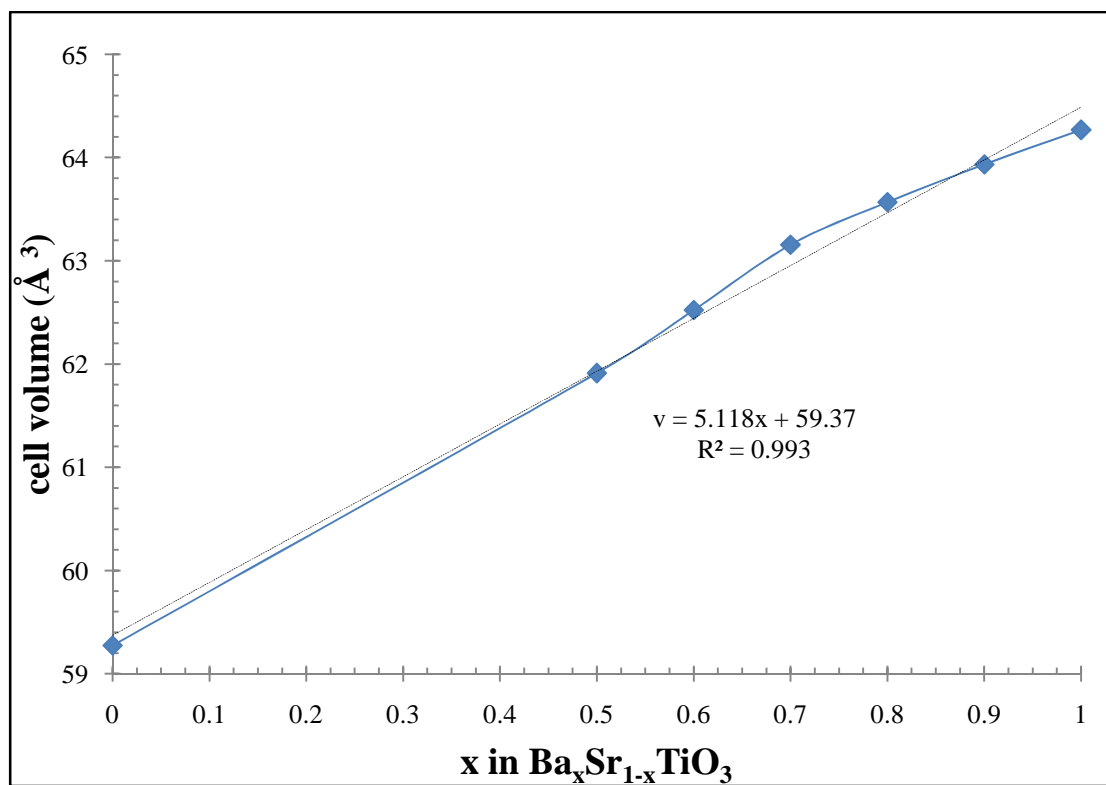


Fig. 3.18: Variation of cell volume vs substitution factor (x)

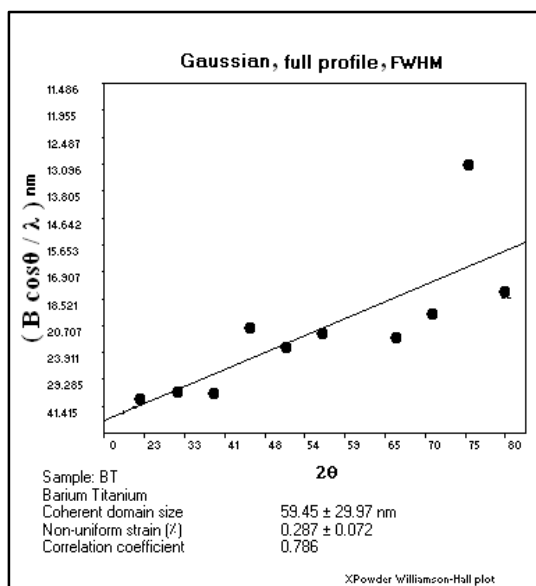


Fig.3.19: Williamson-Hall plot for BT (850 °C/5 hr)

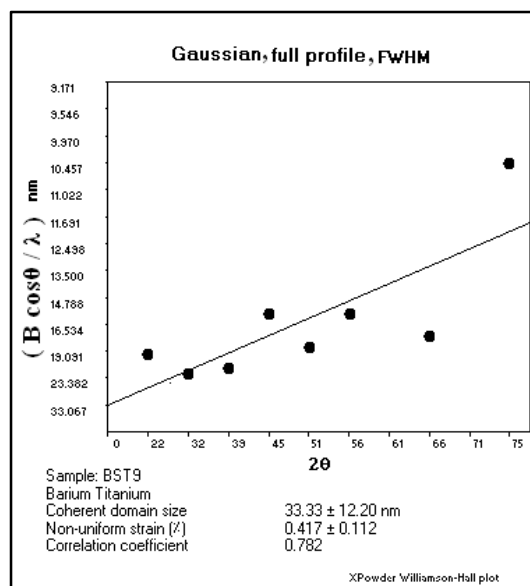


Fig.3.20: Williamson-Hall plot for BST9 (850 °C/5 hr)

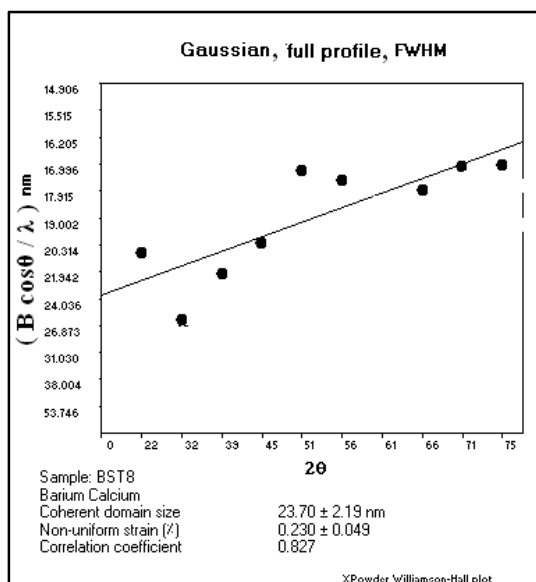


Fig.3.21: Williamson-Hall plot for BST8 (850 °C/5 hr)

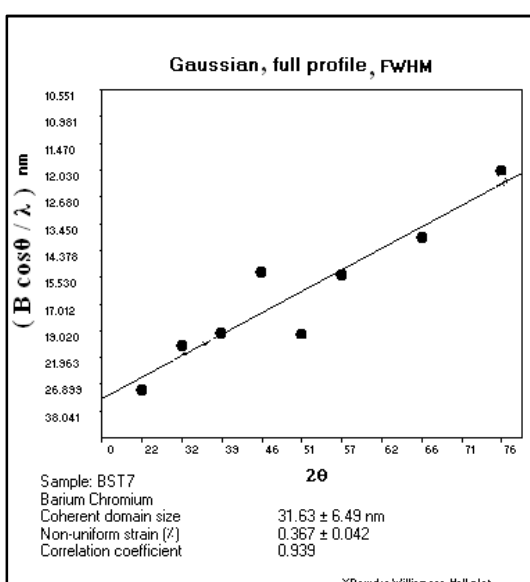


Fig.3.22: Williamson-Hall plot for BST7 (850 °C/5 hr)

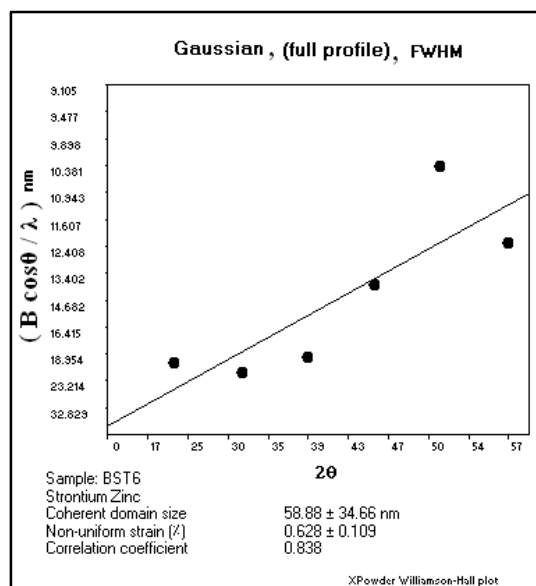


Fig.3.23: Williamson-Hall plot for BST6 (850 °C/5 hr)

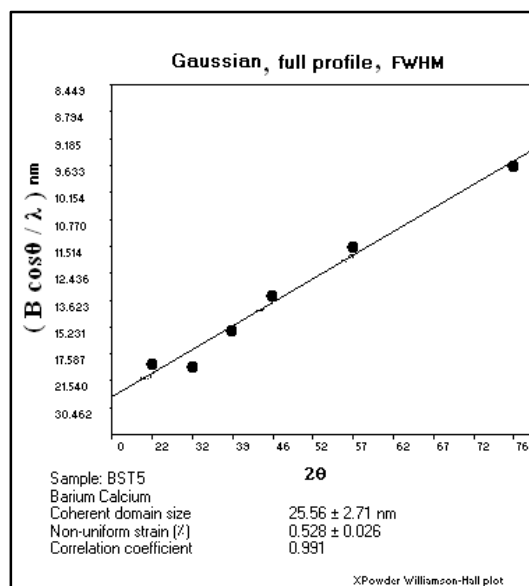


Fig.3.24: Williamson-Hall plot for BST5 (850 °C/5 hr)

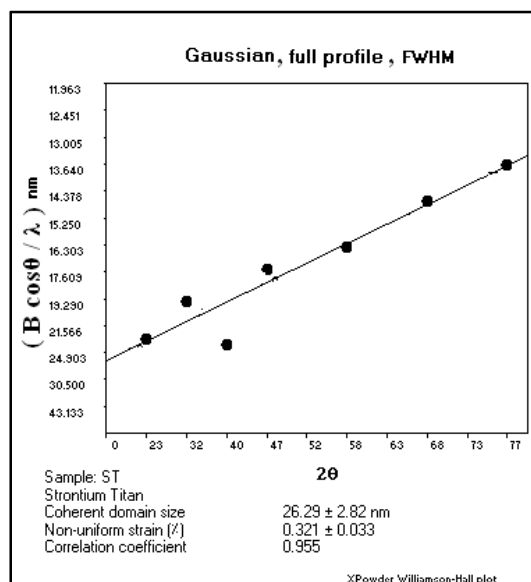


Fig.3.25: Williamson-Hall plot for ST (850 °C/5 hr)

For Fig.3.19 – Fig.3.25, these figures show the crystallite sizes (coherent domain size) and the none-uniform strain for BST samples which calculated from XRD pattern according to Williamson-Hall equation. Crystallite size acts as measurement of crystal growth.

From XRD patterns for BST samples, (BT, BST9, BST8, BST7) have tetragonal lattice (non-centrosymmetric with space group: $P4mm$ [50]) which means that there is no center for symmetry, so these samples have spontaneous polarization related to the crystal structure, while (BST6, BST5 and ST) have cubic lattice (centrosymmetric with space group:

Pm-3m [50]) which means that these samples are centrosymmetric (which posses center of symmetry [50]), so there is no spontaneous polarization for this structure . This means that BT, BST9, BST8 and BST7 samples are in ferroelectric phase or the Curie temperature related to these samples is greater than room temperature, while BST6, BST5 and ST are in paraelectric which means that the Curie temperature is lower than room temperature. The lattice parameters change linearly with the substitution factor (x) and the cell volumes also change linearly with (x). as shown in the following equations.

$$c (\text{\AA}) = 0.120x + 3.898$$

$$a (\text{\AA}) = 0.120x + 3.898 \quad \text{for } 0.7 > x > 0$$

$$a (\text{\AA}) = 0.058x + 3.941 \quad \text{for } x \geq 0.7$$

$$\text{Cell volume } (\text{\AA}^3) = 5.118x + 59.37$$

This linear behavior is due to differences in ion radius ($\text{Ba}^{+2} = 1.35 \text{\AA}$ and $\text{Sr}^{+2} = 1.13 \text{\AA}$)

3.4 FTIR spectroscopy

The FTIR spectrum gave details about the absorption lines related to the bond length between the elements of the compound. FTIR spectra of different samples are shown in the following figures.

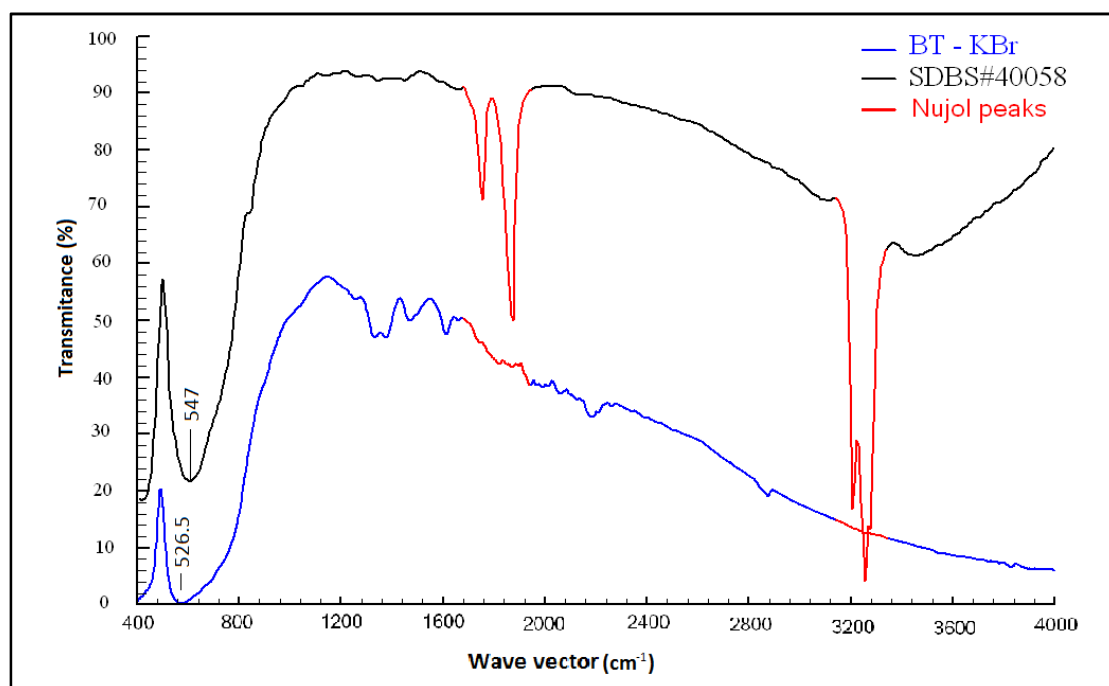


Fig. 3.26: FTIR spectrum for BT

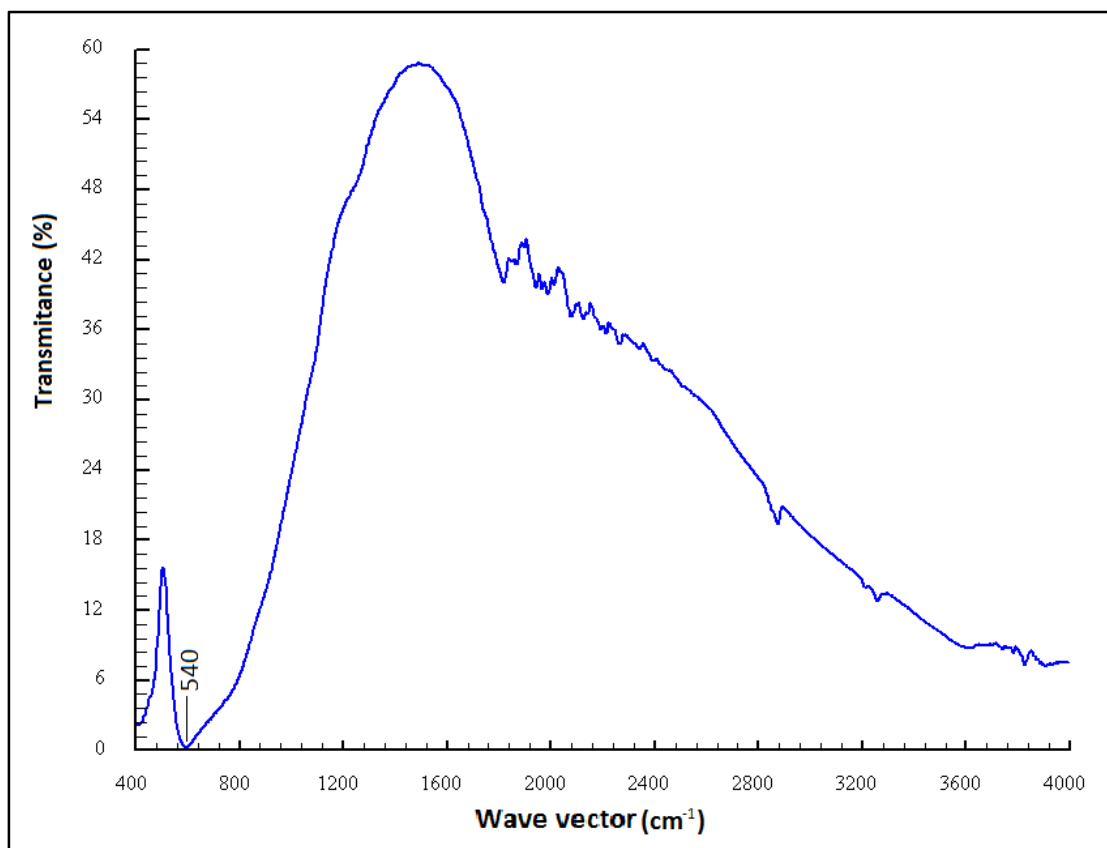


Fig. 3.27: FTIR spectrum for BST5

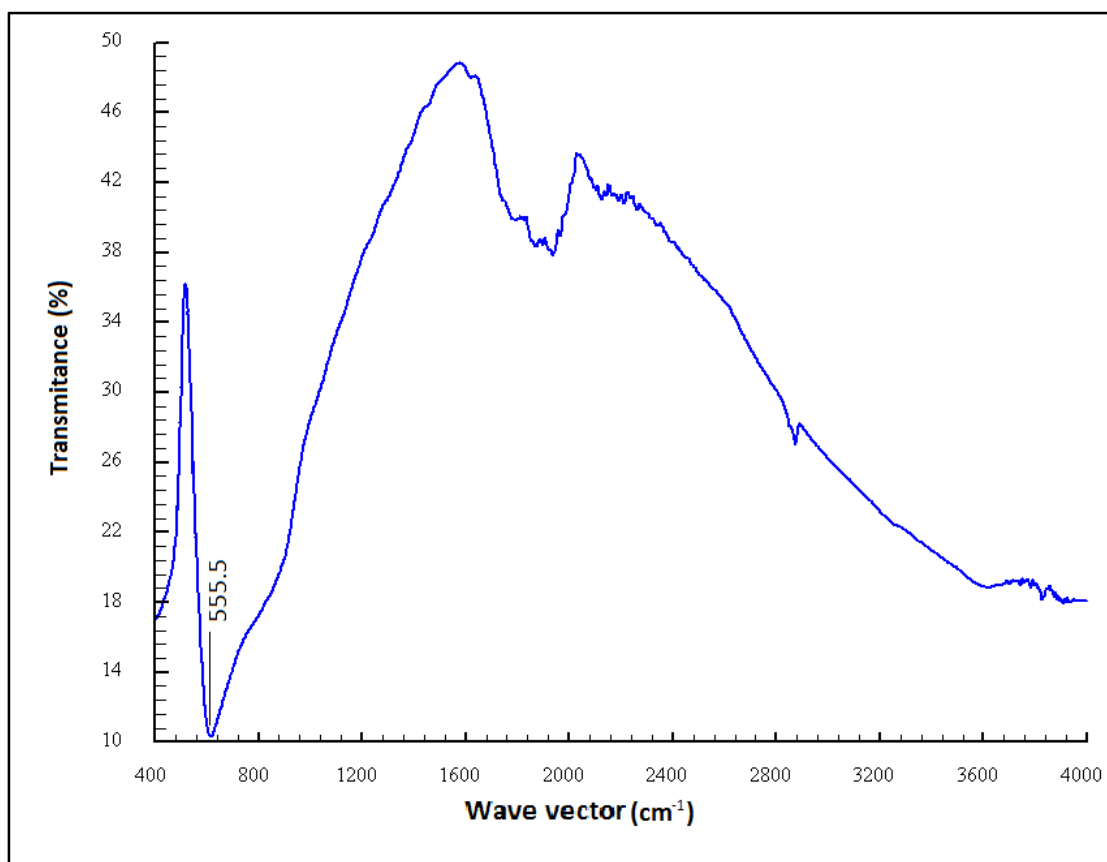


Fig.3.28: FTIR spectrum for ST

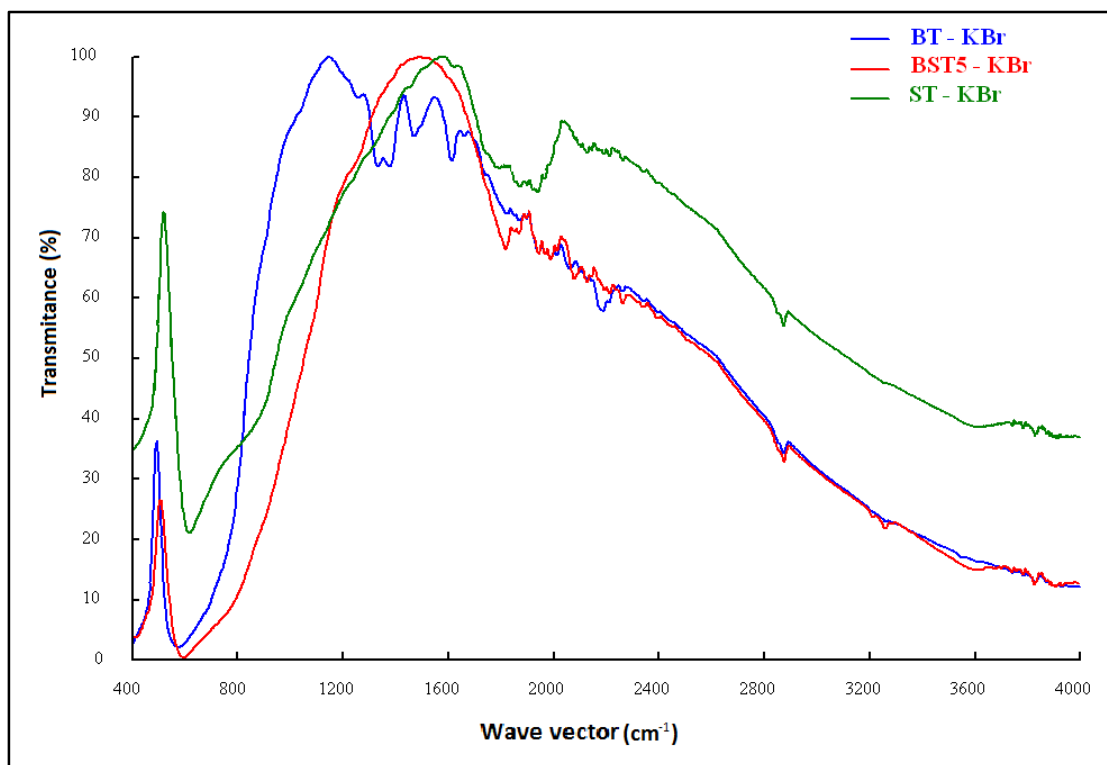


Fig. 3.29: FTIR spectrum for BST samples

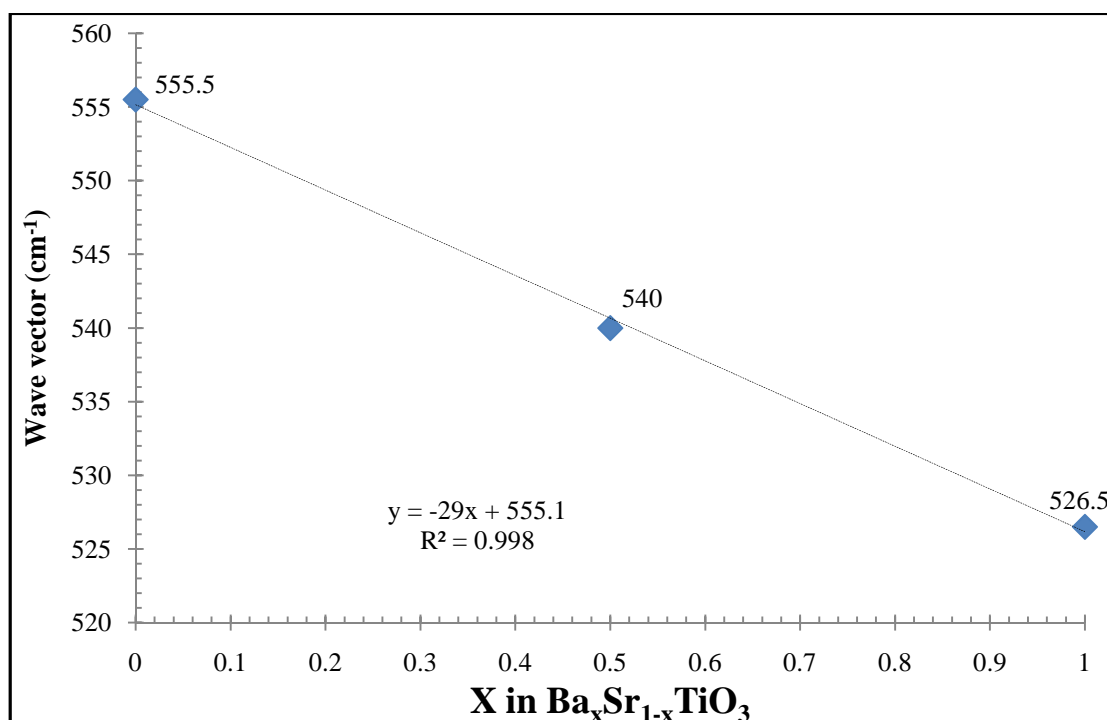


Fig 3.30: Variation of absorption in wave number vs substitution factor (x)

FTIR patterns showed that the absorption peaks in wave vector (555.5 , 540 and 526.5 cm^{-1}) related to ST , BST5 , BT respectively which related to perovskite structure after comparing with SDDBS database #40058 for BT [47] and FDM database #00334 for ST [46] . The wave vector of the

absorption lines changed linearly with the substitution factor (x) according to the following equation which means that the increasing of Sr ions lead to slightly increasing in the wave vector of absorption lines which means that the increasing of Sr ions (decrease in x) lead to decreasing of the bond length and increasing of the bond energy. This result is in agreed with XRD results. The XRD and FTIR results showed that the presence of Perovskite Structure with different lattice parameter which decrease linearly with the substitution factor(x)

$$K (\text{cm}^{-1}) = -29 + 555.1$$

3.5 Dielectric measurements

3.5.1 Frequency measurements

The frequency measurements of dielectric constant for BST sample are shown in the following figures (Fig.3.31 – Fig.3.37) (appendix 3)

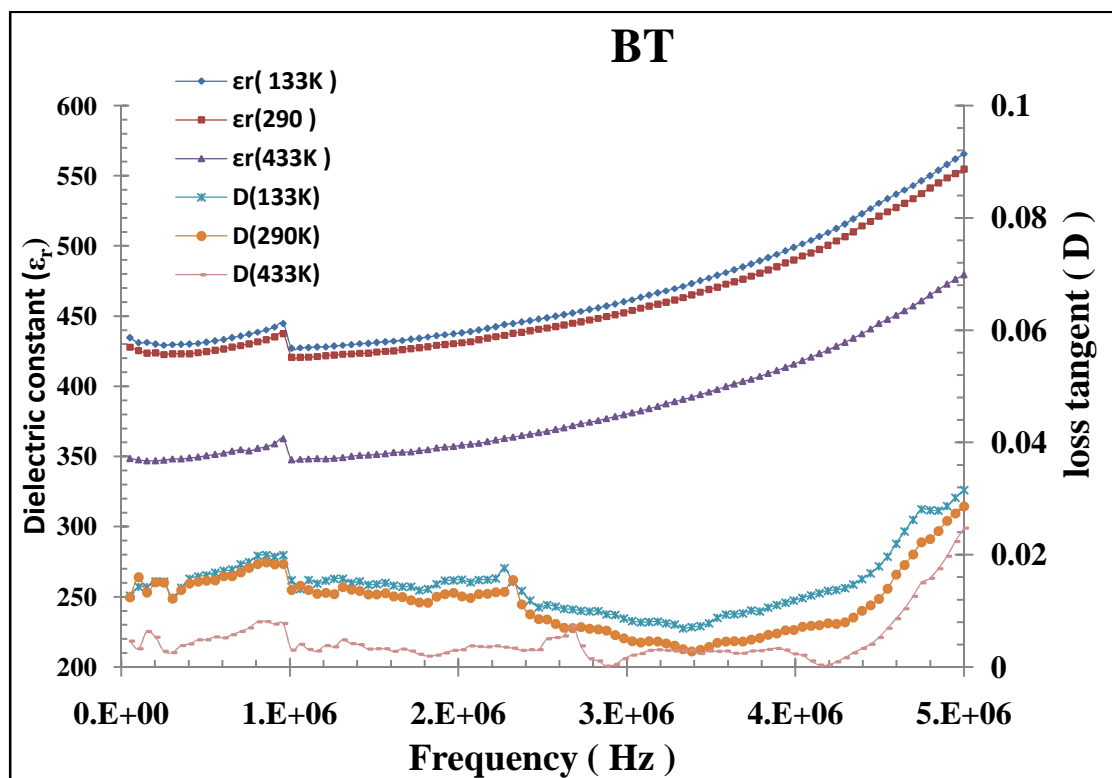


Fig.3.31: Dielectric constant and loss tangent vs frequency for BT

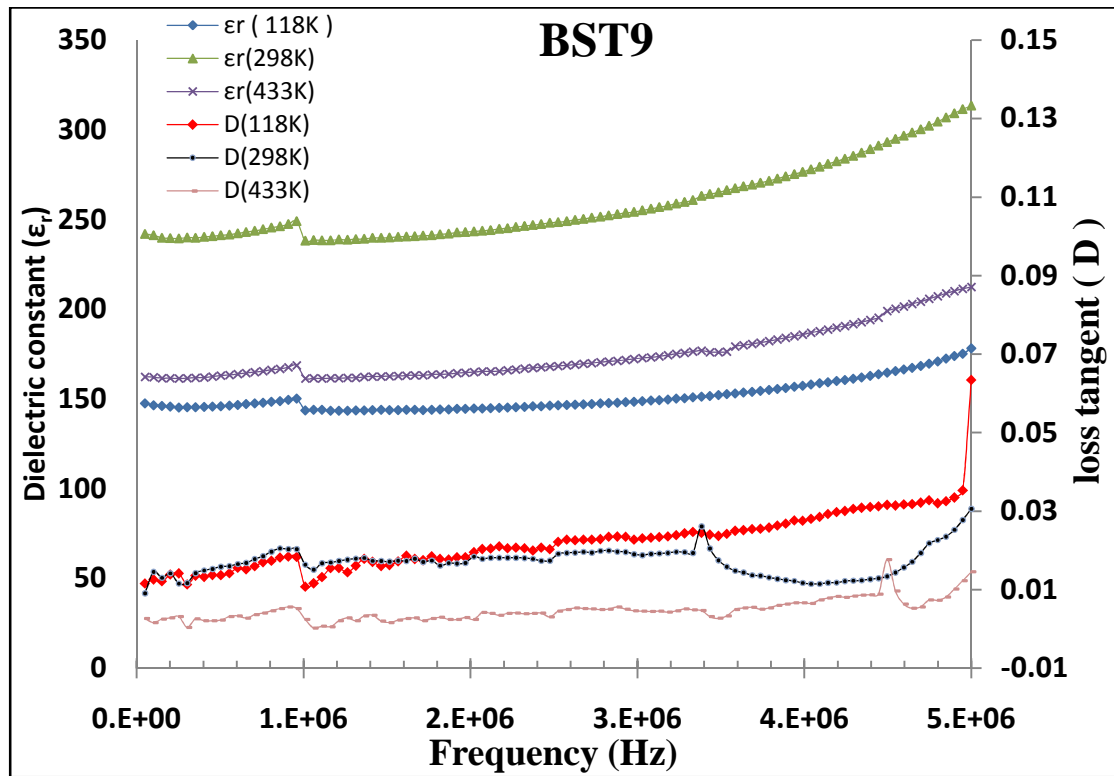


Fig.3.32: Dielectric constant and loss tangent vs frequency for BST9

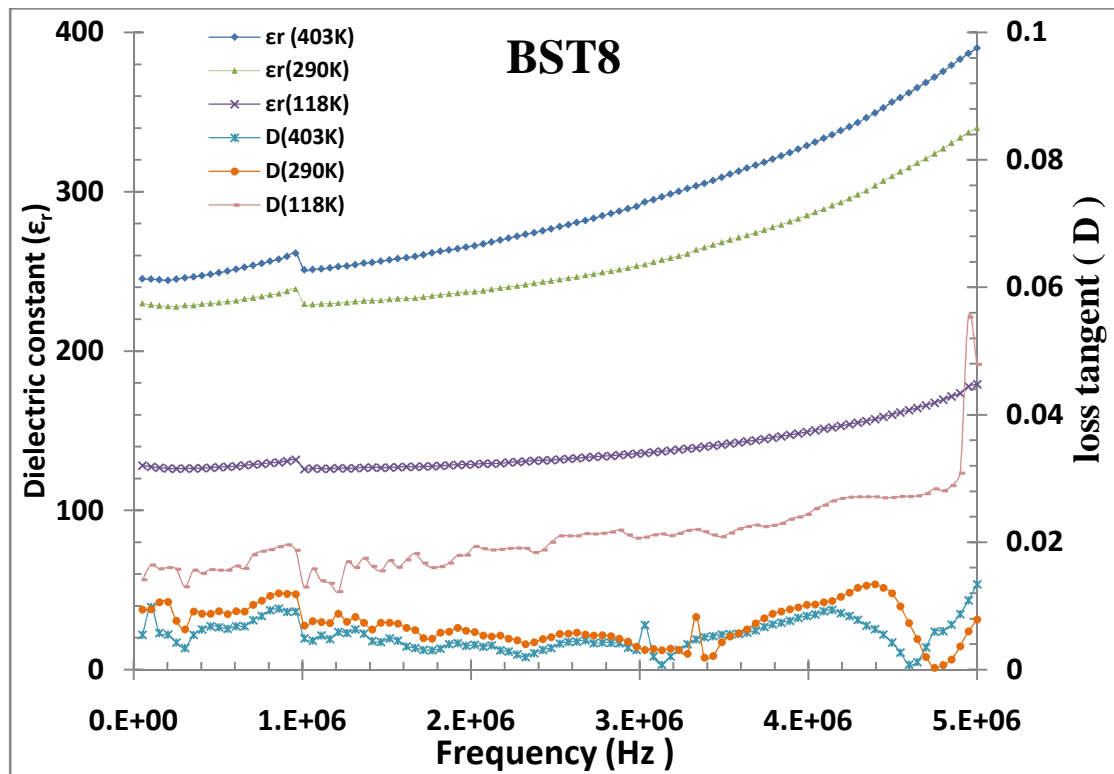


Fig.3.33: Dielectric constant and loss tangent vs frequency for BST8

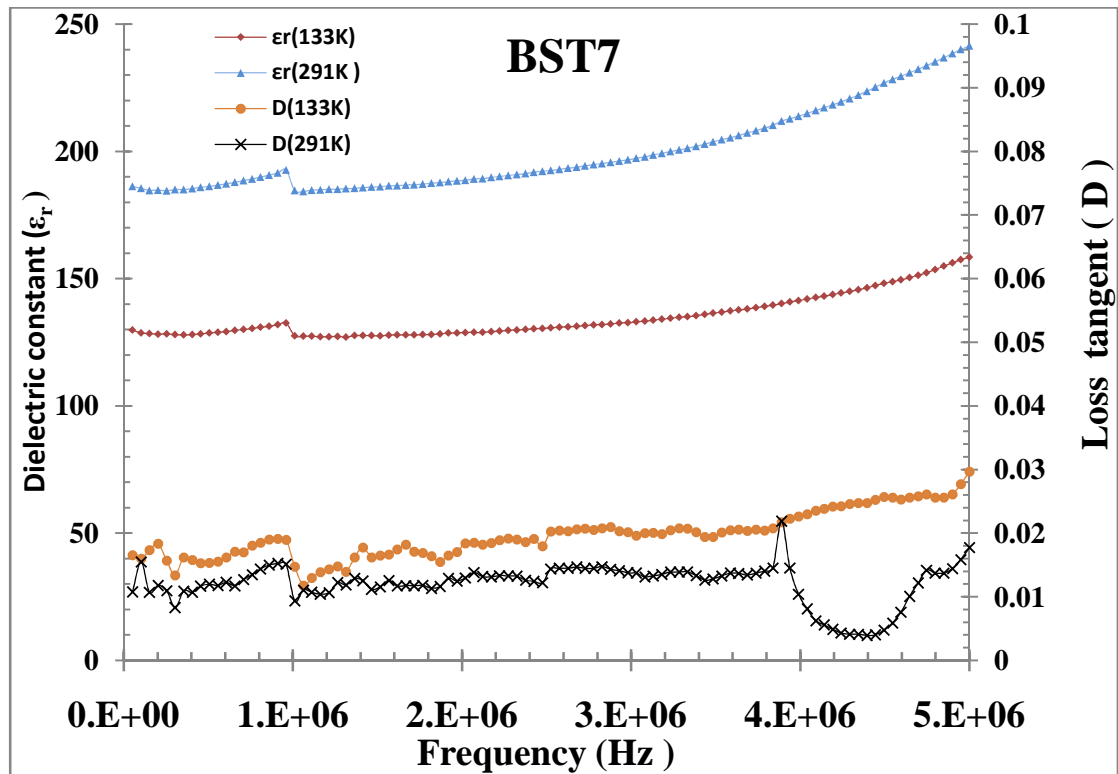


Fig.3.34: Dielectric constant and loss tangent vs frequency for BST7

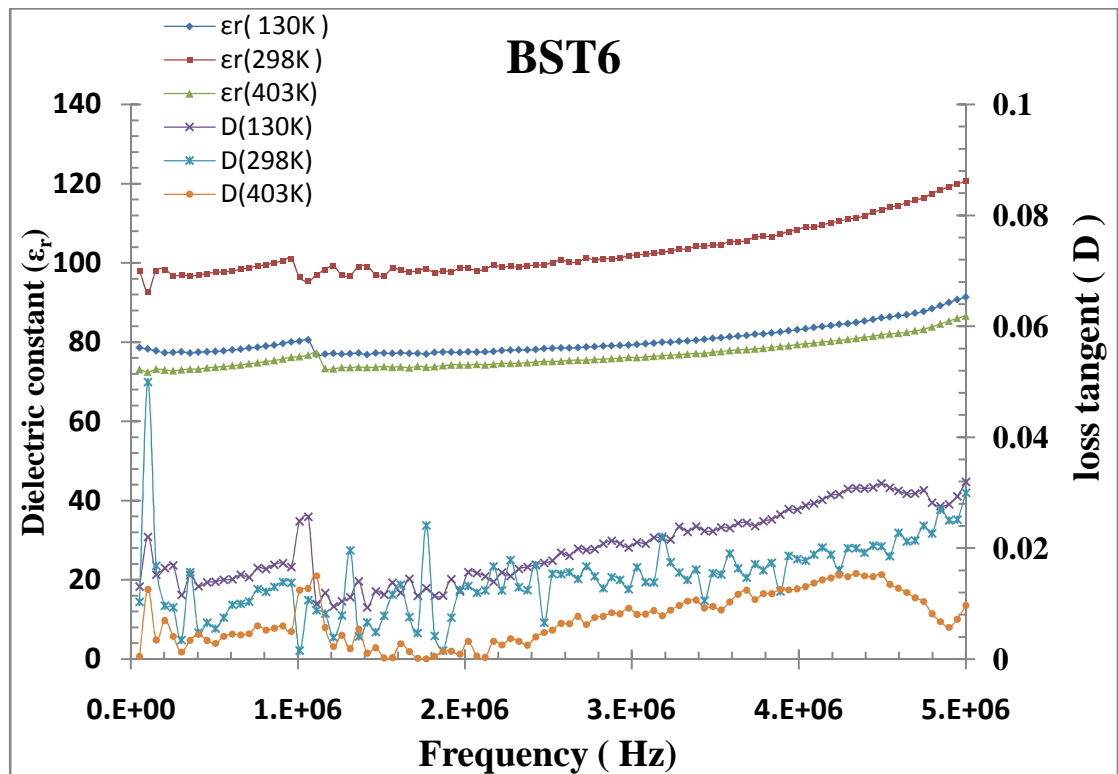


Fig.3.35: Dielectric constant and loss tangent vs frequency for BST6

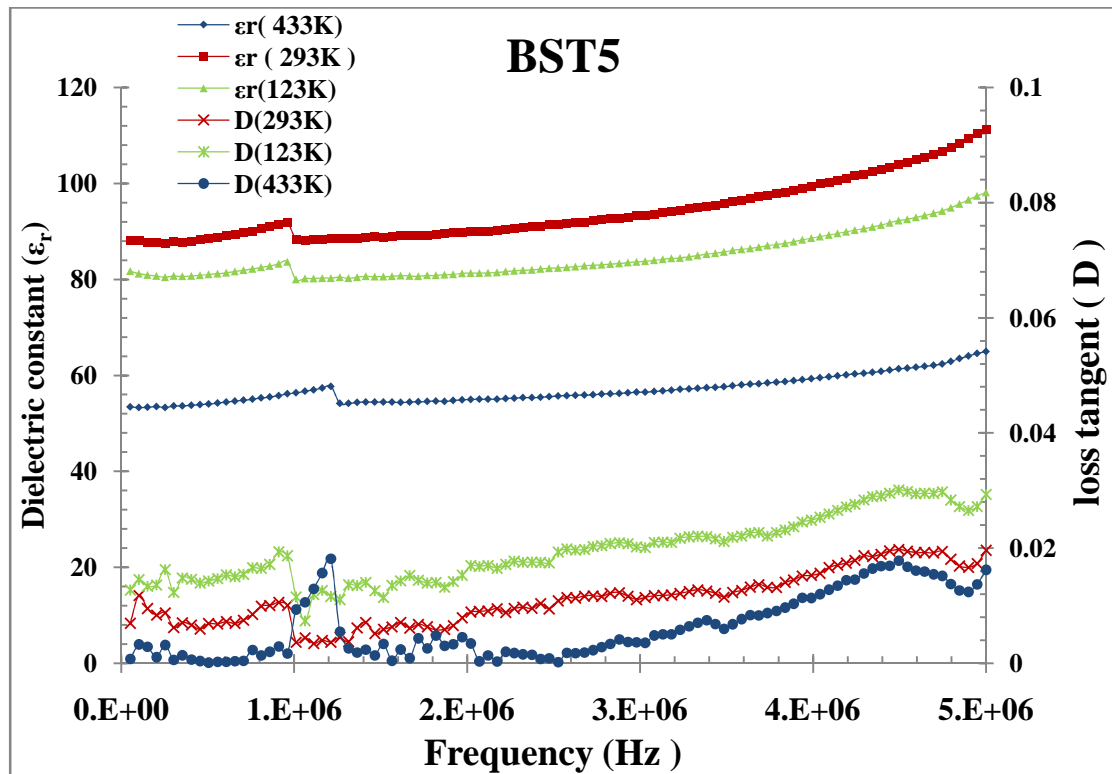


Fig.3.36: Dielectric constant and loss tangent vs frequency for BST5

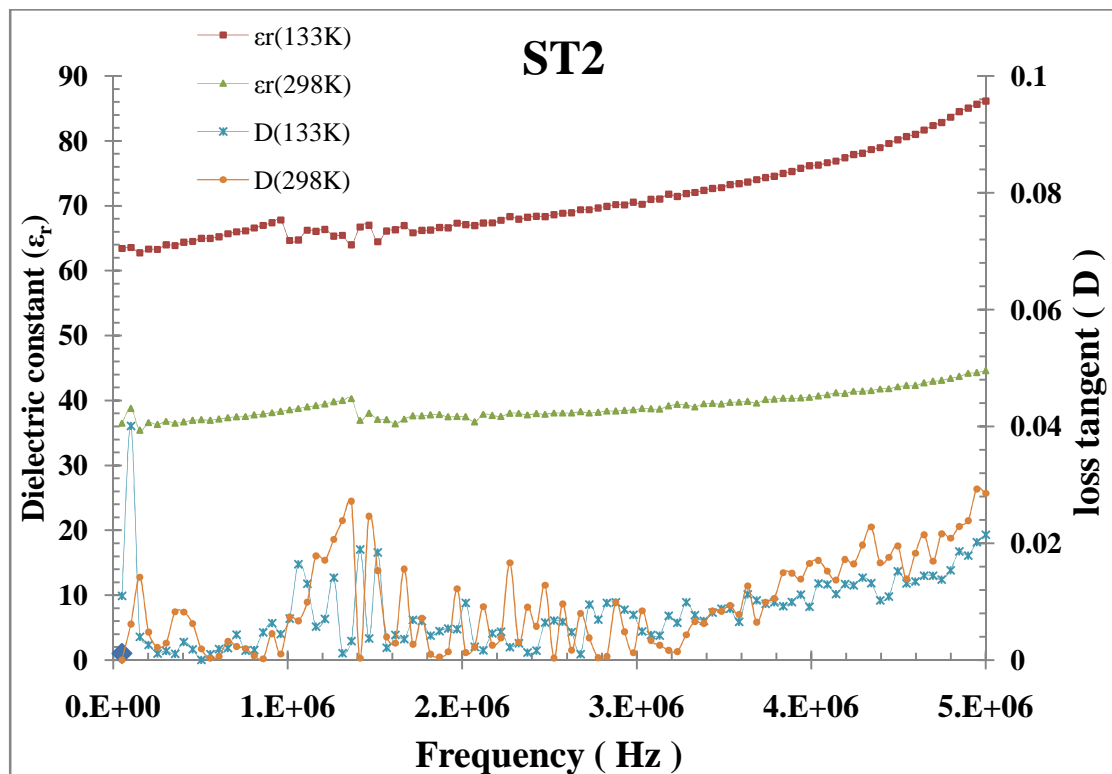


Fig.3.37: Dielectric constant and loss tangent vs frequency for ST

The dielectric constant and loss tangent are slightly increasing with frequency, for BST samples the value of dielectric constant has the maximum value for BT and the minimum value for ST, while for the loss tangent the maximum value is for BT and the minimum value is for BST8

and BST7, which means that BST8, BST7 have very low leakage current which is very important for many applications such as MOSFETs and Microwave applications.

3.5.2 Temperature measurement

The temperature characterization of dielectric constant and loss tangent for BST samples at different frequencies (1 KHz, 10 KHz, 100 KHz and 1 MHz) are shown in the following figures (Fig.3.38 – Fig.3.74).

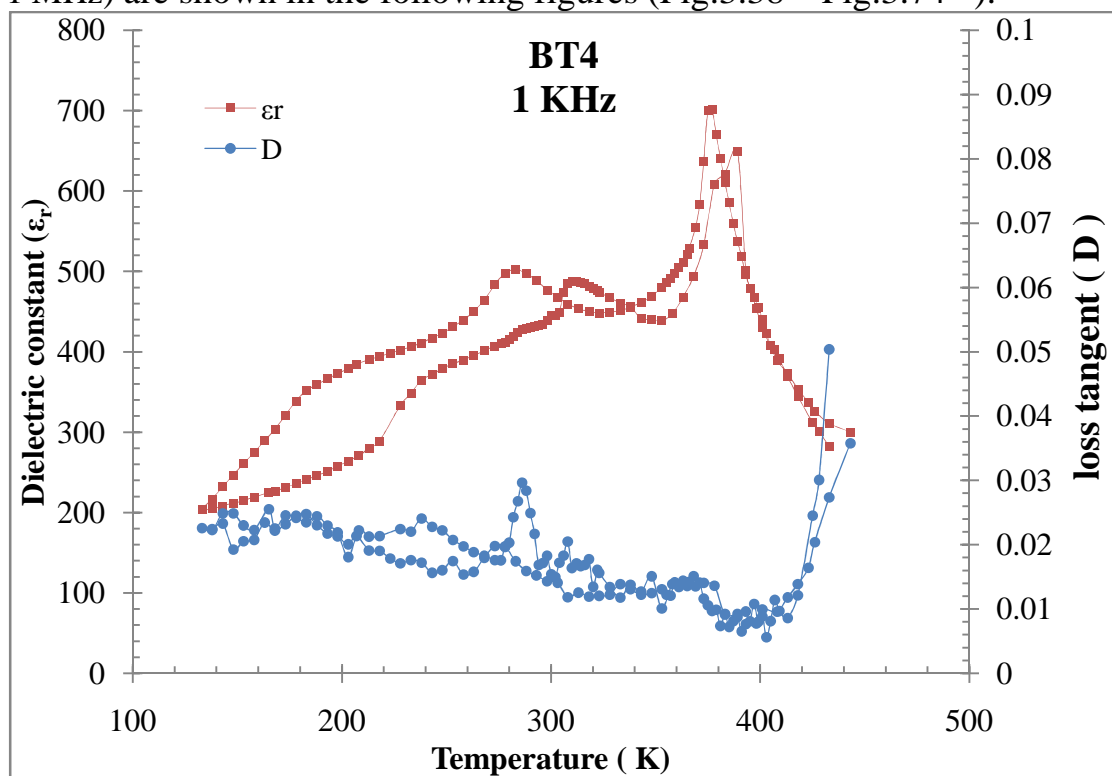


Fig.3.38: The dielectric constant and loss tangent vs temperature for BT at 1 KHz

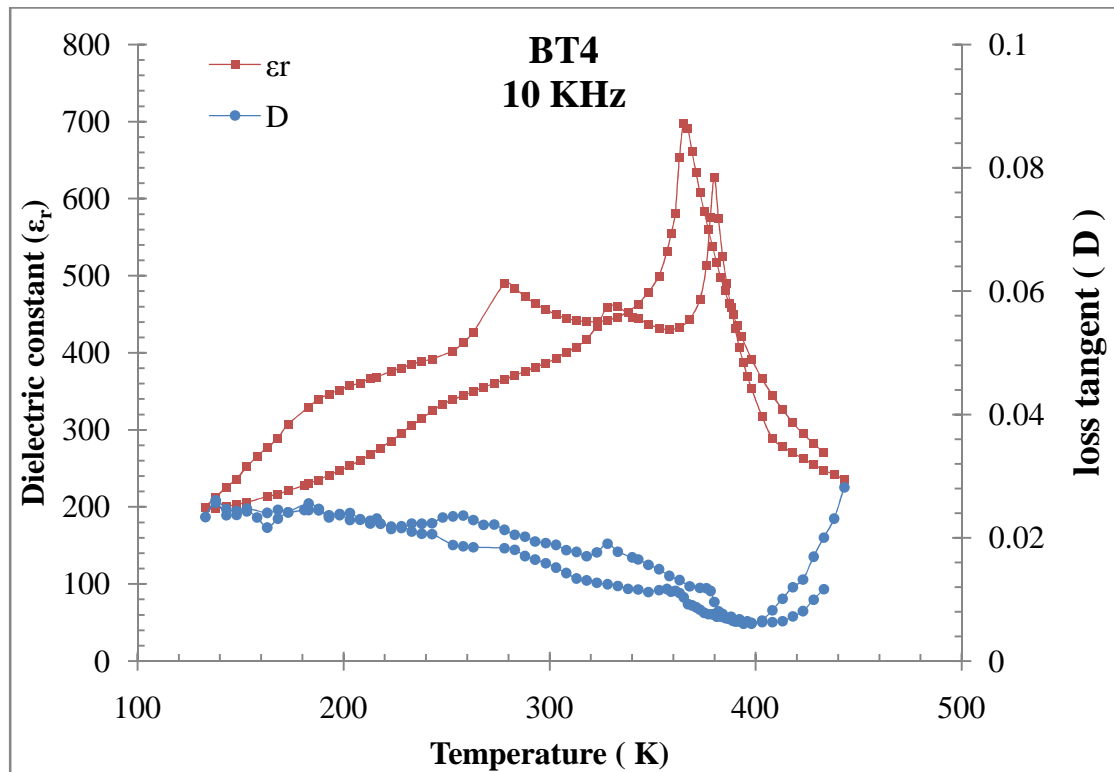


Fig.3.39: The dielectric constant and loss tangent vs temperature for BT at 10 KHz

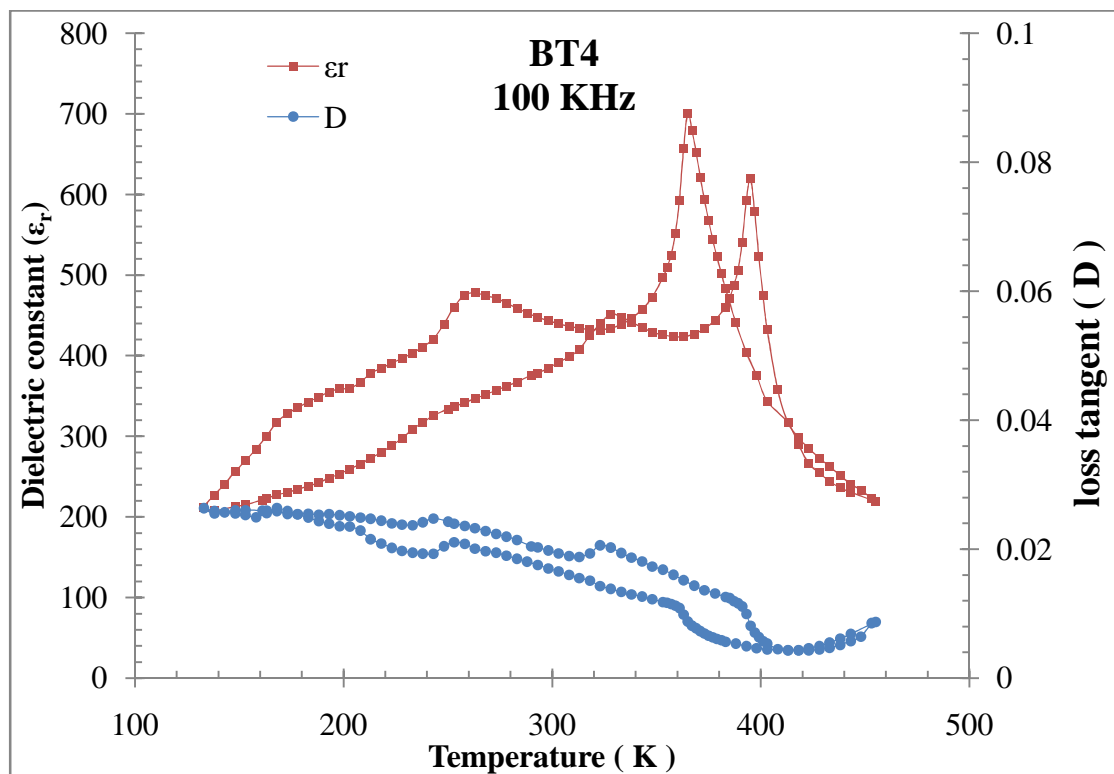


Fig.3.40: The dielectric constant and loss tangent vs temperature for BT at 100 KHz

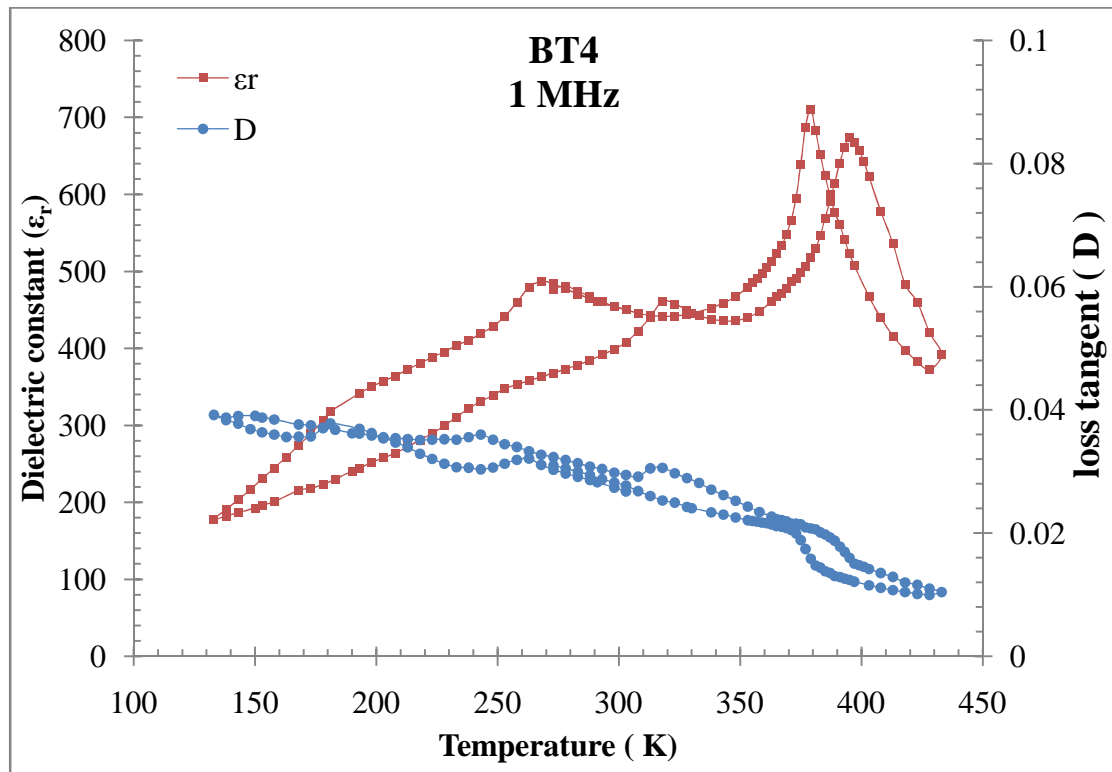


Fig.3.41: The dielectric constant and loss tangent vs temperature for BT at 1 MHz

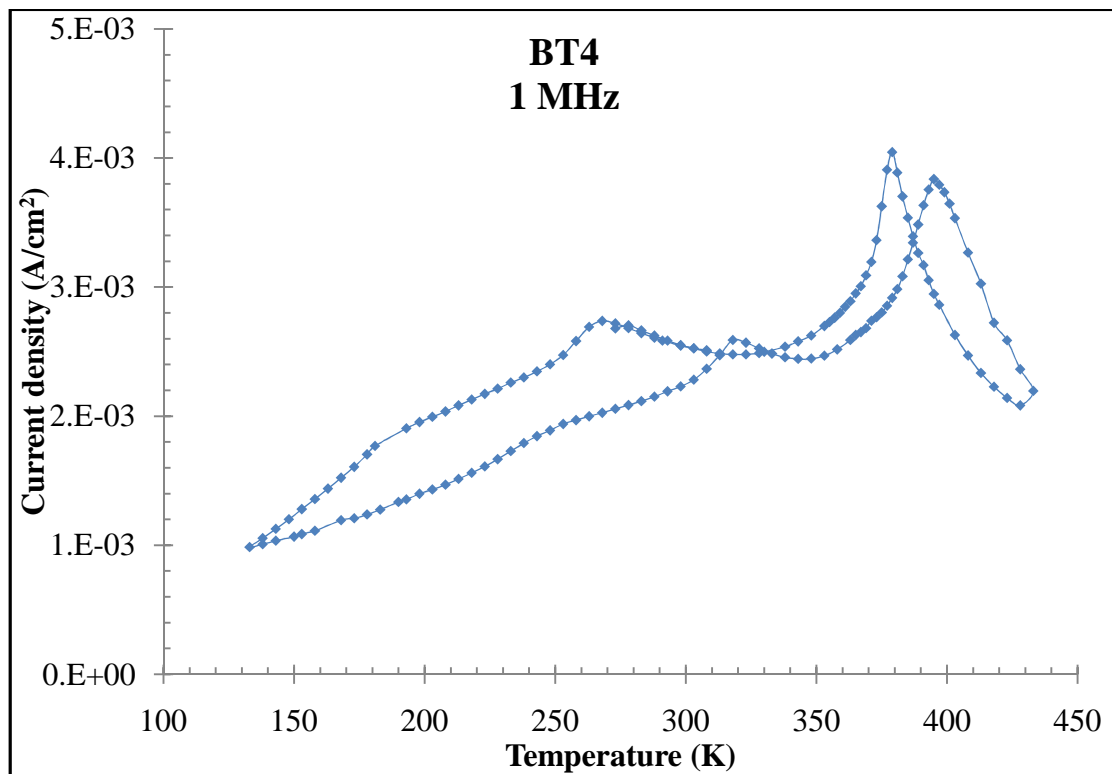


Fig.3.42: The Current density vs temperature for BT4 at 1 MHz

The temperature measurements of dielectric constant and loss tangent (Fig.3.38 – Fig.3.41) for BT at different frequencies (1 KHz, 10 KHz, 100 KHz and 1 MHz) under vacuum conditions for heating and cooling cycle showed that the average value of Curie temperature for BT is 372 K for the cooling cycle while for heating cycle is 401 K. For the temperature measurement of the current density at 1 MHz (Fig.3.42), there is a transition at $T= 365$ K and $T=400$ K for cooling and heating cycle respectively.

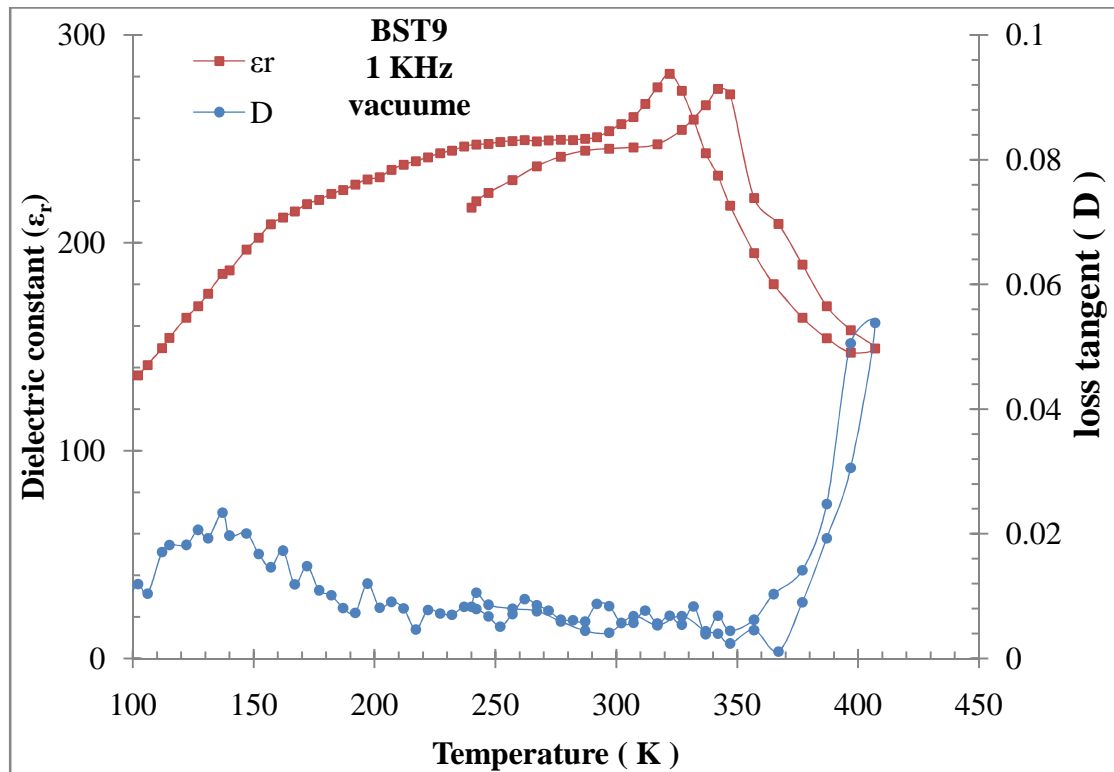


Fig.3.43: The dielectric constant and loss tangent vs temperature for BST9 at 1 KHz

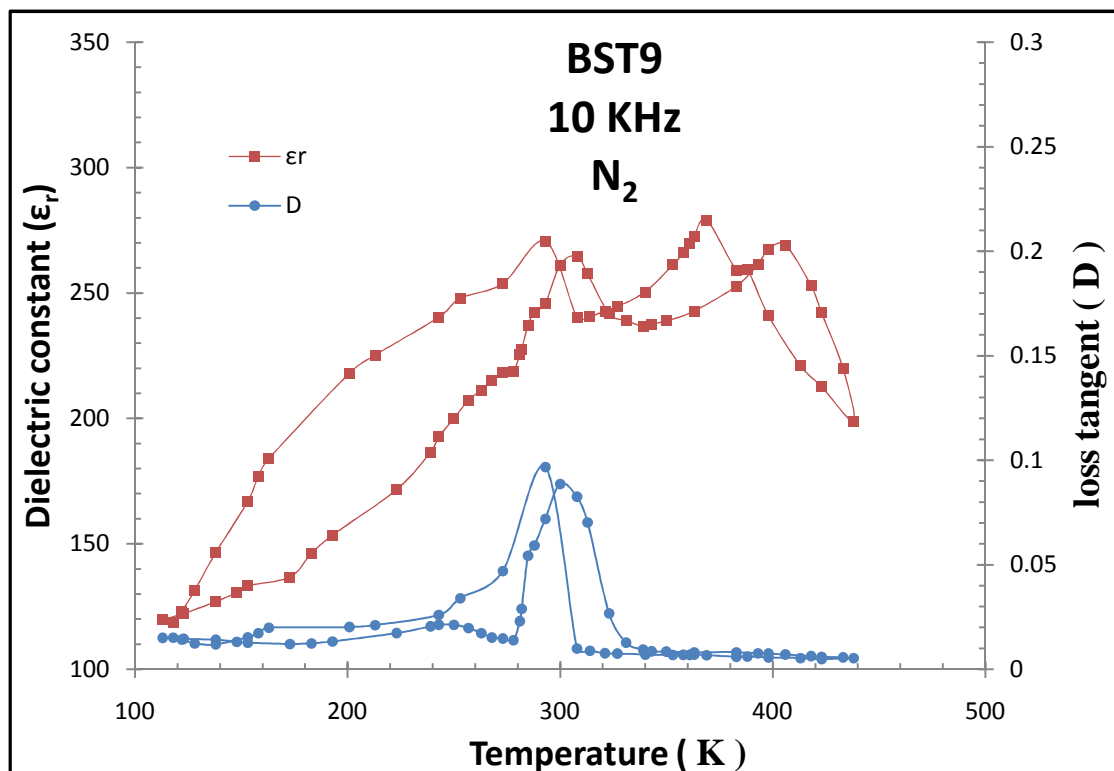


Fig.3.44: The dielectric constant and Loss tangent vs temperature for BST9 at 10 KHz

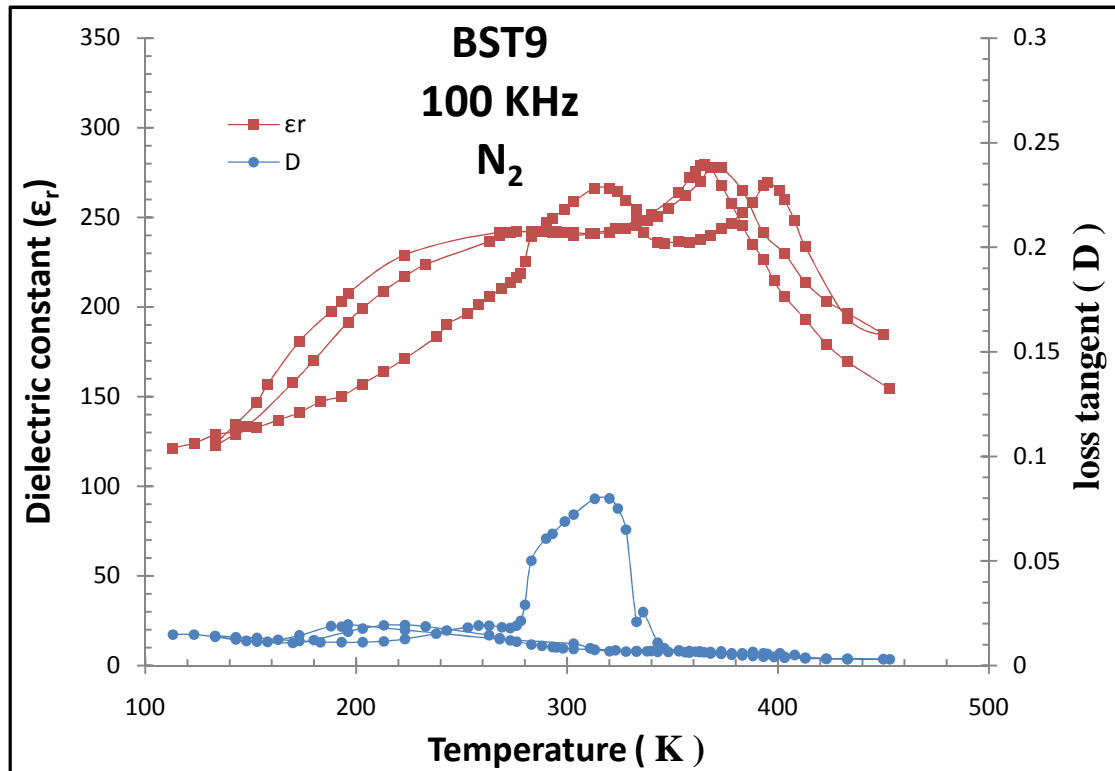


Fig.3.45: The dielectric constant and loss tangent vs temperature for BST9 at 100 KHz

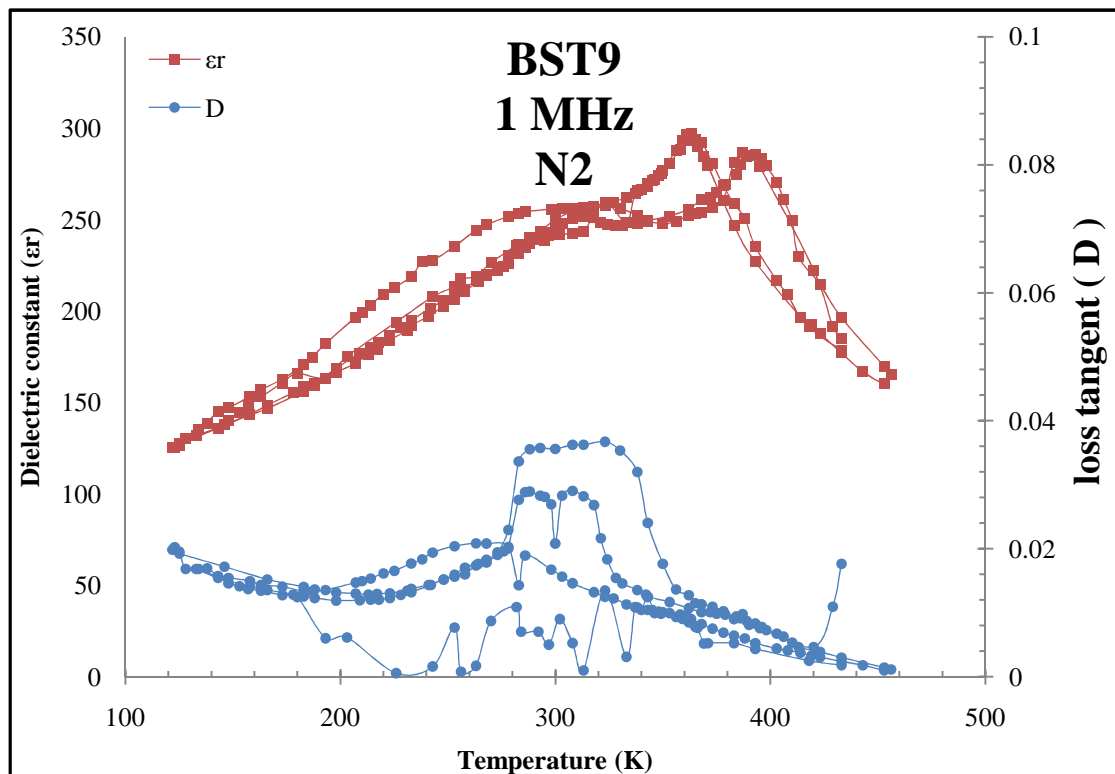


Fig.3.46: The dielectric constant and loss tangent vs temperature for BST9 at 1 MHz

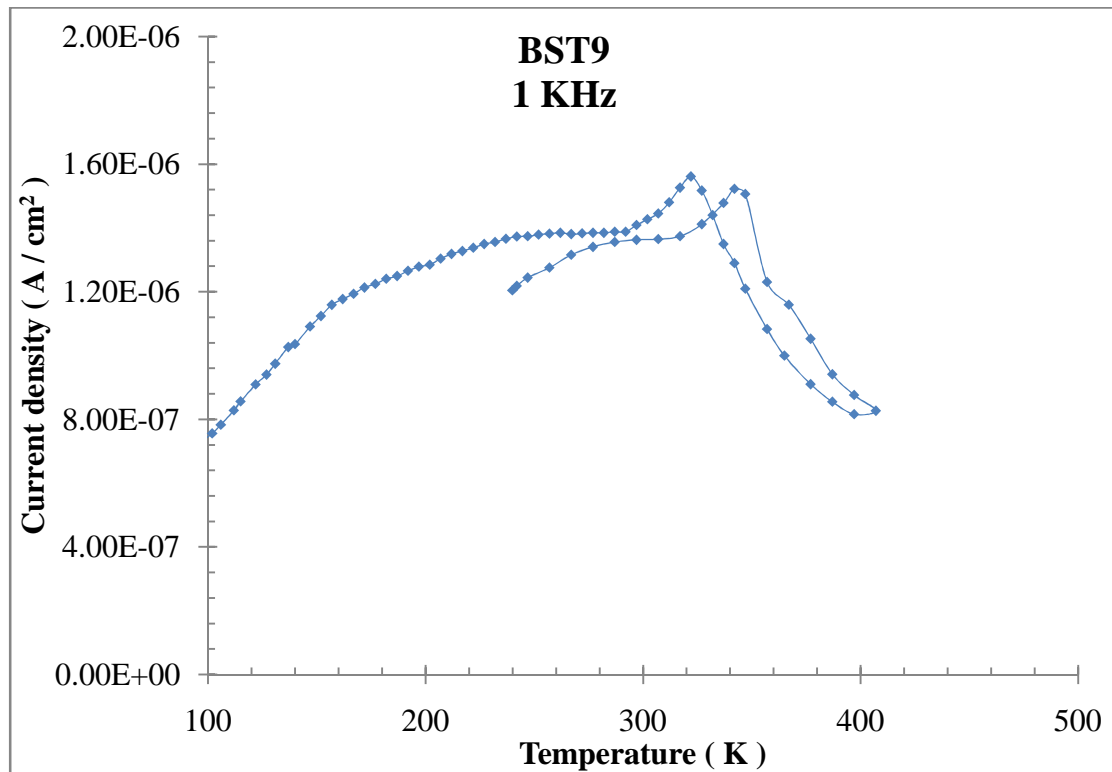


Fig.3.47: The Current density vs temperature for BST9 at 1 KHz.

The temperature measurements of dielectric constant and loss tangent (Fig.3.43) under vacuum conditions (Fig.3.44– Fig.3.46) under Nitrogen pressure for BST9 at different frequencies (1 KHz, 10 KHz, 100 KHz and 1 MHz) for heating and cooling cycle showed that the average value of Curie temperature for BST9 is 364.8 K for the cooling cycle while for heating cycle is 388.8 K. For the temperature measurement of the current density was performed at 1 KHz under vacuum condition (Fig.3.47), there is a transition at $T= 358$ K and $T=378$ K for cooling and heating cycle respectively.

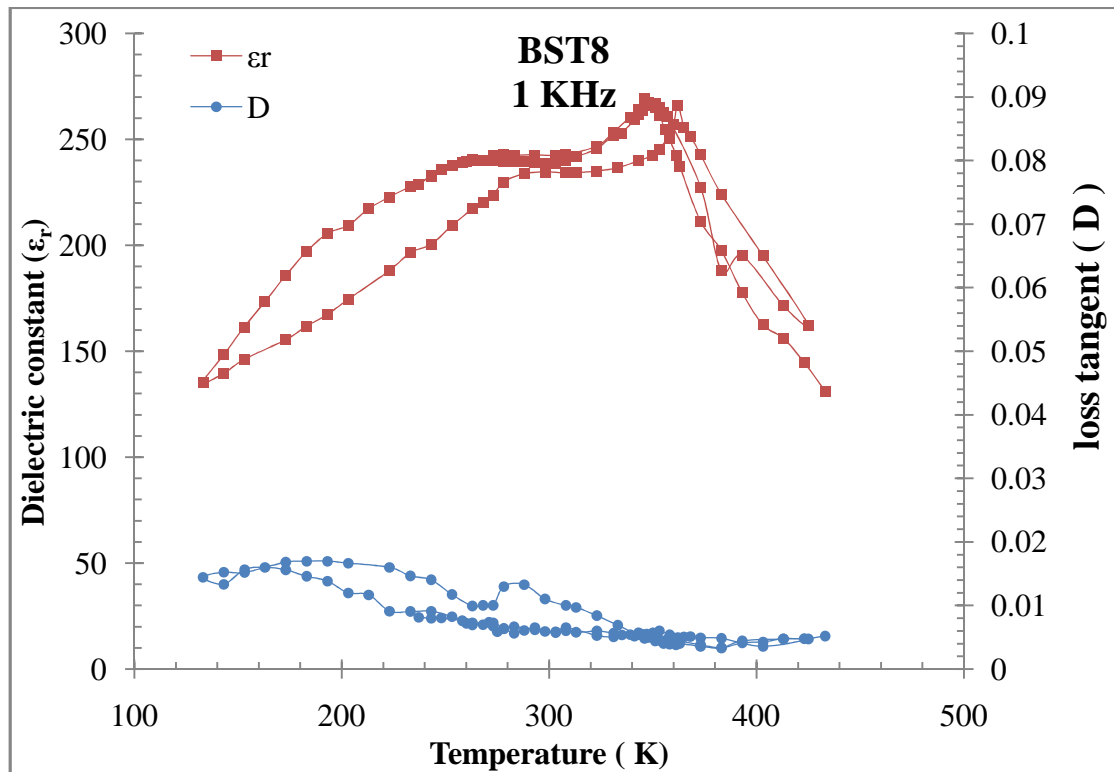


Fig.3.48: The dielectric constant and loss tangent vs temperature for BST8 at 1 KHz

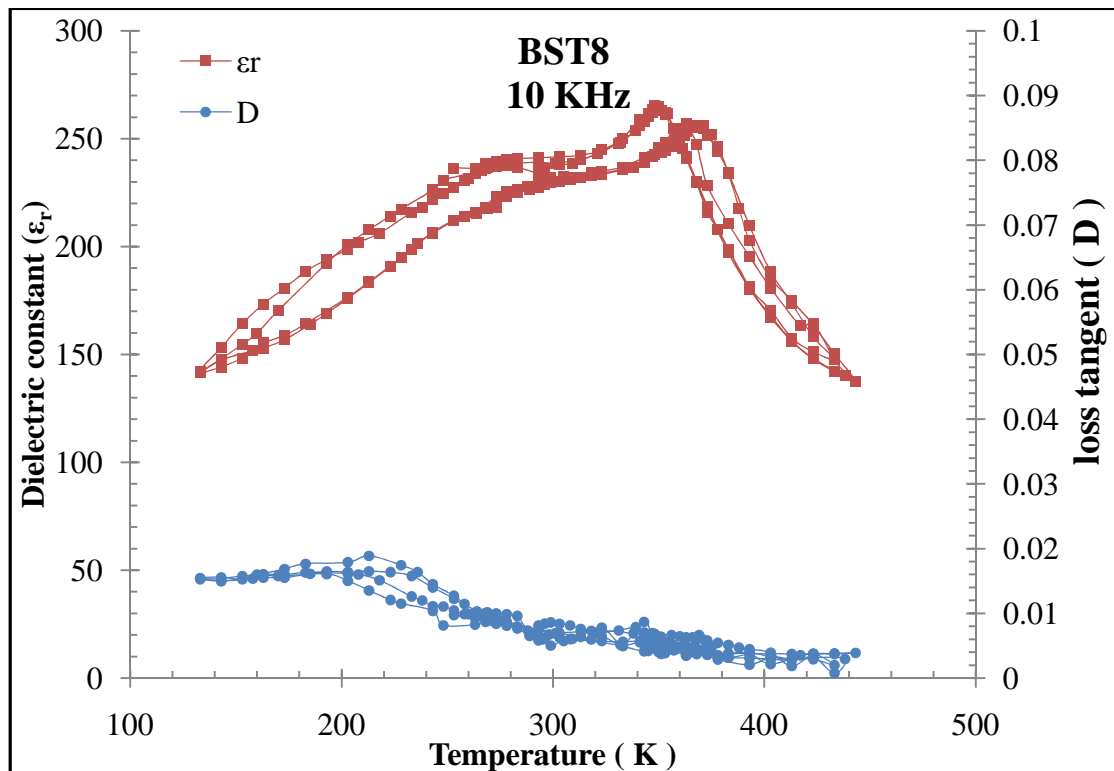


Fig.3.49: The dielectric constant and loss tangent vs temperature for BST8 at 10 KHz.

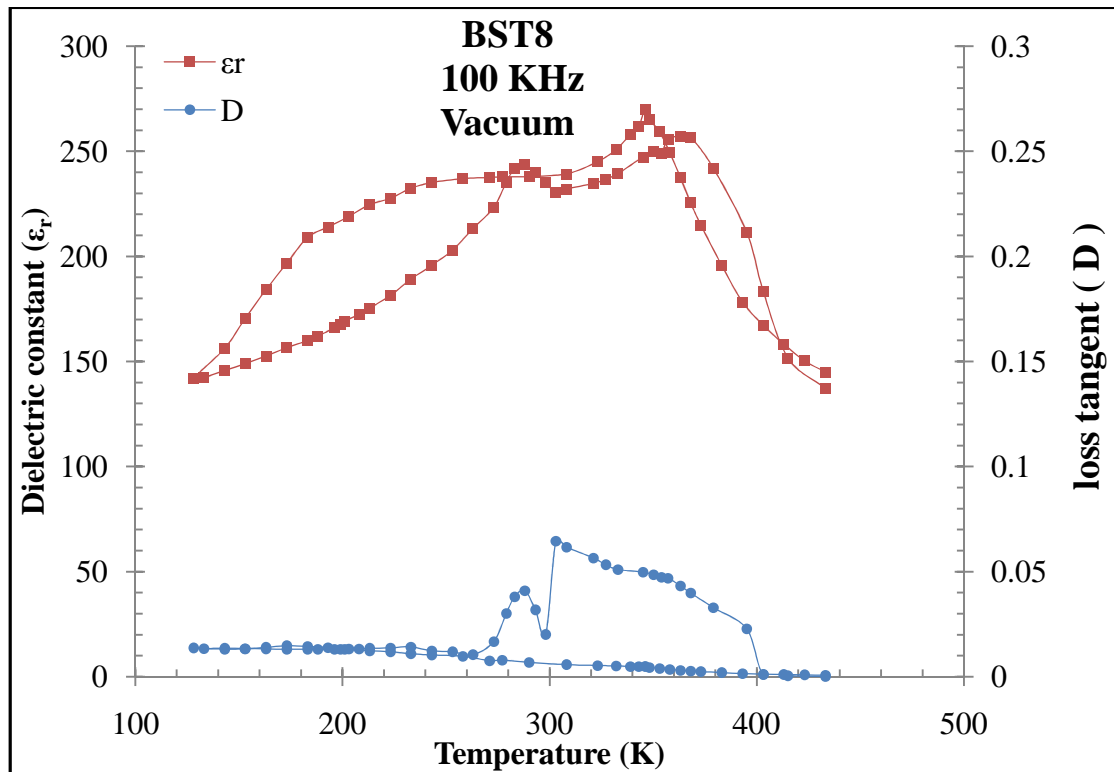


Fig.3.50: The dielectric constant and loss tangent vs temperature for BST8 at 100 KHz

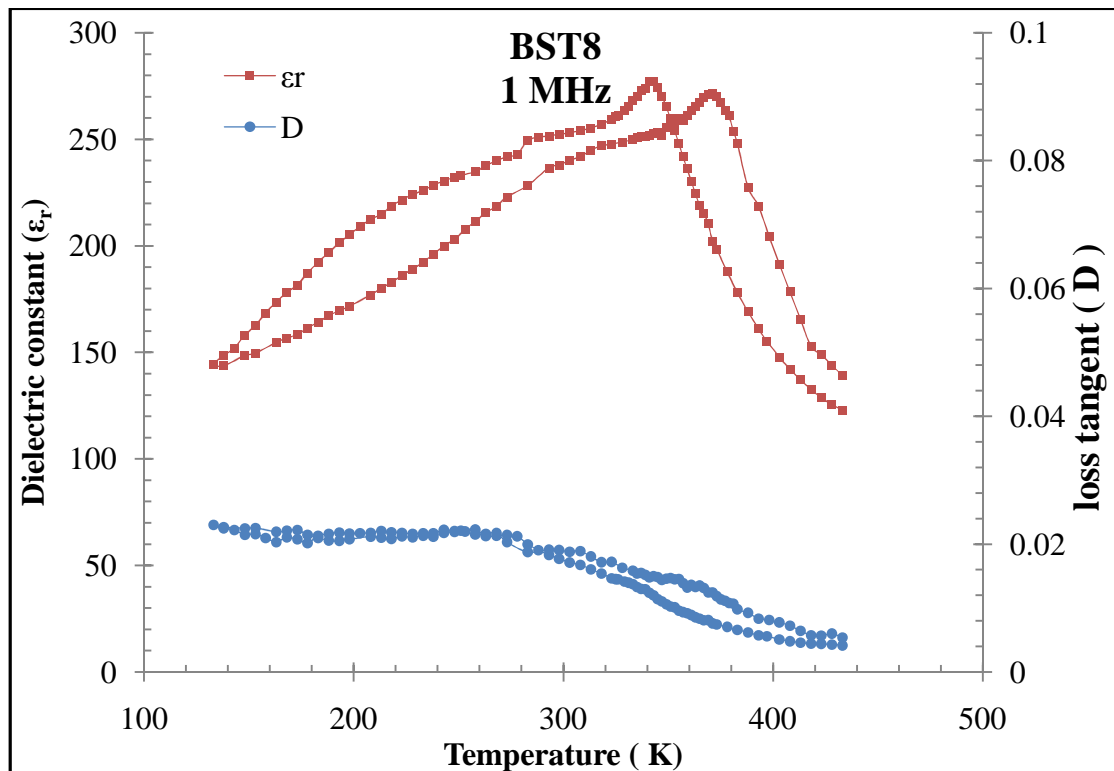


Fig.3.51: The dielectric constant and loss tangent vs temperature for BST8 at 1 MHz

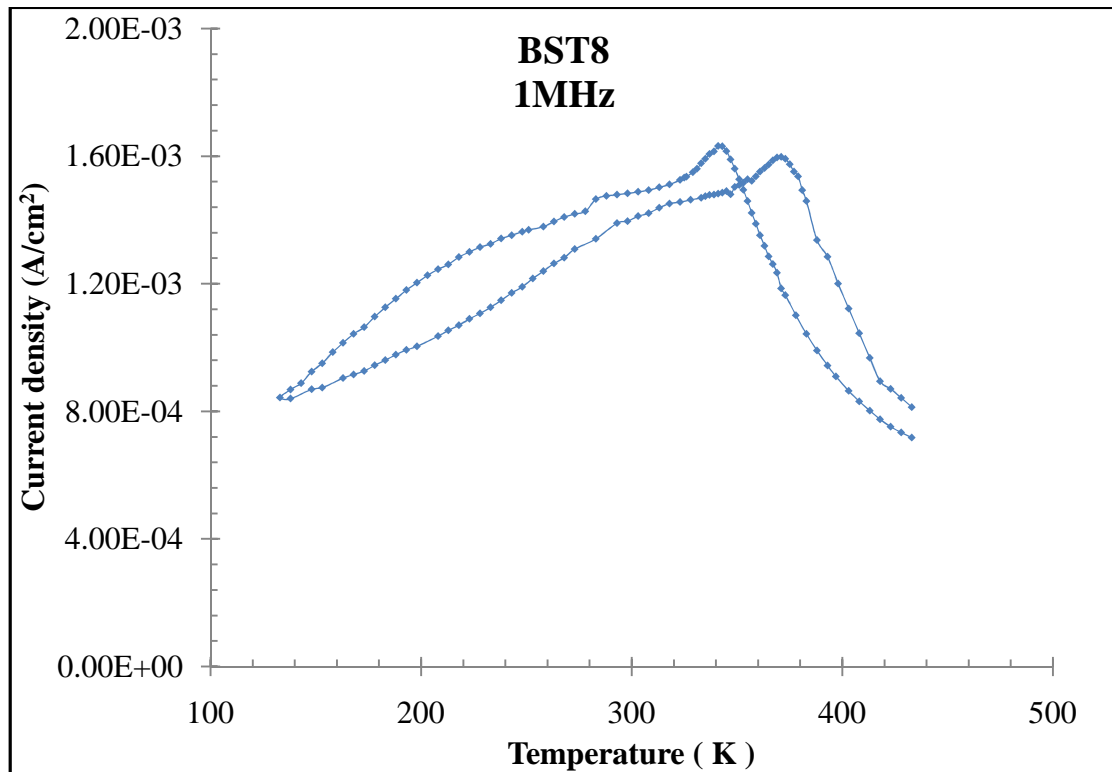


Fig.3.52: The Current density vs temperature for BST8 at 1 MHz.

The temperature measurements of dielectric constant and loss tangent (Fig.3.48 – Fig.3.51) for BST8 at different frequencies (1 KHz, 10 KHz, 100 KHz and 1 MHz) under vacuum conditions for heating and cooling cycle showed that the average value of Curie temperature for BST8 is 346.7 K for the cooling cycle while for heating cycle is 367 K . For the temperature measurement of the current density at 1 MHz under vacuum conditions (Fig.3.52), there is a transition at $T= 340$ K and $T=370$ K for cooling and heating cycle respectively.

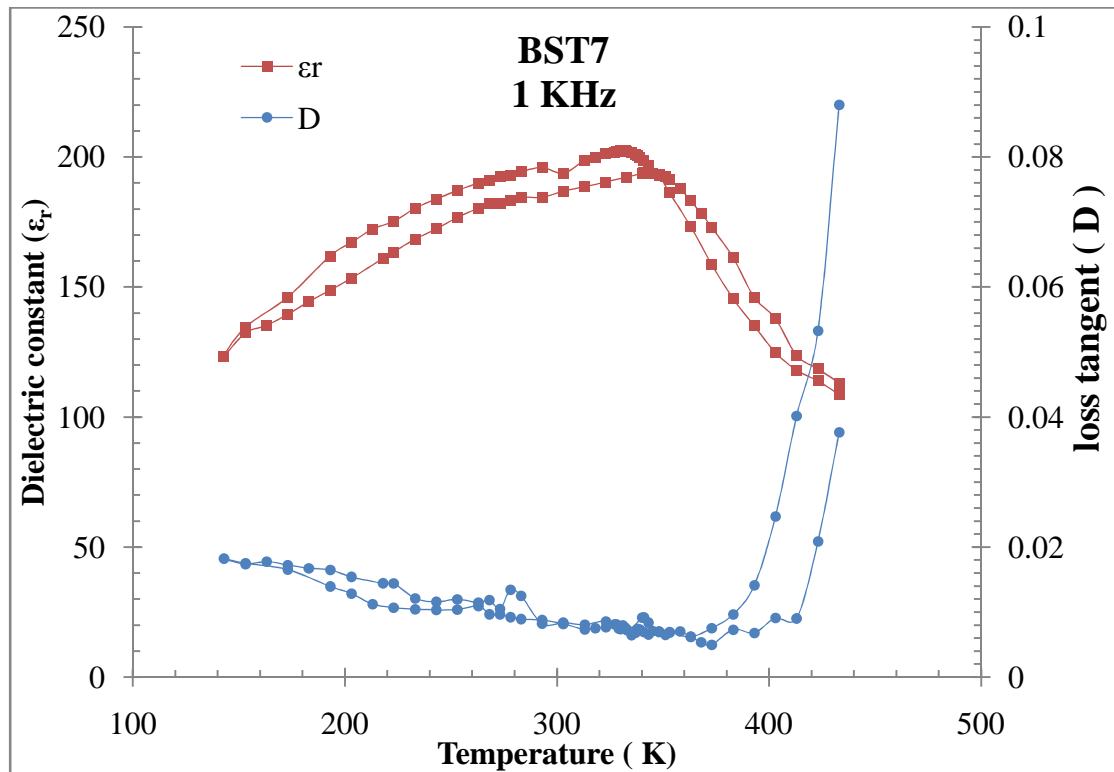


Fig.3.53: The dielectric constant and loss tangent vs temperature for BST7 at 1 KHz.

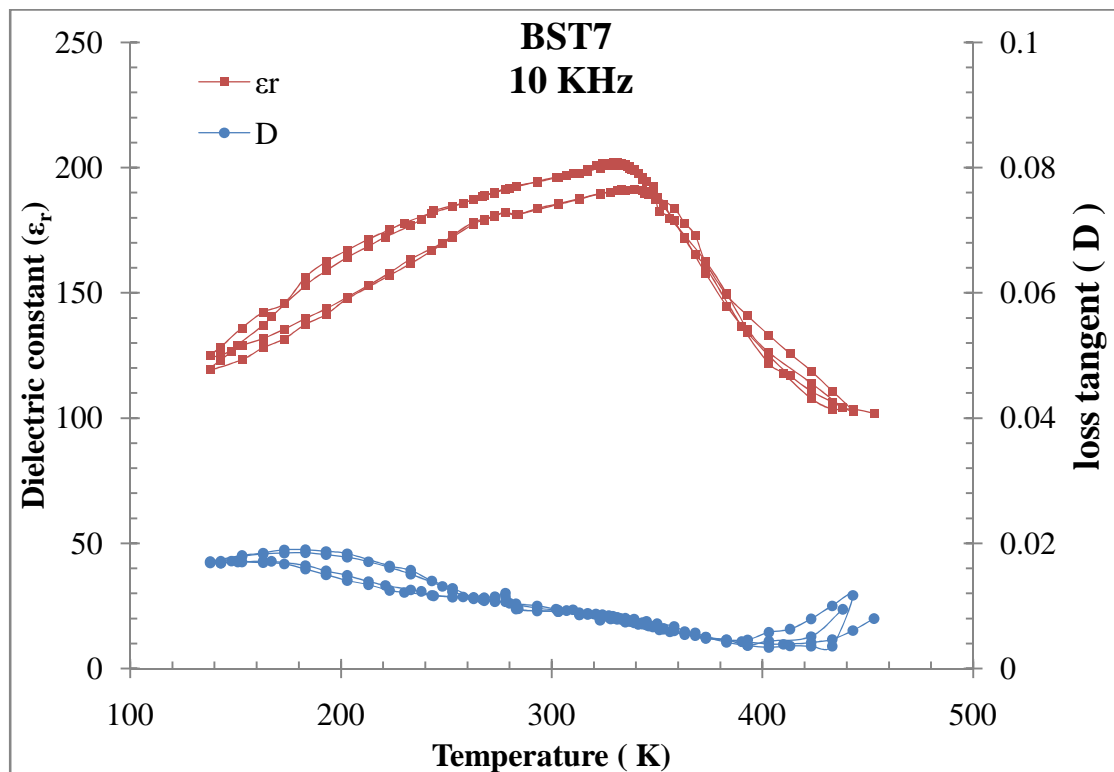


Fig.3.54: The dielectric constant and loss tangent vs temperature for BST7 at 10 KHz

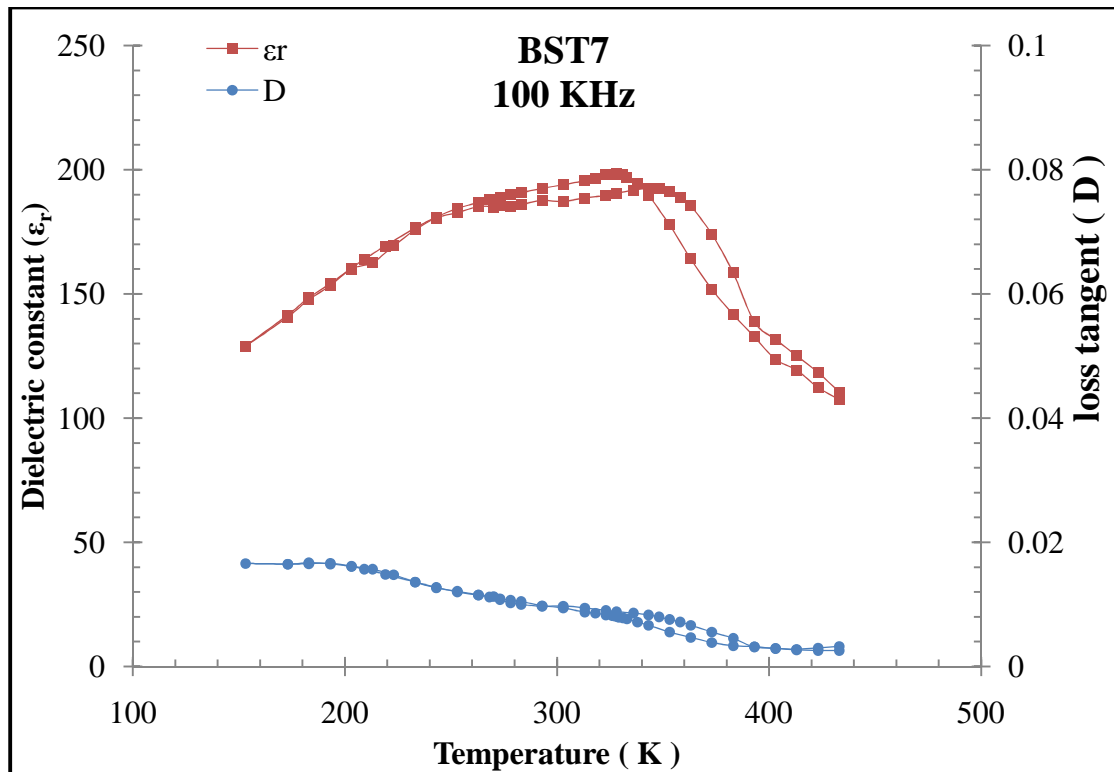


Fig.3.55: The dielectric constant and loss tangent vs temperature for BST7 at 100 KHz

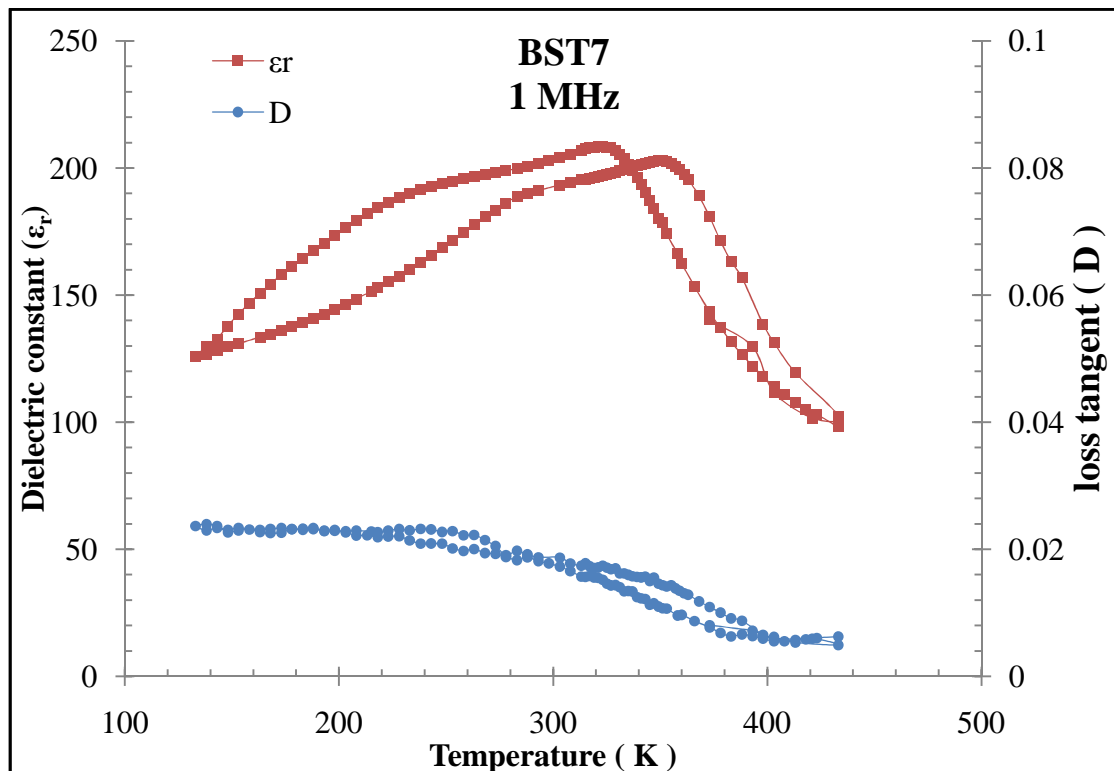


Fig.3.56: The dielectric constant and loss tangent vs temperature for BST7 at 1 MHz

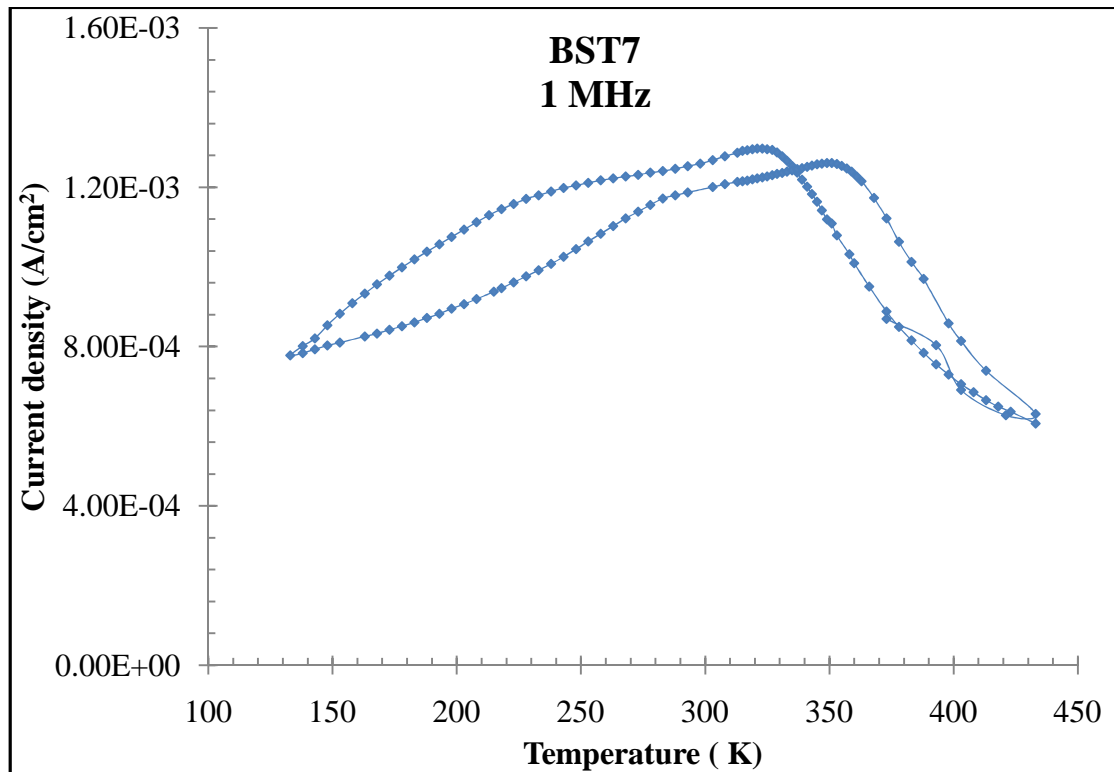


Fig.3.57: The current density vs temperature for BST7 at 1 MHz

The temperature measurements of dielectric constant and loss tangent (Fig.3.53 – Fig.3.56) for BST7 at different frequencies (1 KHz, 10 KHz, 100 KHz and 1 MHz) under vacuum conditions for heating and cooling cycle showed that the average value of Curie temperature for BST7 is 329 K for the cooling cycle while for heating cycle is 341K . For the temperature measurement of the current density at 1 MHz under vacuum conditions (Fig.3.57), there is a transition at $T= 323$ K and $T=349$ K for cooling and heating cycle respectively.

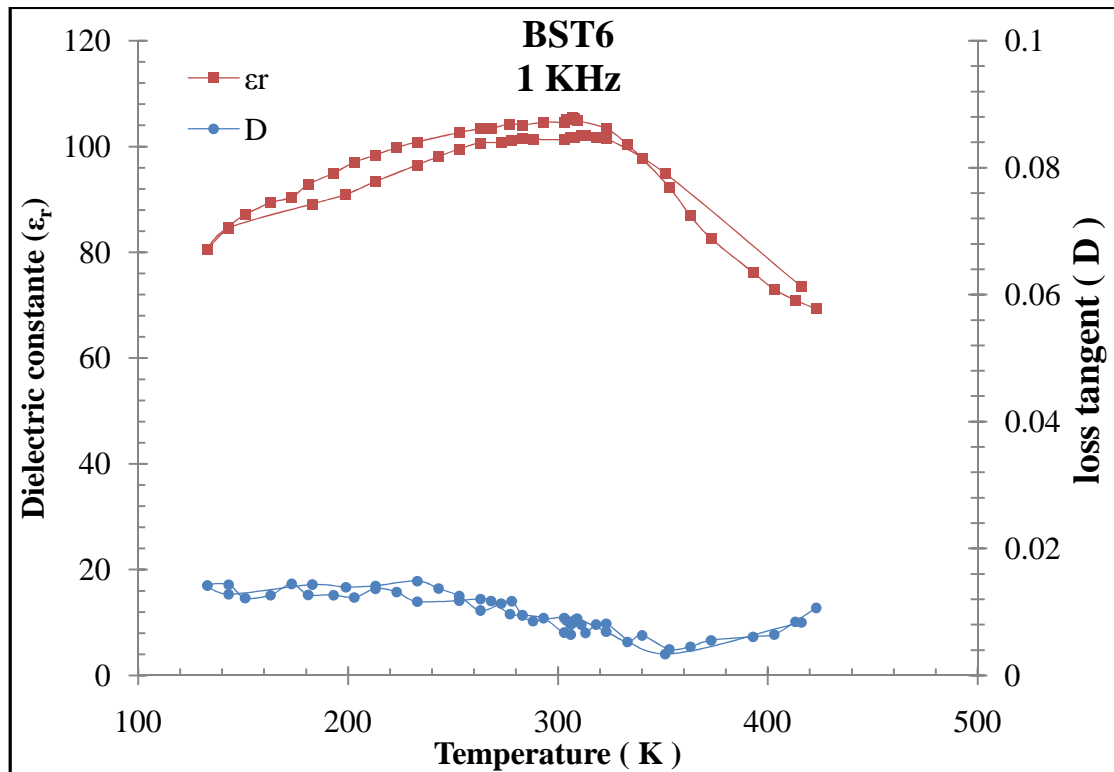


Fig.3.58: The dielectric constant and loss tangent vs temperature for BST6 at 1 KHz

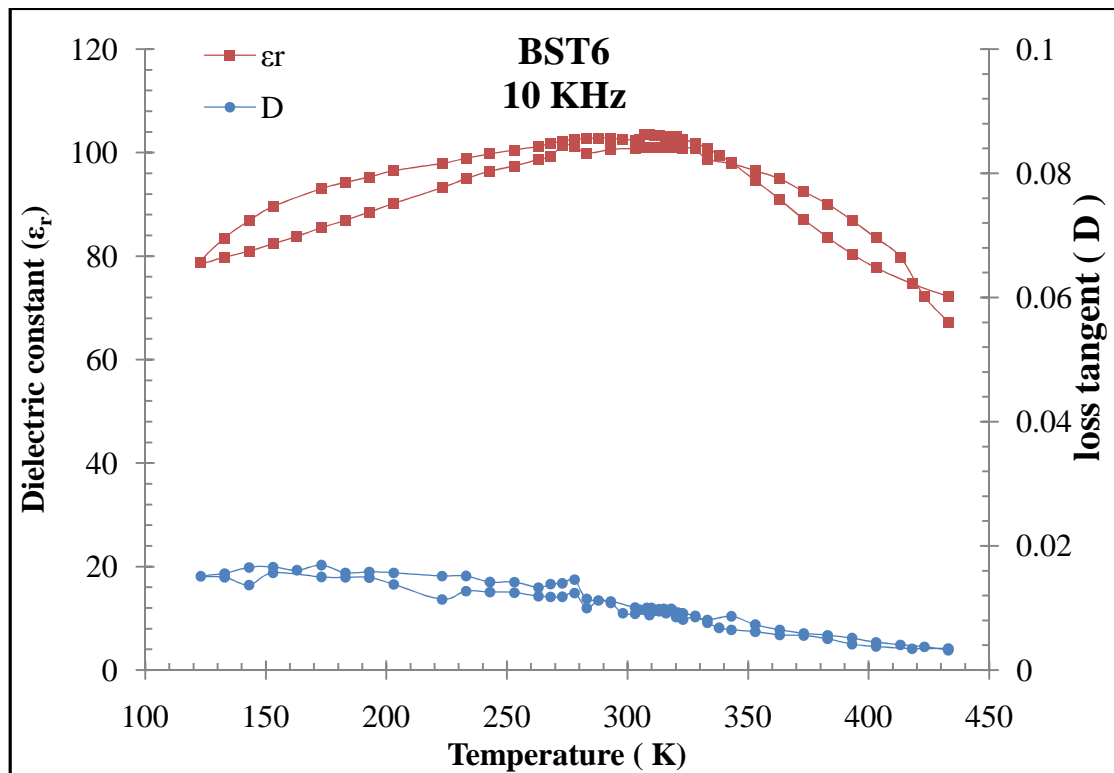


Fig.3.59: The dielectric constant and loss tangent vs temperature for BST6 at 10 KHz

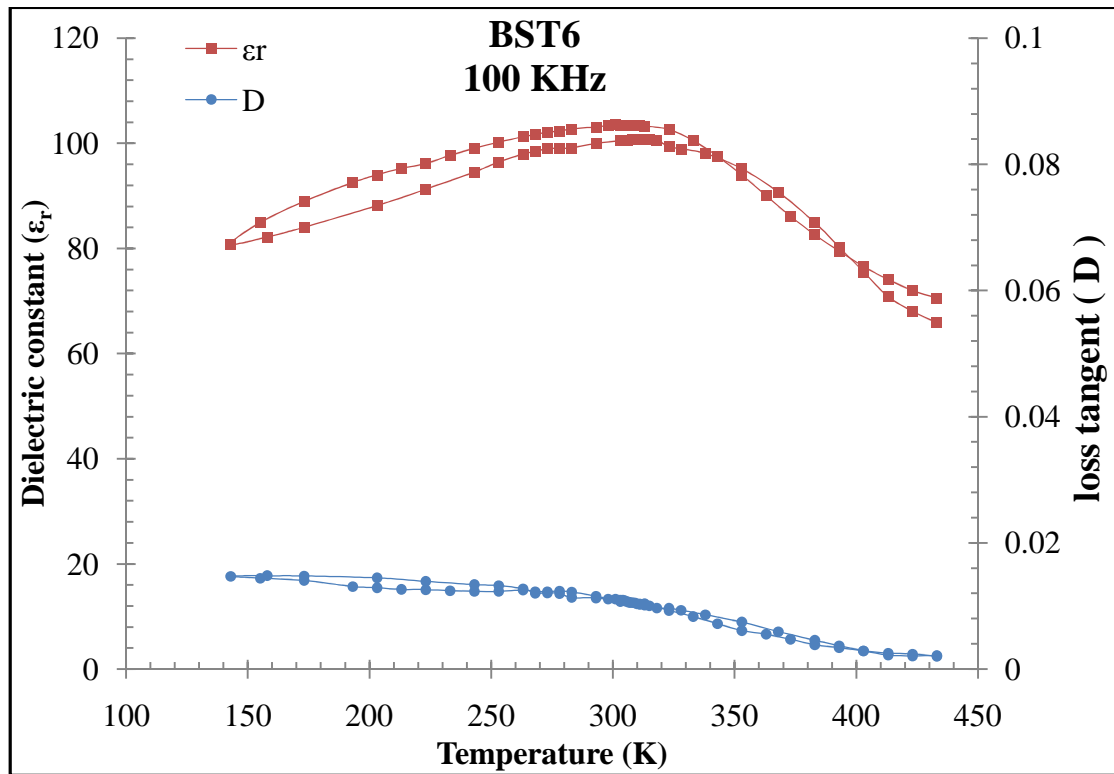


Fig.3.60: The dielectric constant and loss tangent vs temperature for BST6 at 100 KHz

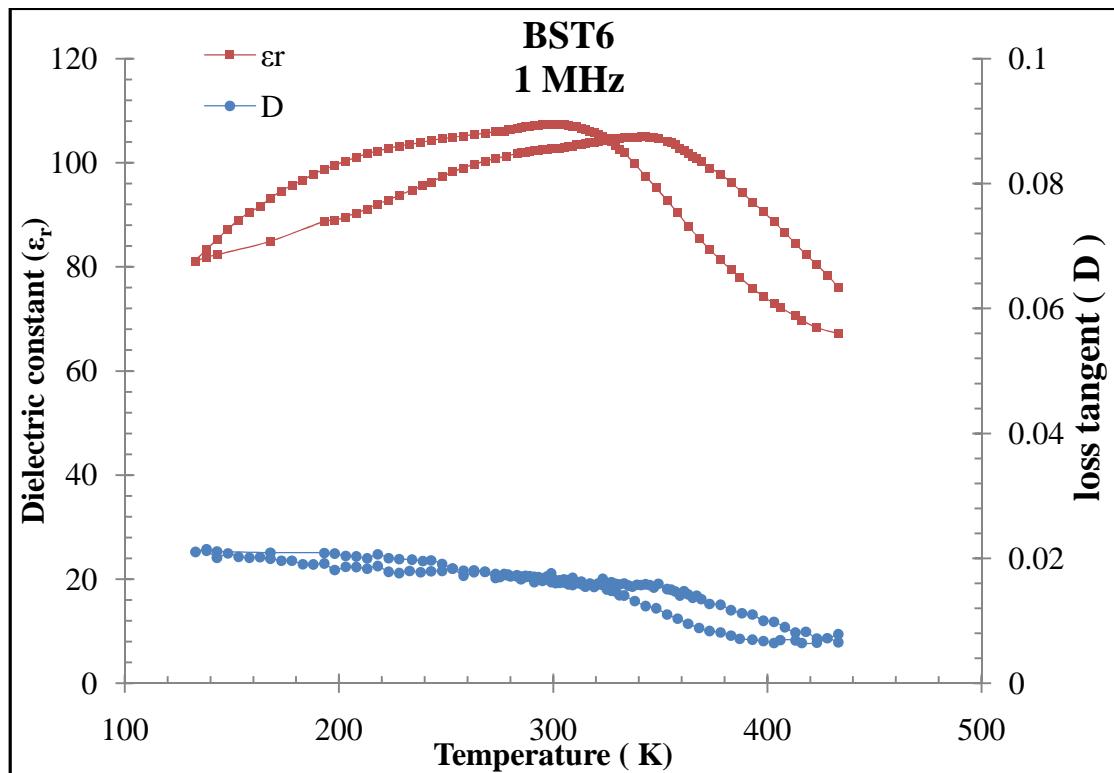


Fig.3.61: The dielectric constant and loss tangent vs temperature for BST6 at 1 MHz

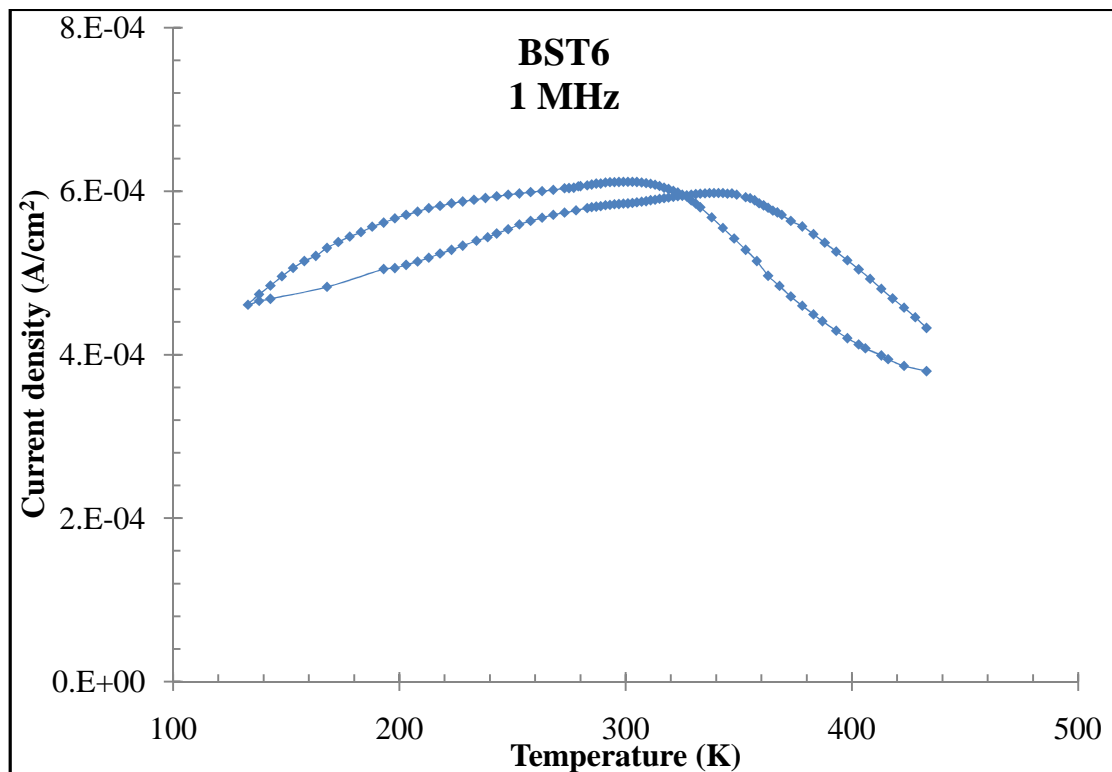


Fig.3.62: The Current density vs temperature for BST6 at 1 MHz

The temperature measurements of dielectric constant and loss tangent (Fig.3.58 – Fig.3.61) for BST6 at different frequencies (1 KHz, 10 KHz, 100 KHz and 1 MHz) under vacuum conditions for heating and cooling cycle showed that the average value of Curie temperature for BST6 is 307 K for the cooling cycle while for heating cycle is 312 K . For the temperature measurement of the current density at 1 MHz under vacuum conditions (Fig.3.62), there is a transition at $T= 300$ K and $T=340$ K for cooling and heating cycle respectively

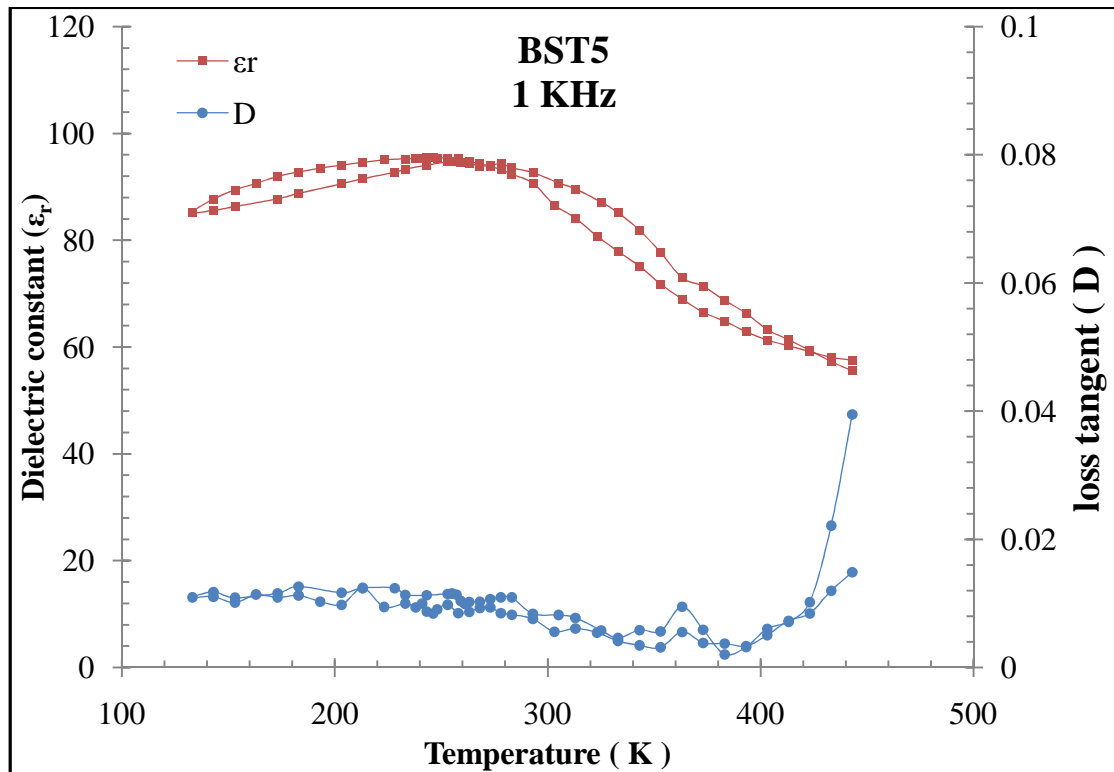


Fig.3.63: The dielectric constant and loss tangent vs temperature for BST5 at 1 KHz

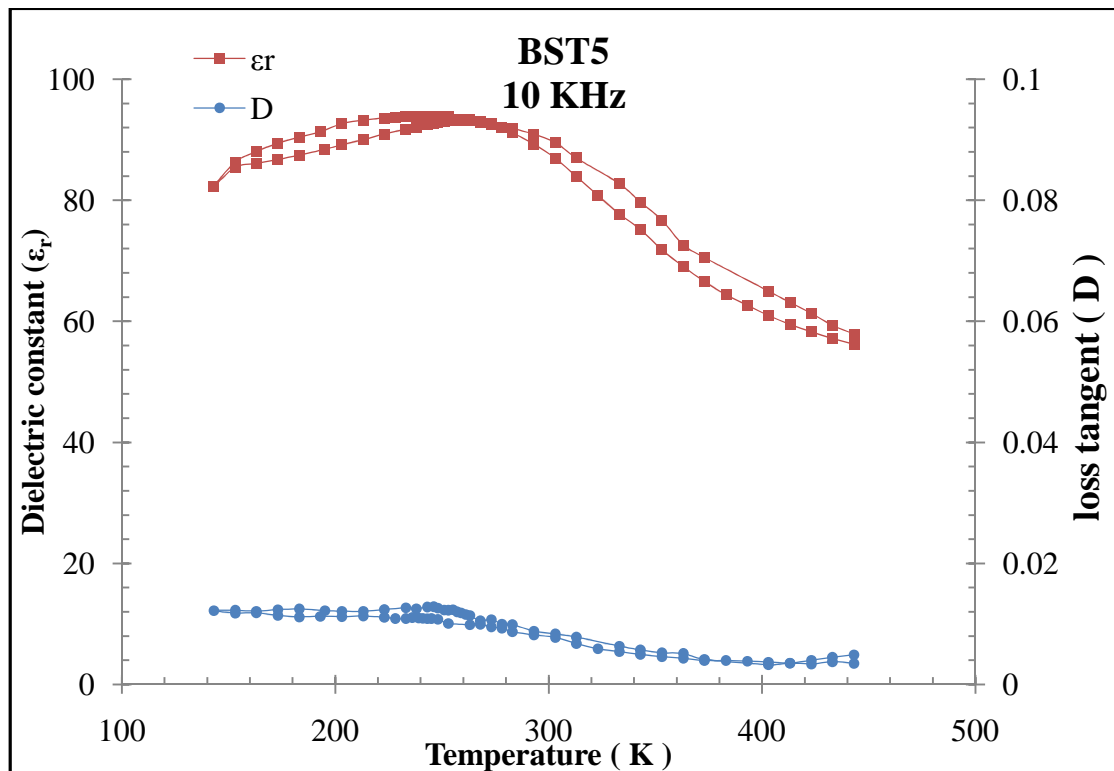


Fig.3.64: The dielectric constant and loss tangent vs temperature for BST5 at 10 KHz

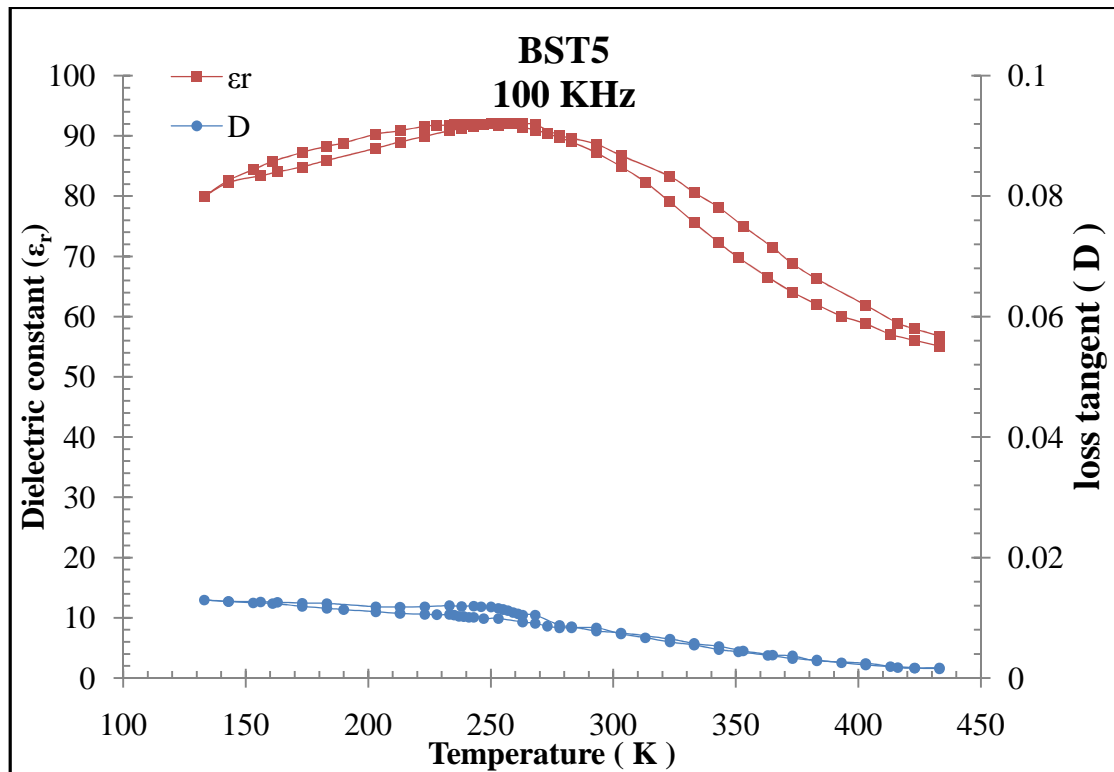


Fig.3.65: The dielectric constant and loss tangent vs temperature for BST5 at 100 KHz

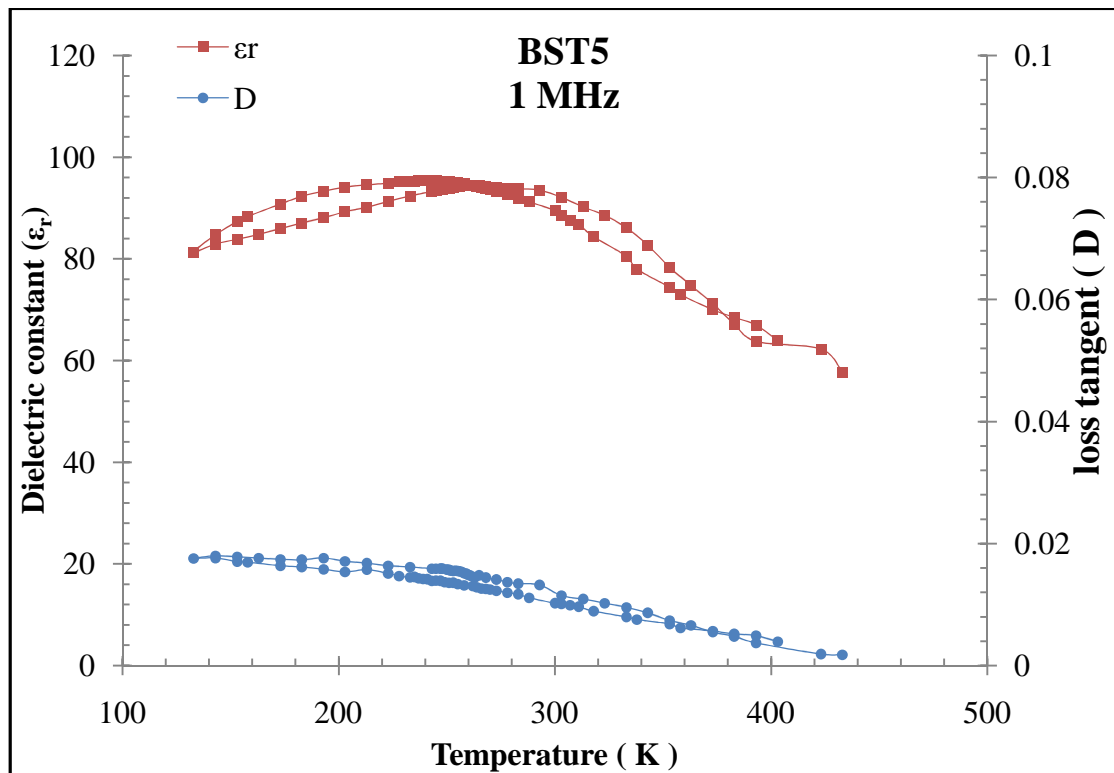


Fig.3.66: The dielectric constant and loss tangent vs temperature for BST5 at 1 MHz

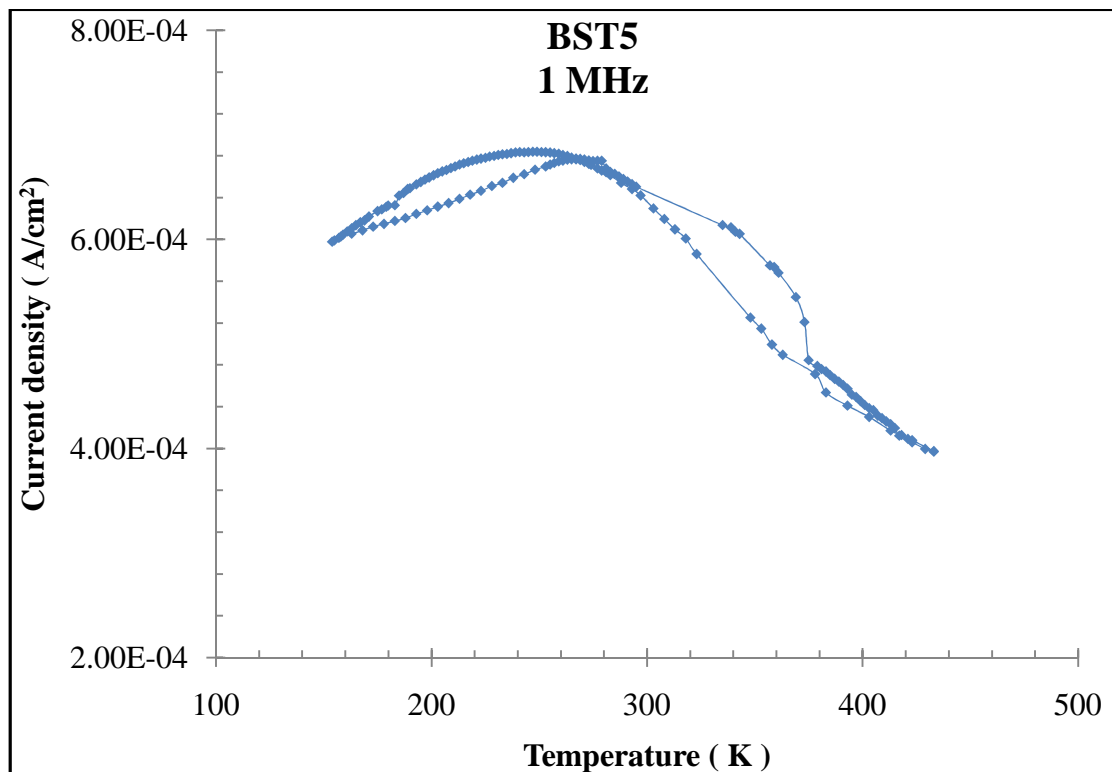


Fig.3.67: The Current density vs temperature for BST5 at 1 MHz

The temperature measurements of dielectric constant and loss tangent (Fig.3.63 – Fig.3.66) for BST5 at different frequencies (1 KHz, 10 KHz, 100 KHz and 1 MHz) under vacuum conditions for heating and cooling cycle showed that the average value of Curie temperature for BST5 is 244 K for the cooling cycle while for heating cycle is 217 K . For the temperature measurement of the current density at 1 MHz under vacuum conditions (Fig.3.67), there is a transition at $T= 247$ K and $T=243$ K for cooling and heating cycle respectively

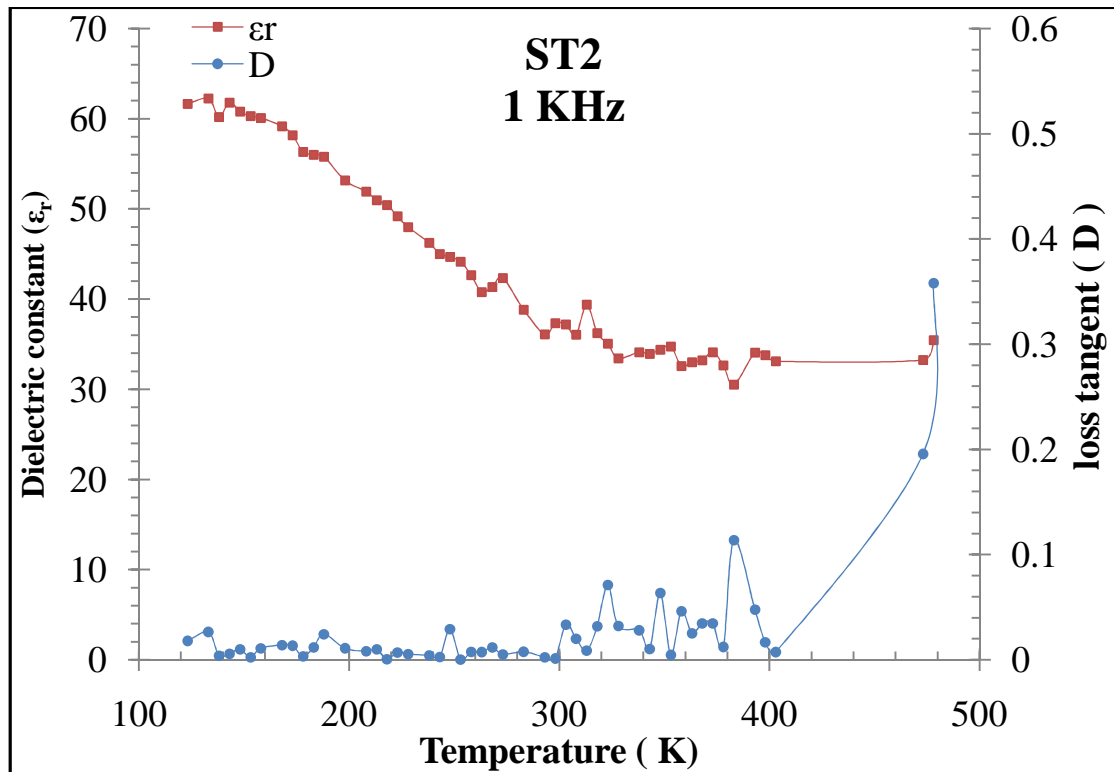


Fig.3.68: The dielectric constant and loss tangent vs temperature for ST at 1 KHz

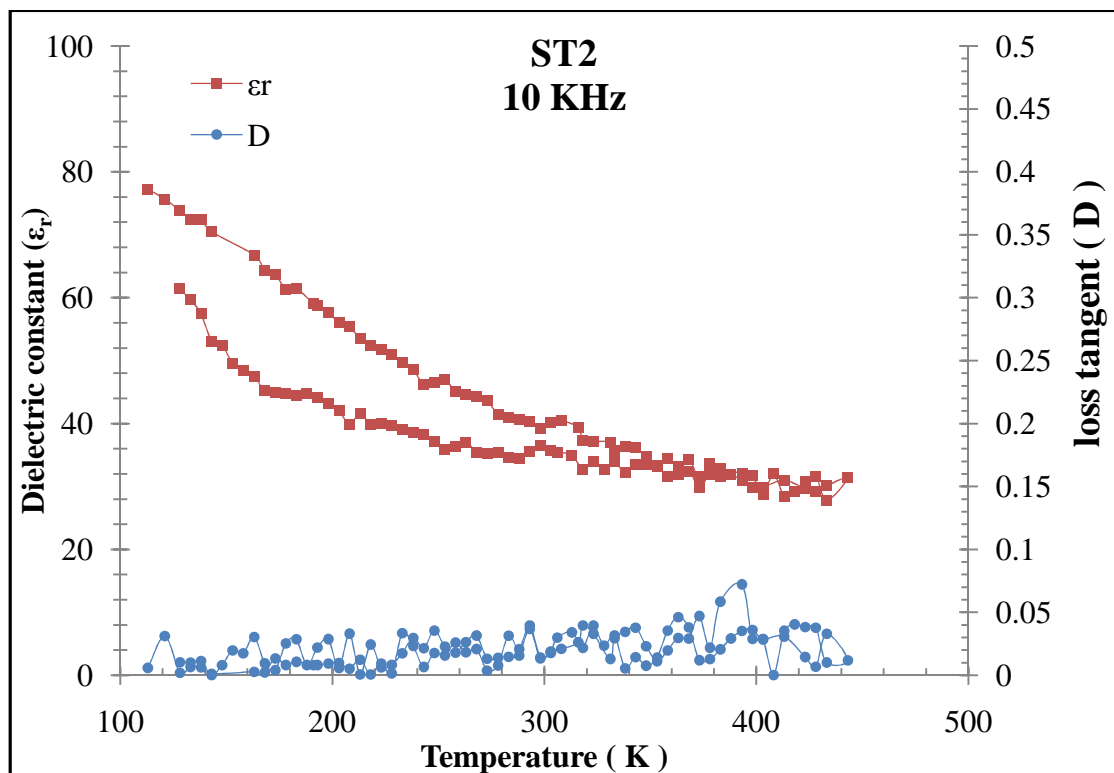


Fig.3.69: The dielectric constant and loss tangent vs temperature for ST at 10 KHz

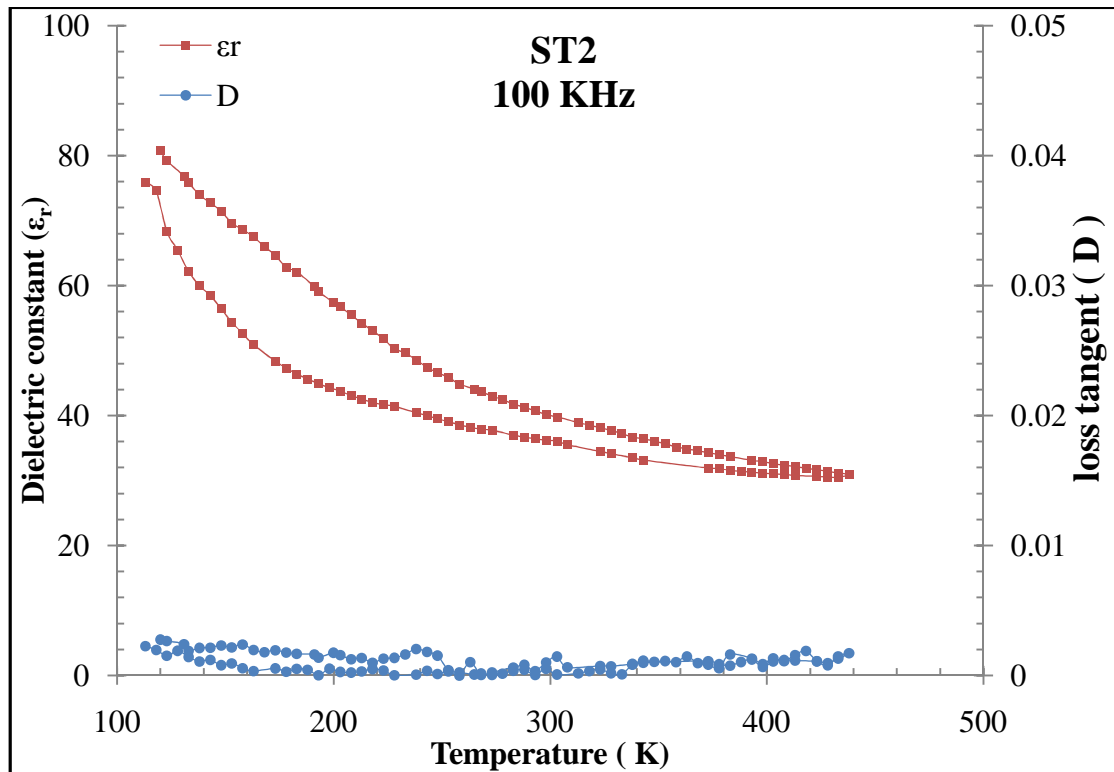


Fig.3.70: The dielectric constant and Loss tangent vs temperature for ST at 100 KHz

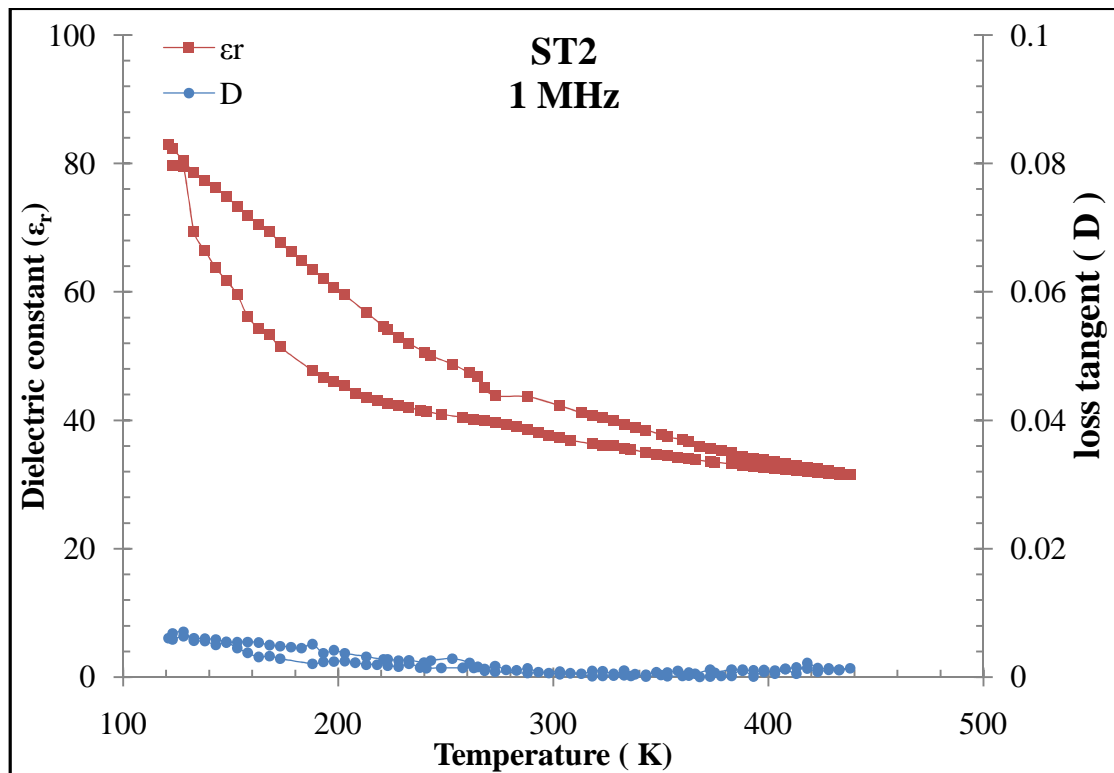


Fig.3.71: The dielectric constant and loss tangent vs temperature for ST at 1 MHz

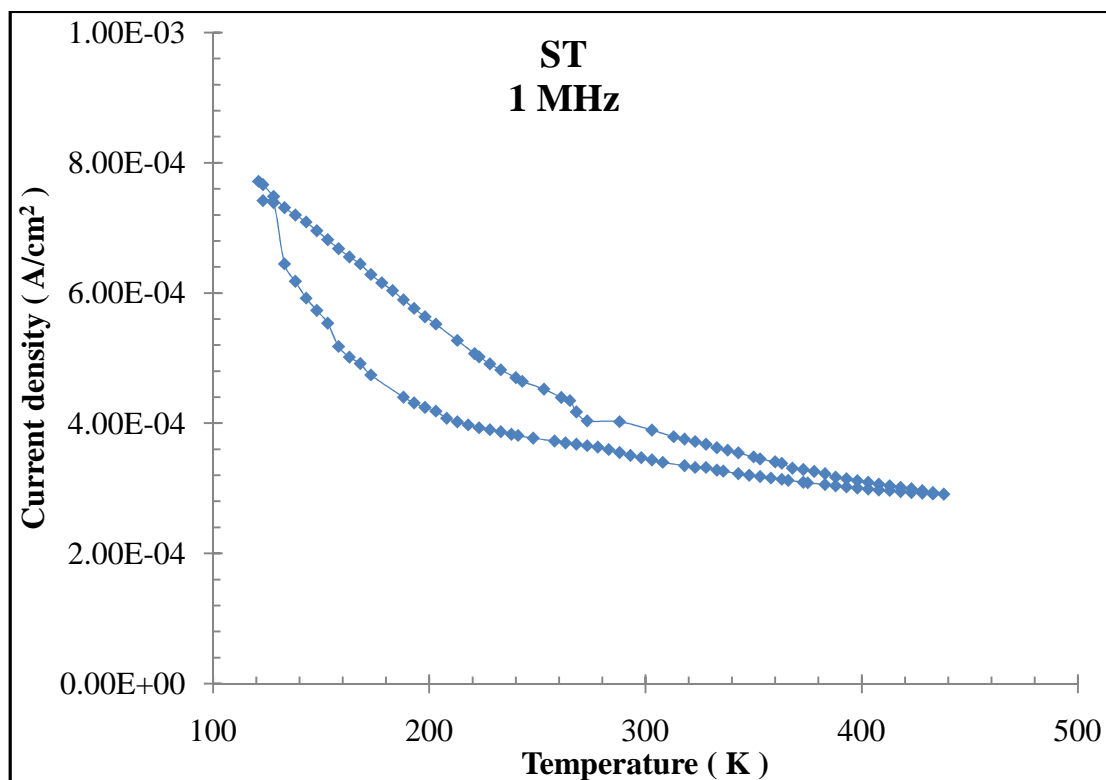


Fig.3.72: The Current density vs temperature for ST at 1 MHz

The temperature measurements of dielectric constant and loss tangent (Fig.3.68 – Fig.3.71) for ST at different frequencies (1 KHz, 10 KHz, 100 KHz and 1 MHz) under vacuum conditions for heating and cooling cycle showed that the value of Curie temperature for ST is lower than liquid Nitrogen temperature (77 K).

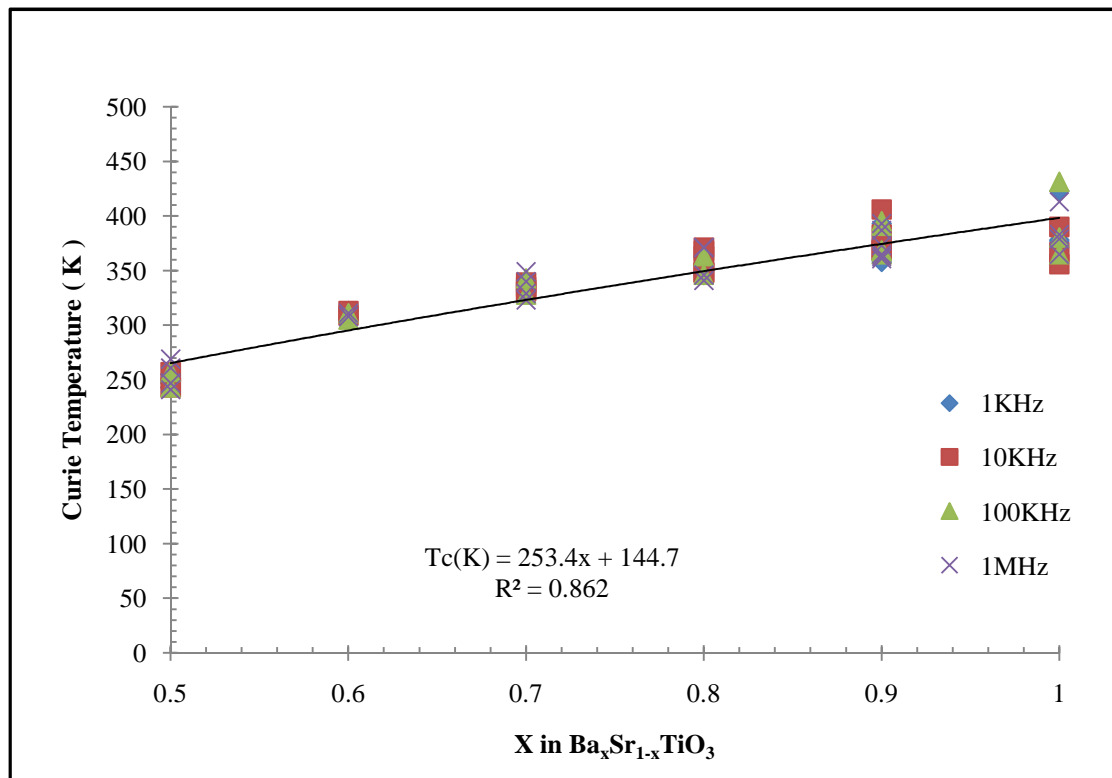


Fig.3.73: Curie temperature (K) vs substitution factor for BST samples at different frequencies (appendix 4).

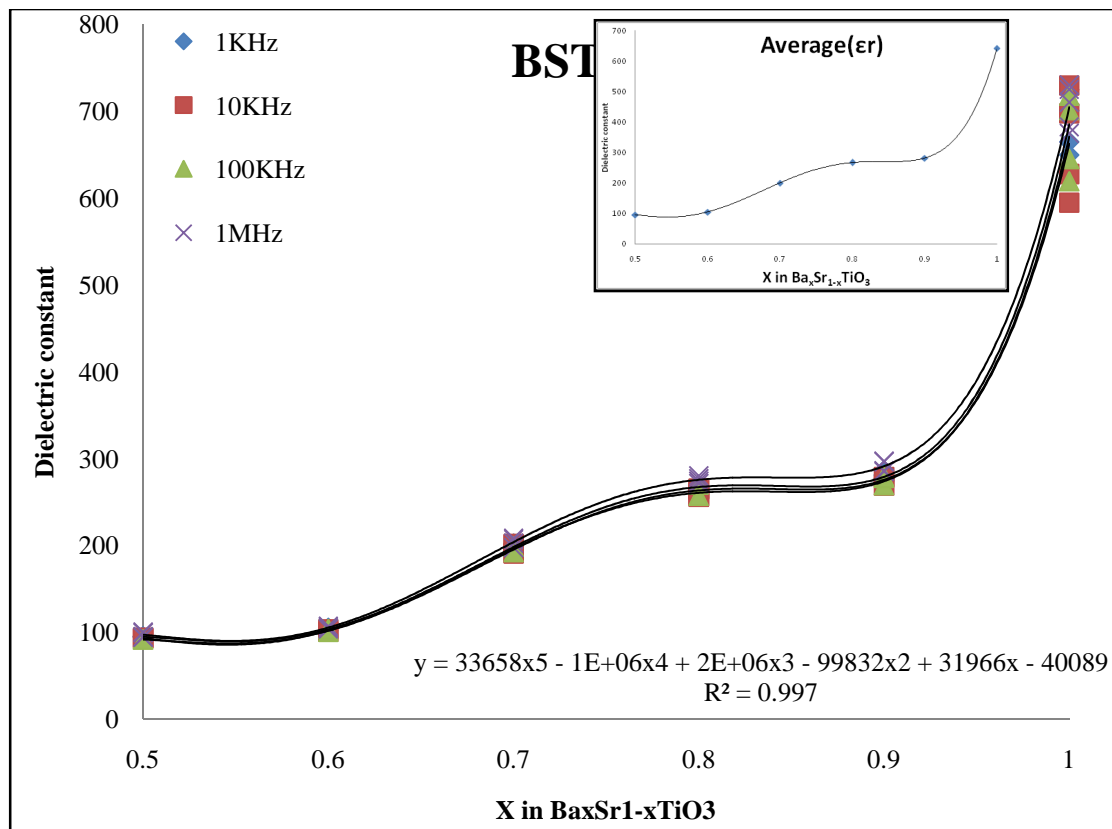


Fig.3.74: Maximum value of Dielectric constant (at T_c) vs substitution factor for BST samples at different frequencies .

For temperature characterization of dielectric constant and loss tangent, the Curie temperature is the temperature of the maximum value of dielectric constant (the transition from ferroelectric phase to paraelectric phase). Curie temperature changes linearly with the substitution factor (x) i.e the increasing of Sr ions leads to decrease the Curie temperature, the estimated equation that describe the changing of Curie temperature with the substitution factor (x) is shown in the following equation

$$T_c(\text{K}) = 253.4x + 144.7$$

The changing of the dielectric constant (at Curie temperature or the maximum value of dielectric constant) with the substitution factor (x) is non-linear as shown in the following equation.

$$\epsilon_r = 33658X^5 - 1E+06X^4 + 2E+6X^3 - 99832X^2 + 31966X - 40089$$

3.6 Transmission electron microscope

Transmission electron microscope (TEM) image for BST5 showed that the particle size is in the range (68 – 99 nm) with agglomeration (Fig.3.75.A). Selected Area Electron Diffraction (SAED) pattern showed that the powder have polycrystalline structure as shown in (Fig.3.75.B.)

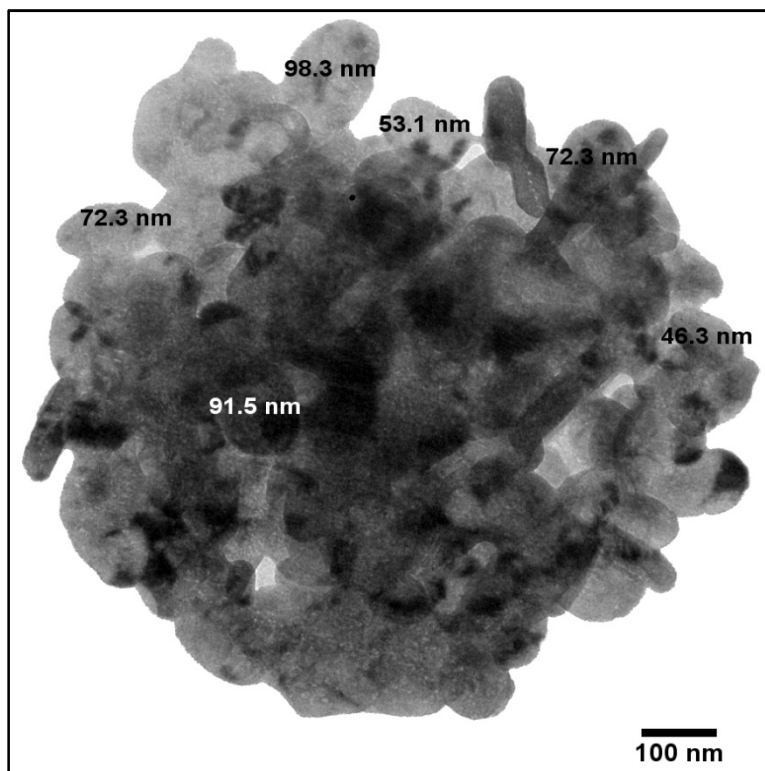


Fig.3.75 .A : TEM image for BST5

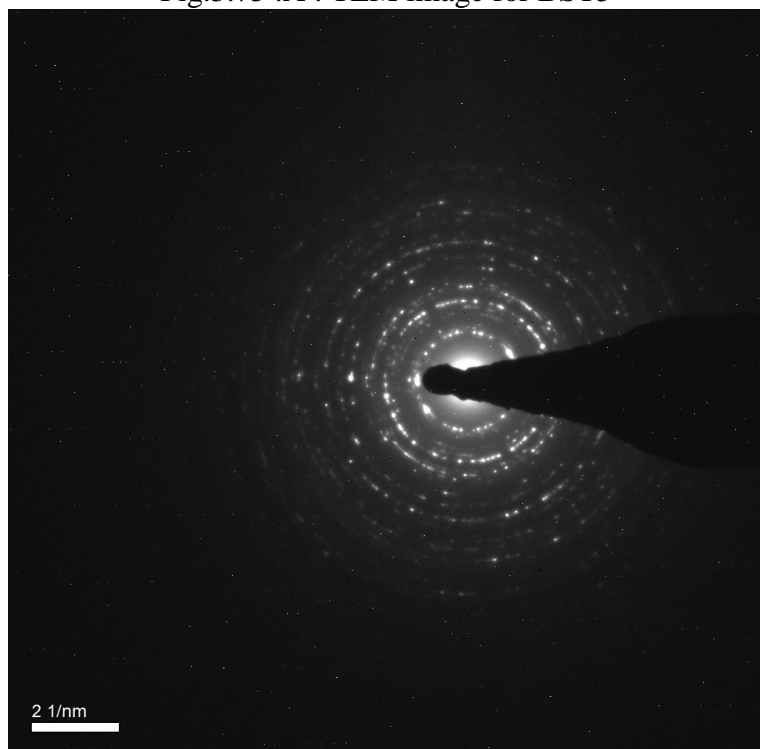


Fig.3.75.B:SAED pattern for BST5

TEM image for BST6 showed that the particle size is in the range (77 – 140 nm) with agglomeration (Fig.3.76.A ; Fig.3.77.A) . SAED pattern (Fig.3.76.B) showed that the powder have polycrystalline structure. Whereas SAED pattern (Fig.3.77.B) is belong to the particle surrounded by the yellow circle in Fig.3.77.A, so this pattern may be either Superstructure or single crystal

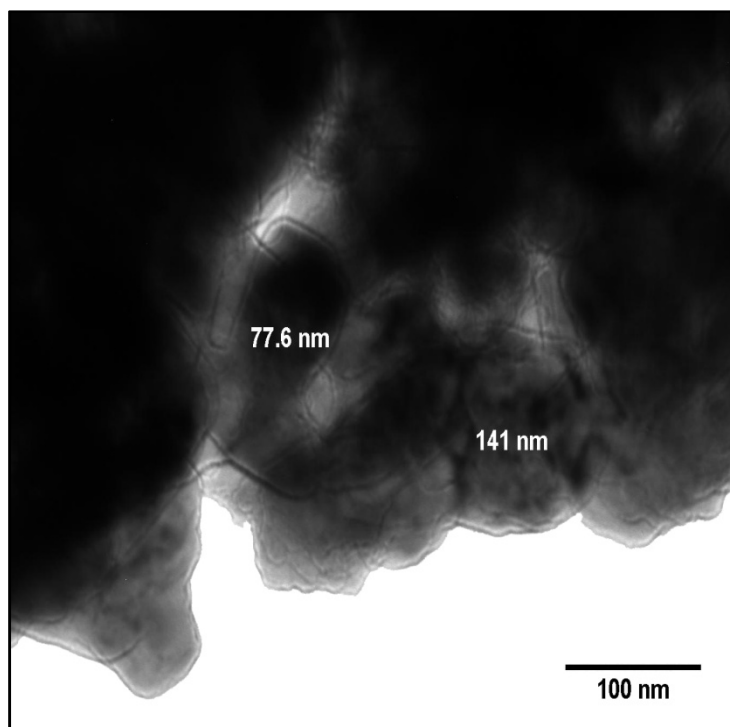


Fig.3.76.A : TEM image for BST6

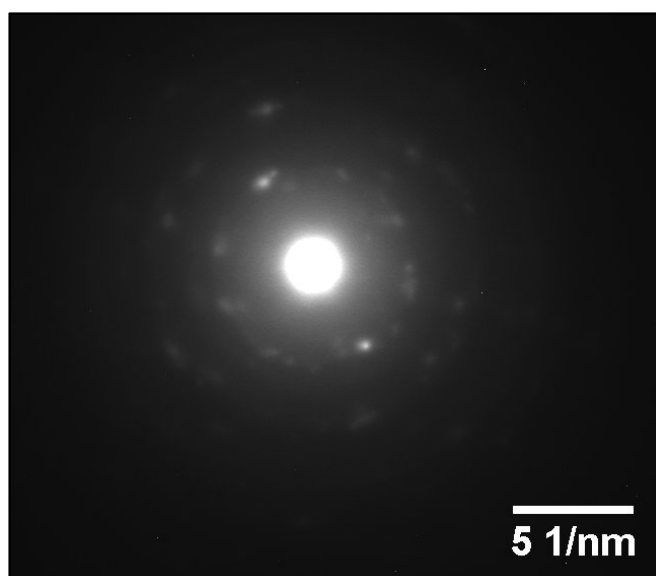


Fig.3.76.B:SAED pattern for BST6

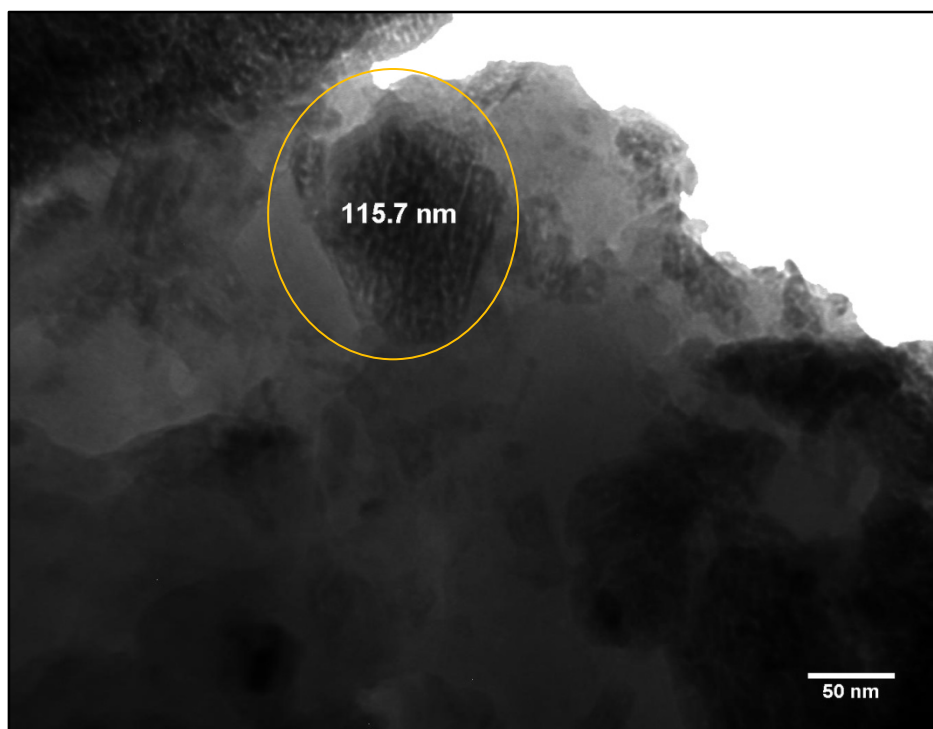


Fig.3.77.A : TEM image for BST6

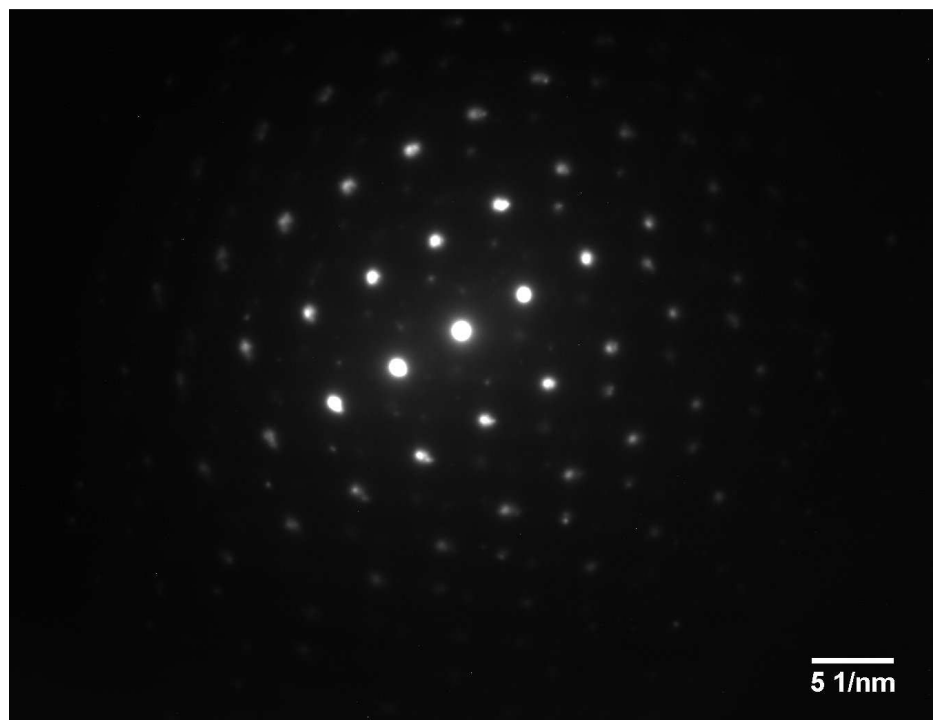


Fig.3.77.B: SAED pattern for BST6

TEM image for BST8 showed that the particle size is in the range (36 – 50 nm) with low agglomeration (Fig.3.78.A). SAED pattern (Fig.3.78.B) showed that the powder have polycrystalline structure.

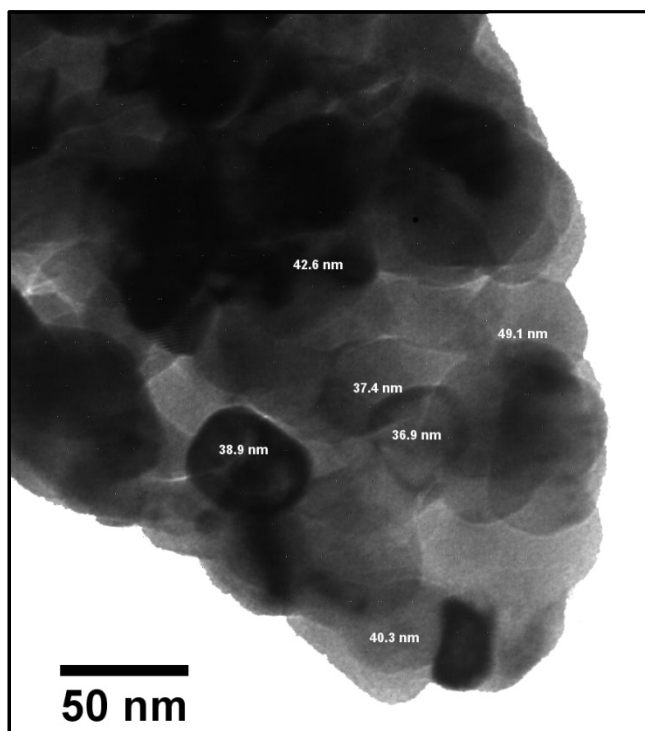


Fig.3.78.A : TEM image for BST8

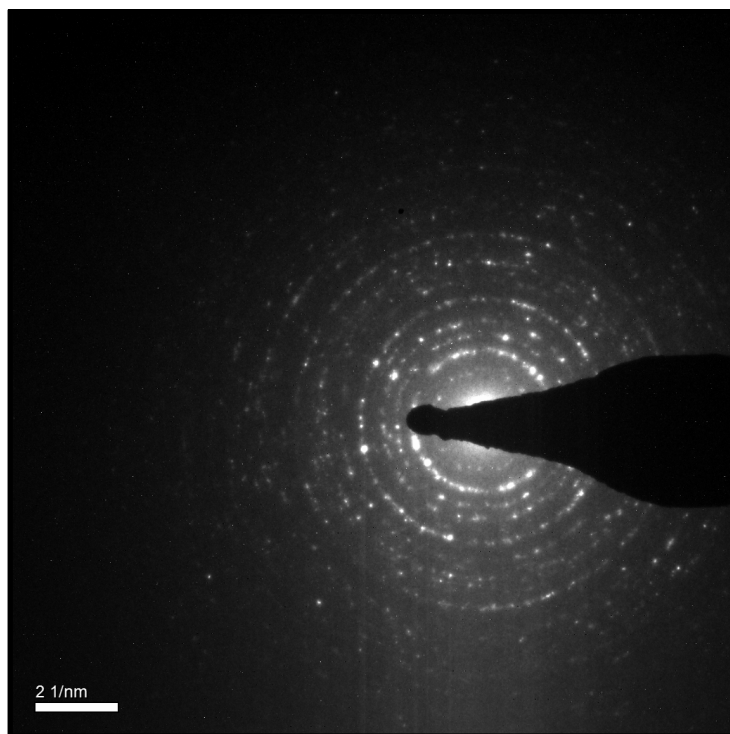


Fig.3.78.B: SAED pattern for BST8

BST system ($\text{Ba}_x\text{Sr}_{1-x}\text{TiO}_3$) is a solid solution between BaTiO_3 and SrTiO_3 as mentioned elsewhere, so BST have adjustable physical properties by varying the substitution factor (x). The Curie temperature which considered as the main feature of ferroelectric materials, the values of Curie temperature (T_c) for all ferroelectric solid solutions like $\text{Ba}_x\text{Ca}_{1-x}\text{TiO}_3$ (BCT), $\text{BaZr}_x\text{Ti}_{1-x}\text{O}_3$ (BZT), $\text{PbTi}_x\text{Zr}_{1-x}\text{O}_3$ (PZT), $\text{PbMn}_x\text{Nb}_{1-x}\text{O}_3$ (PMN) and $\text{Ba}_x\text{Sr}_{1-x}\text{TiO}_3$ etc. are not fixed but could be adjusted.

For our case (BST system) the value of Curie temperature (T_c) could be adjusted between $T_c=400$ K to $T_c=23$ K for BT and ST respectively depending on the value of the substitution factor (x) as concluded in above equation $\{T_c(\text{K}) = 253.4x + 144.7\}$, which is in agreement with thermodynamic expectations $\{T_c(\text{K}) = 370x + 23\}$ [4], also the experimental results of this study in agreement with theoretical ($x - T$) phase diagram of order transitions (P4mm – Pm-3m transition) [26]. Fig.3.78 shows the differences of the results of this study with Mantese *et al*, [4] and Shirokov *et al*, [26].

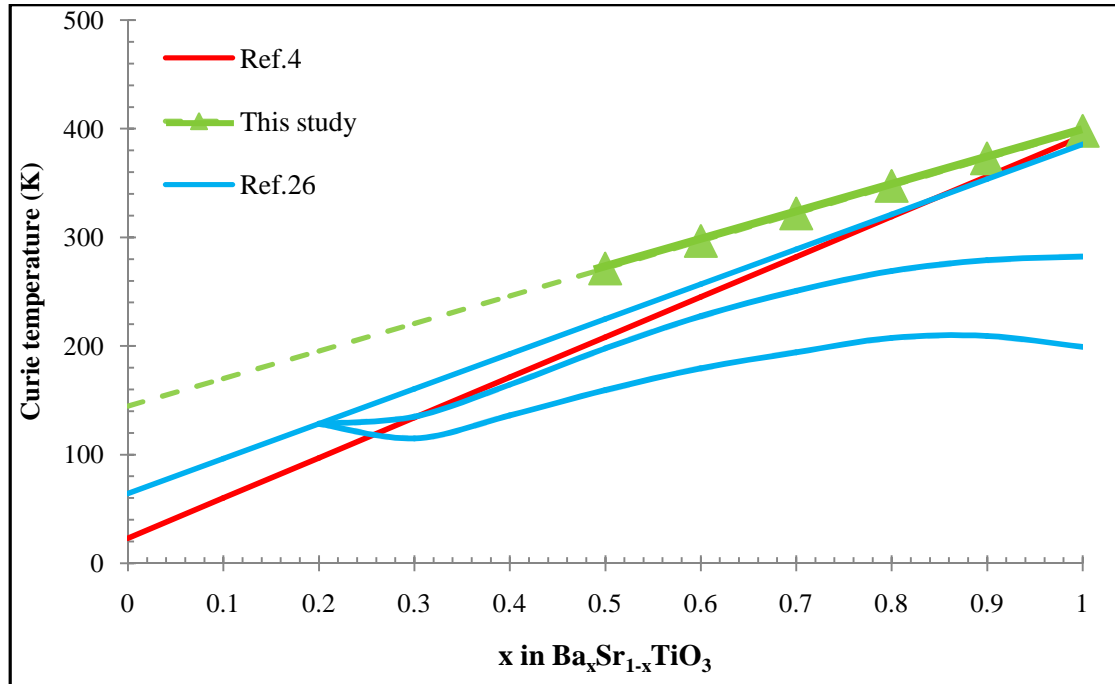


Fig.3.78: Theoretical and experimental Curie temperature vs substitution factor (x) for BST system.

Dielectric constant (ϵ_r) also can be adjusted by changing the substitution factor (x) according to Eq.3.6 ($\epsilon_r = 33658X^5 - 1E+06X^4 + 2E+6X^3 - 99832X^2 + 31966X - 40089$), which is derived from this study.

The density changes with the substitution factor (x), the increasing of (x) means increasing of Ba^{+2} will result raising in density, this increasing in density is due to the differences between Ba^{+2} and Sr^{+2} molar mass and ionic radius. The differences between the experimental densities (Geometrical density) shown in Table 3.2 means that the ceramic porosity of BST samples increase when (x) decrease.

The difference between Ba^{+2} and Sr^{+2} in ionic radius (A site of perovskite ABX_3) means that BT and ST have different values of tolerance factor (τ) or $\tau(BT) > \tau(ST)$, and this means that both BT and ST have different crystal structures (both belong to perovskite).

All these changes in physical properties (Curie temperature, dielectric constant and density) of BST system are related to the changing of substitution factor (x). The changes of substitution factor (x) of BST samples lead to change the crystal structure, lattice parameters, space groups as shown in Table.3.2 and Fig.(3.17 ; 3.18), so the changes in physical properties are due to changes in the crystal structures.

Samples BT, BST9, BST8 and BST7 have tetragonal structure belongs to space group: $P4mm$ (non-centrosymmetric), while BST6, BST5 and ST samples have cubic structure belongs to space group: $Pm-3m$ (centrosymmetric), which confirm that BT, BST9, BST8 and BST7 samples have Curie temperature $>$ room temperature and BST6, BST5, ST samples have Curie temperature $<$ room temperature.

For BST7, BST6 and BST5 and other compounds $x=0.7 - 0.5$, Curie temperatures were around room temperature as well. These samples are suitable for medical and environmental applications, transducers and other applications related to pyroelectric properties such as thermal imaging (IR camera).

From studying of dielectric measurements, the samples BST8, BST7, BST6 and BST5 have very low values of loss tangent (D), so these samples are suitable for many applications especially for microwave applications and electronic devices such as MOSFETs.

From dielectric measurements and structural analysis (XRD, FTIR, TEM) it can be expected that there is a regular (adjustable) changing of the piezoelectric coefficient (d_{33}), electrochemical coupling (κ) and pyroelectric coefficient (ρ_t) versus substitution factor (x), i.e. (d_{33} , κ and ρ_t) can be adjusted by changing (x)

Conclusions

&

Recommendations

3.7 Conclusions

For this study, it can be concluded that:

1. Oxalate method was the best , since it is very easy and need short time and power , so it can be considered as promising method to prepare perovskite precursors like BZT , PZT , BCT , BCZT Tungsten bronze structure .
2. Estimation of experimental equation that describe the changing of Curie temperature and dielectric constant for BST system with the substitution factor (x). And estimate experimental equations for the changing of structural properties with the substitution factor (x).
3. The compounds BST7, BST6 and BST5 and other compounds $x=0.5$ to 0.7 , the Curie temperatures were around room temperature. These samples are suitable for medical and environmental applications, transducers and other applications related to piezoelectric properties such as thermal imaging (IR camera). While the compounds BST8, BST7, BST6 and BST5 had very low values of loss tangent (D), so these samples are suitable for many applications especially for microwave applications and electronic devices such as MOSFETs.
4. From dielectric measurements and structural analysis (XRD, FTIR, TEM) it can be expected that there are a regular (adjustable) changing of the piezoelectric coefficient (d_{33}), electrochemical coupling (κ) and pyroelectric coefficient (ρ_t) versus substitution factor (x), i.e. (d_{33} , κ and ρ_t) can be adjusted by changing (x)
5. In this study the dielectric measurement were done under N_2 , He, Ar pressure and under vacuum. We conclude that the best condition for dielectric measurement was under vacuum.

3.8 Recommendations:

- 1- Studying the effect of the substitution factor(x) on the piezoelectric coefficient (d_{33}) and electrochemical coupling (κ) and pyroelectric coefficient (ρ_t).
- 2- Studying the effect of frequency on d_{33} , κ and ρ_t .
- 3- Studying the microwave properties for BST system in ceramics.
- 4- Studying the effect of doping with Nb, Ta and Ln for some of BST samples, which expect to have numerous application in microwave.
- 5- Preparing BST system as thin film to design a waveguide and phase shifter.
- 6- Trying to prepare BST system as a single crystal and study the changes in their physical properties with (x).
- 7- Trying to build a theoretical model for perovskite solid solutions.

References

References

1. Kao, K. (2004). Dielectric Phenomena in Solids . Elsevier Academic Press , USA
2. Xu, H. ; Gao, L . ; Guo , J . (2002). Preparation and characterizations of tetragonal barium titanate powders by hydrothermal method. J. Eur . Ceram. Soc. **22** . 1163–1170 .
3. Guo , L . ; Luo , H . ; Gao , J ; Guo , L . and Yang , J . (2006). Microwave hydrothermal synthesis of barium titanate powders. Materials Lett . **60** : 3011–3014.
4. Mantese , J . and Alpay , S . (2005). Graded Ferroelectrics, Transpacitors and Transponent. Chapter 2 , p 48 . Springer , USA.
5. Barnes, P. (2003). Exploring Structural Changes and Distortions in Quaternary Perovskite and Defect Pyrochlores Using Powder Diffraction Techniques. Ph.D thesis . School of the Ohio State University , USA .
6. . Muller , K . and Kool , W . (Eds.) . (2010) . Properties of Perovskites and other Oxides . World Scientific Publishing Co. Pte. Ltd.,UK .
7. Thomas, R . ; Skumryev, V . ;. Coey, J. and S. Wirth . (1999) . High magnetic field studies of 3d and 4f magnetism in $(R_{0.7}A_{0.3})MnO_3$; $R=La^{3+}, Pr^{3+}, Nd^{3+}$, $A=Ca^{2+}, Sr^{2+}, Ba^{2+}, Pb^{2+}$. J. Appl. Phys. **85** , 5384-5386 .
8. Moulson , A. and Herbert , J..(2003) . Electroceramics . John Wiley & Sons Ltd., England
9. Kim , S. ; Lee , M . ; Noh , T . and Lee , C . .(1996) . preparation of barium titanate by homogeneous precipitation. J . Materials Sci . **31** : 3643- 3645 .
10. Hwu , J. ; Yu , W . ; Yang , W . ; Chen, Y. and Chou , Y . (2005).Characterization of dielectric barium titanate powders prepared by homogeneous precipitation chemical reaction for embedded capacitor applications. Material. Res . Bull . **40** : 1662–1679
11. Al-Darub , M. (2000) .Studying the Physical Properties of Ferrite Type LiFe5O8 Prepared by Using Freeze – Drying Method . MSc. Thesis , Saddam University , College of Science , Department of Physics . Baghdad , Iraq .
12. Byrappa , K . and Ohachi , T . (2003) . Crystal Growth Technology . Springer – Verlag , Berlin, Heidelberg , New York .
13. Jhung , S . ; Lee , J . ;Yoon , J . ; Hwang , Y . Hwang , Y . ; Park , S . and Chang , J .(2004). Effects of reaction conditions in microwave synthesis of nanocrystalline barium titanate. Materials Lett . **58** : 3161–3165.

14. Xu , M . ; Lu , Y . ; Liu , Y . ; Shi , S . ; Qian , T . ; Lu , D . (2006). Sonochemical synthesis of monosized spherical BaTiO₃ particles. Powder Technol. **161** : 185 – 189.
15. Yan , T . ; Liu , X . ; Wang , N . and Chen , J . (2005) Synthesis of monodispersed barium titanate nanocrystals hydrothermal recrystallization of BaTiO₃ nanospheres. J. Crystal Growth **281** : 669–677 .
16. Zhigang , S . ; Zhang W . ; Chen , J . and Yun , J . (2006) . Low temperature one step synthesis of Barium titanate: particle formation mechanism and large-scale synthesis. Chinese J. Chem. Eng., **14** : 642-648.
17. Somani , V . and Kalita , S . (2007). Synthesis and characterization of nanocrystalline Barium Strontium Titanate powder via sol-gel processing . J . Electroceram **18**:57–65 .
18. Simon-Seveyrat, L . ; Hajjaji, A . ; Emziane, Y . ; Guiffard, B . and Guyomar, D. (2007). Re-investigation of synthesis of BaTiO₃ by conventional solid-state reaction and oxalate coprecipitation route for piezoelectric applications. Ceram. Int. **3** : 35-40 .
19. Shen , W . (2010) . Investigation of Resistive Switching in Barium Strontium Titanate Thin Films for Memory Applications . Verlag , Germany .
20. Rahaman , M . (2007). Ceramic Processing and Sintering . 2nd Ed. Marcel Dekker Inc . , New York , USA .
21. Kajtoch , C . ; Gabryoe , M . ; Tejchman , W . and Handke , B . (2008). Structural and dielectric properties of polycrystalline (Ba_{0.9}Sr_{0.1})TiO₃ . Arch. Materials Sci. Engin. **33** : 89-92.
22. Kajtoch , C . ; Bak , W . ; Gabryoe , M . ; Mroczka , K . ; Handke , B . and Starzyk , F .(2009). Diffused phase transition of polycrystalline (Ba_{0.80}Sr_{0.20})TiO₃. Arch . Materials Sci . Engin . **39**: 88-91.
23. Wang , T . ; Jin , D . ; Cheng , J . ; and Li , J . (2010). Intragrain Compositional Gradient BariumStrontium Titanate Ceramics Fabricated by a Solassisted Sintering Technology. IEEE . International Symposium on the Applications of Ferroelectrics (ISAF) (August 2010), pp. 1-4 .
24. Ioachim , A . ; Toacsan , M . ; Banciu , M . ; Nedelcu , L . ; Dutu , ; Antohe , S . ; Berbecaru , C . ; Georgescu , L . ; Stoica , G. and Alexandru , H .(2007). Transitions of barium strontium titanate ferroelectric ceramics for different strontium content. Thin Solid Films . **515**: 6289–6293 .
25. Berbecaru , C . ; Alexandru , H . ; Porosnicu , C . ; Velea , A . ; Ioachim , A . ; Nedelcu , L . ; and Toacsan , M . (2008). Ceramic materials Ba_(1-x)Sr_xTiO₃ for electronics - Synthesis and characterization. Thin Solid Films . **516** : 8210–8214.

26. Shirokov , V . ; Torgashev , V . and Bakirov , A . ; Lemanove , V . (2008). Concentration phase diagram of $Ba_xSr_{1-x}TiO_3$ solid solutions . APS/paper. pp 1-8 .
27. Gabryoe , M . (2008). Dielectric properties of polycrystalline $(Ba_{0.60}Sr_{0.40})Ti_{0.8}O_3$. Arch . Materials Sci . Engin . **34**: 27-30 .
28. Nedelcu , L . ; Ioachim , A . ; Toacsan , M . ; Banciu , M . ; Pasuk , I . ; Berbecaru , C. and Alexandru , H . (2011). Synthesis and dielectric characterization of $Ba_{0.6}Sr_{0.4}TiO_3$ ferroelectric ceramics. Thin Solid Films . **519** : 5811–5815 .
29. Uchino , K . (2000) . Ferroelectric Devices . Marcel Dekker , New York .
30. Maune , H.; Sazegar , M . ; Zheng , Y. and Jakoby , R. (2011) . Memory Effects in Ferroelectric Thick Film Varactors based on Barium Strontium Titanate . Proceeding RWS'10 Proceedings of the 2010 IEEE conference on Radio and wireless symposium . pp 134-137 .
31. Cardona , A . (2010) . Tunable $BaSrTiO_3$ Applications for the RF Front End . IEEE International Microwave Symposium . May 23-28, 2010 , California
32. Gurumurthy , V . (2007) . Barium Strontium Titanate Films for Tunable Microwave and Acoustic Wave Applications . MSc . thesis Department of Electrical Engineering , College of Engineering , University of South Florida .
33. Serraiocco , J. (2003) . Compact Phase Shifter Design Using Barium Strontium Titanate Thin-Film Varactors . MSc. Thesis . Electrical and Computer Engineering , University of California .
34. Wee , F . and Malek , F . (2010). Barium strontium titanate (BST) array antenna covered with dielectric resonator superstrates for high gain and high directive antenna . IEEE International Symposium on the Applications of Ferroelectrics (ISAF) (August 2010), pp112-115 .
35. Blattau , N . ; Barker , D. and Hillman , C. (2004) . Lead Free Solder and Flex Cracking Failures in Ceramic Capacitors . 24th Capacitor and Resistor Technology Symposium, San Antonio, Texas, March 29 - April 1, 2004.
36. Guangneng , F . ; Lixia , H. and Xueguang , H . (2005). Synthesis of single-crystal $BaTiO_3$ nanoparticles via a one-step sol-precipitation route. J. Crystal Growth **279** : 493–489 .
37. Kholam , Y . ; Bhoraskar , S . ; Deshpande , S . ; Potdar , H . ; Pavaskar , N . ; Sainkar , S. and Date , S . (2003) . Simple chemical route for the quantitative precipitation of barium–strontium titanyl oxalate precursor leading to $Ba_{1-x}Sr_xTiO_3$ powders. Materials Lett . **57**: 1871–1879 .
38. Kao, Ch. And Yang, W. (1999). Preparation of Barium Strontium Titanate

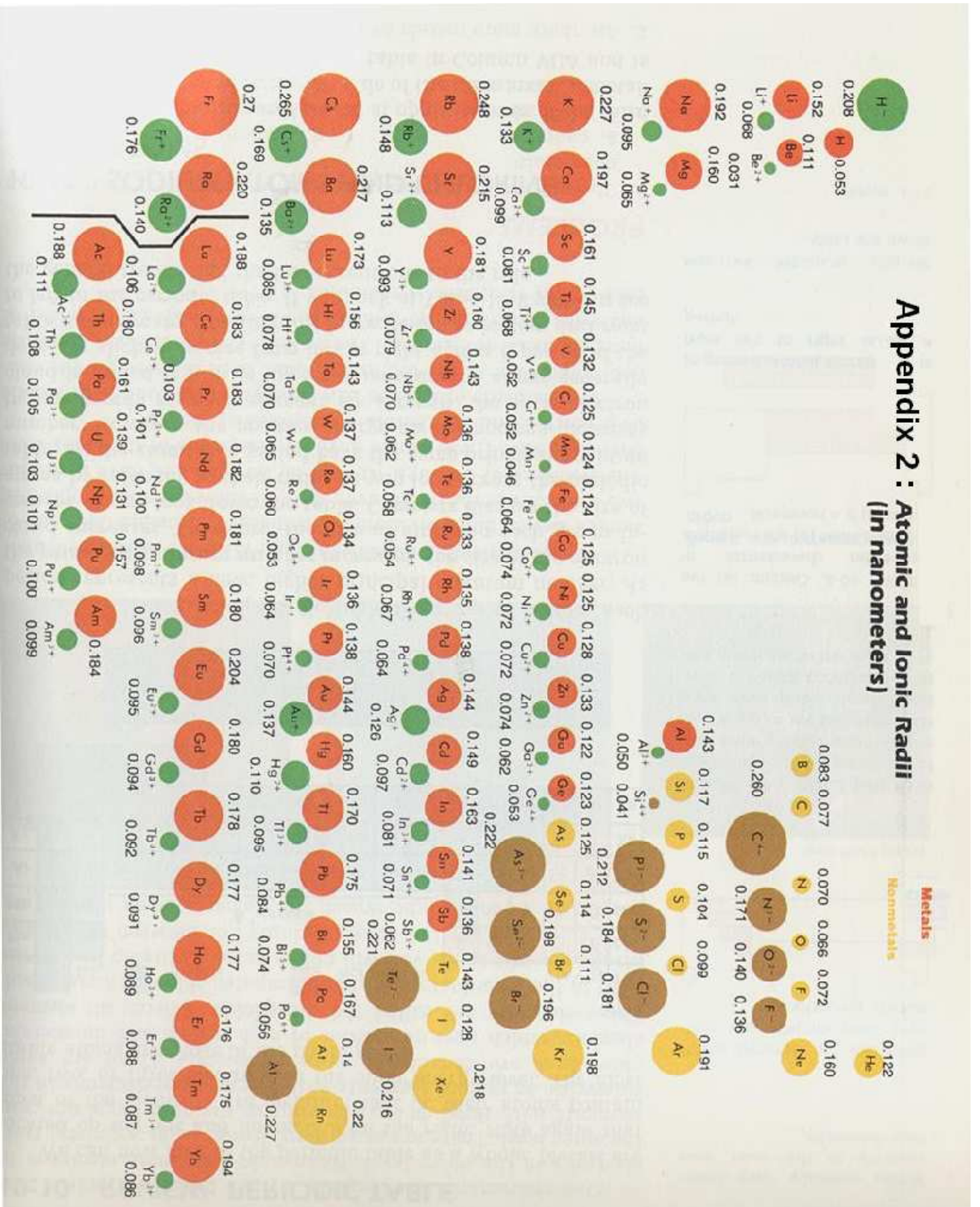
- Powder from Citrate Precursor. Appl. Organometal. Chem. **13**: 383–397
39. Guinebretière , R .(2007) . X-ray Diffraction by Polycrystalline Materials. ISTE Ltd . USA .
 40. Xpowder Ver. 2004.04.70 PRO , <http://www.xpowder.com> .
 41. Crystal impact software , <http://www.crystalimpact.com>
 42. Refine95 software . university of Arizona . downs@geo.arizona.edu
 43. PDF2 database (powder diffraction file) from International Center for Diffraction Data) , <http://www.icdd.com/> .
 44. Crystallography Open Database (COD) , from International Union for Crystallography (IUCr) , <http://www.crystallography.net/> .
 45. Essential FTIR Software. V1.50.282 . <http://www.essentialftir.com/> .
 46. FDM Library (Fiveash Data Management) , http://www.fdmspectra.com/FDM_Library_Search.htm .
 47. Spectral Database for Organic Compounds SDBS , National Institute of Advanced Industrial Science and Technology (AIST), Japan . http://riodb01.ibase.aist.go.jp/sdbs/cgi-bin/cre_index.cgi?lang=eng .
 48. Tao , H . (2004) . BST-Based Low Temperature Co-fired Ceramic (LTCC) Modules for Microwave Tunable Component . PhD thesis . Department of Electrical and Information Engineering and InfoTech . Oulu, University of Oulu , Finland .
 49. Kittel, C. (2004) . Introduction to Solid State Physics. 8th Edition . John Wiley , USA .
 50. Hahn , T. (Ed.) . (2005) . International Tables for Crystallography . Volume A. Space-group symmetry, Springer, USA .

Appendix

Appendix 1 : Calculations of theoretical density

x	Sample	molar mass (g / mol)	cell volume (\AA^3)	Na (mol ⁻¹)	Density (g/ Cm ³)
0	SrTiO ₃	183.49	59.27	6.02E+23	5.14
0.5	Ba _{0.5} Sr _{0.5} TiO ₃	208.34	61.91	6.02E+23	5.59
0.6	Ba _{0.6} Sr _{0.4} TiO ₃	213.31	62.52	6.02E+23	5.67
0.7	Ba _{0.7} Sr _{0.3} TiO ₃	218.28	63.16	6.02E+23	5.74
0.8	Ba _{0.8} Sr _{0.2} TiO ₃	223.25	63.57	6.02E+23	5.83
0.9	Ba _{0.9} Sr _{0.1} TiO ₃	228.22	63.94	6.02E+23	5.93
1	BaTiO ₃	233.19	64.27	6.02E+23	6.03

Appendix 2 : Atomic and Ionic Radii (in nanometers)



Appendix 3 : Equation that was used in dielectric calculations

$$1- \epsilon_r = \frac{C \times t}{A \times \epsilon^0}$$

where ϵ_r is dielectric constant , C is the capacitance , t is the disc thickness , A is the area of disc and ϵ^0 is vacuum permittivity = $8.85E-12$

$$2- D = \tan(\delta)$$

$$\text{Where } \delta = \left(\frac{\epsilon''}{\epsilon'} \right)$$

ϵ'' is the imaginary part of dielectric constant and ϵ' is the real part of dielectric constant

Appendix 4: Readings of Curie temperature vs substitution factor (x)

Cooling cycle		Curie temperature (K)			
Sample	x	T _c (K) 1KHz	T _c (K) 10KHz	T _c (K) 100KHz	T _c (K) 1MHz
BaTiO ₃	1	378	356	380	383
	1	377	367	365	365
	1				379
Ba _{0.9} Sr _{0.1} TiO ₃	0.9	363	368	368	365
	0.9	358	369	365	361
	0.9			368	363
Ba _{0.8} Sr _{0.2} TiO ₃	0.8	346	348	346	346
	0.8	349	348		341
	0.8		349		
Ba _{0.7} Sr _{0.3} TiO ₃	0.7	330	331	328	329
	0.7		332		323
Ba _{0.6} Sr _{0.4} TiO ₃	0.6	307	309	305	308
	0.6	305			
Ba _{0.5} Sr _{0.5} TiO ₃	0.5	243	243	243	241
	0.5	247			247
N ₂	Ar	He	Vacuum		

Appendix 4 (cont.)

Heating cycle		Curie temperature			
Sample	x	Tc (K) 1KHz	Tc (K) 10KHz	Tc (K) 100KHz	Tc (K) 1MHz
BaTiO ₃	1	423	390	431	413
	1	383	380	395	395
Ba _{0.9} Sr _{0.1} TiO ₃	0.9	393	383	391	373
	0.9	378	406	395	393
	0.9				387
Ba _{0.8} Sr _{0.2} TiO ₃	0.8	362	368	363	371
	0.8		363		371
	0.8		371		
Ba _{0.7} Sr _{0.3} TiO ₃	0.7	341	339	343	340
	0.7		335		349
Ba _{0.6} Sr _{0.4} TiO ₃	0.6	313	313	311	311
Ba _{0.5} Sr _{0.5} TiO ₃	0.5	255	257	257	261
	0.5				269
N ₂		Ar		He	Vacuum

نشر جزء من نتائج هذه الدراسة على شكل موديلات بلورية (CIF files) في قاعدة بيانات عالمية وهي قاعدة بيانات علوم البلورات والمواد COD database التابعة للاتحاد العالمي لعلوم البلورات IUCr .

من جهة أخرى تم دراسة بعض الخواص الفيزيائية للأقرص السيراميكية الناتجة مثل قياس الكثافة نظريا وعمليا وبعده طرق وحساب جودة الكبس Compactness و استنتاج معادلة توضح تغيرها مع عامل التعويض Substitution factor (x)

درست خواص العزل الكهربائي وبطريقتين الأولى بتغيير التردد وثبوت درجة الحرارة ، والثانية بتغيير درجة الحرارة وثبوت التردد لقياس ثابت العزل الكهربائي (ϵ_r) Dielectric constant والخسارة الكهربائية Loss tangent ، من دراسة خواص العزل الكهربائي تم استنتاج درجات حرارة كيوري Curie temperature (T_c) وثابت العزل الكهربائي وتم استنتاج معادلة عملية توضح تغير درجة حرارة كيوري مع عامل التعويض ومعادلة أخرى توضح تغير ثابت العزل الكهربائي مع عامل التعويض (x) .

وظهر أن العينات BST5 , BST6 , BST7 لها درجة حرارة كيوري قريبة من حرارة الغرفة والتي من المتوقع أن تكون لها تطبيقات عديدة خاصة في المجالات الطبية والبيئية . والعينات BST5 إلى BST8 لها قيمة قليلة من الخسارة الكهربائية لذلك فمن المتوقع ان تجد استخدامات في تطبيقات المايكروويف Microwave والاتصالات .

الملخص

المواد الفيروكهربائية Ferroelectric materials مواد عازلة كهربائياً تمتلك استقطاباً كهربائياً ذاتياً Spontaneous polarization ، وهذا الاستقطاب يمكن عكسه بتطبيق مجال كهربائي خارجي ضمن مدى معين من درجات الحرارة . تمتاز هذه المواد بان لها تراكيب بلورية خاصة وهذه التراكيب تكون غير متماثلة بلوريا (Non-centroemmytric) . تعد المواد الفيروكهربائية مواد ذات أهمية صناعية كبيرة حيث تدخل في العديد من التطبيقات في الصناعة والطب والبيئة والاتصالات .

أهم هذه المواد الفيروكهربائية التي تدخل في التطبيقات هي تلك المواد التي لها تركيب بلوري من نوع بيروفسكايت Perovskite وأهمها تيتانات الباريوم BaTiO₃ وتيتانات السترونشيوم SrTiO₃ وغيرها . هناك طرق عديدة لتحضير هذه المواد التي تختلف من حيث الأهمية والكلفة وهي الطرق الكيميائية والطرق الفيزيائية .

في هذه الدراسة تم تحضير مادة Ba_xSr_{1-x}TiO₃ حيث (x) يمثل عامل التعويض وهو، x = 1 , 0.9 , 0.8 , 0.7 , 0.6 , 0.5 , 0 Oxalate co-precipitation بطريقة الاوكزالات method حيث كانت هذه الطريقة سهلة ولا تتطلب الكثير من الوقت والطاقة أثناء عملية التحضير وتعطي نتائج جيدة وقد تم تحضير مساحيق نانوية وبحجم حبيبي يتراوح بين (50 إلى 140 نانومتر)، ثم تمت عملية كبس المساحيق باستخدام قوالب خاصة ذات قطر 1 سنتيمتر وعند ضغط 125 ميكاباسكال ، ثم أجريت عليها عملية الفخر Sintering وتحت ظروف مفرغة من الهواء وبدرجة حرارة 1200 درجة مئوية لمدة 8 ساعات .

المسحوق الناتج هو متعدد التبلور Polycrystalline ، تم تحديد كل التركيب البلوري و المجموعة الفراغية Space group و الأبعاد البلورية و طاقة الأصرة والحجم الحبيبي باستخدام عدة تقنيات تحليلية مثل حيود الأشعة السينية XRD ، مطيافية الأشعة تحت الحمراء FTIR والمجهر الإلكتروني النافذ TEM . وتم تحليل النتائج باستخدام عدة برامج خاصة بالفحوص التركيبية كبرامج تحليل حيود الأشعة السينية ومطيافية الأشعة تحت الحمراء وبرامج المجاهر والتي سهلت عمليات التحليل والحسابات والتي سهلت أيضا من إجراء المقارنات ببعض قواعد البيانات العالمية مثل قاعدة بيانات حيود الأشعة السينية PDF2 وقاعدة بيانات علوم البلورات والمواد COD وقاعدة بيانات مطيافية رامان والأشعة تحت الحمراء . كما تم

المخلص

الأهداء

اللهم منك واليك

ثم

الى كل من ساهم في انجاز هذا
العمل

أَعُوذُ بِاللَّهِ مِنَ الشَّيْطَانِ الرَّجِيمِ

بِسْمِ اللَّهِ الرَّحْمَنِ الرَّحِيمِ

﴿ ءَاتُونِي زُبَرَ الْحَدِيدِ ^ط حَتَّىٰ إِذَا سَاوَىٰ بَيْنَ الصَّدَفَيْنِ قَالَ أَنْفُخُوا ^ط

حَتَّىٰ إِذَا جَعَلَهُ نَارًا قَالَ ءَاتُونِي أُفْرِغْ عَلَيْهِ قِطْرًا ﴿٩٦﴾ فَمَا

أَسْطَعُوا أَن يَصْفُوهُ وَمَا سَمِعُوا لَهُ نِقْبًا ﴿٩٧﴾ ﴾

الكهف: ٩٦ - ٩٨



جمهورية العراق
وزارة التعليم العالي والبحث العلمي
جامعة النهرين
كلية العلوم

تحضير وتوصيف المركبات الفيروكهربائية $Ba_xSr_{1-x}TiO_3$

أطروحة

مقدمة الى كلية العلوم في جامعة النهرين وهي جزء من متطلبات نيل درجة
الماجستير في علوم الفيزياء

من قبل

نذير بشير محمود

بكالوريوس علوم فيزياء 2008

باشراف

الاستاذ الدكتور عماد خضير الشكرجي

نيسان 2012

جماد الاول 1433